Modeling Vadose Zone Wells and Infiltration Basins to Compare Recharge Efficiency in Unconfined Aquifers

by

Erik Mark Patton

B.S., United States Military Academy, 2008
M.S., Missouri University of Science and Technology, 2014

A THESIS

submitted in partial fulfillment of the requirements for the degree

MASTER OF SCIENCE

Department of Geology
College of Arts and Sciences

KANSAS STATE UNIVERSITY
Manhattan, Kansas

2017

Approved by:

Major Professor
Dr Saugata Datta

Copyright

Abstract

In specific lithologic and hydrogeological settings, Managed Aquifer Recharge (MAR) projects using vadose zone wells have the potential to outperform infiltration basins in terms of volume of water recharged. Numerical modeling can assist in determining which recharge method is most efficient in infiltrating water to unconfined alluvial aquifers of differing unsaturated zone lithologic complexities. The Sagamore Lens Aquifer (SLA) in Cape Cod, Massachusetts is an example of an aquifer with minimal lithologic complexity while the Hueco Bolson Aquifer (HBA) near El Paso, Texas has greater lithologic complexity. This research combines two U.S. Geological Survey numerical models to simulate recharge from infiltration basins and vadose wells at these two locations. VS2DTI, a vadose zone model, and MODFLOW-2005, a saturated zone model, were run sequentially at both sites and with both vadose well and infiltration basin recharge methods simulated. Results were compared to determine the relative effectiveness of each method at each location and to determine the effects of vadose zone complexity on recharge. At the HBA location, soil samples were tested for conductivity and grain size distribution and a microgravity survey was begun to constrain the models.

The infiltration basin structure proved to be more efficient, infiltrating more water volume at both locations. Lithologic complexity formed perched conditions in the HBA model, significantly affecting infiltration rates from both infiltration methods at that location. Methods and conclusion from this study can assist in the modeling and design of future MAR projects, especially in locations with thick or lithologically complex vadose zones.

Table of Contents

List of Figures

List of Tables

Acknowledgements

A special thanks goes to my committee members without whom this research would not be possible:

- Dr Pamela Kempton, for her fantastic thesis edits and who, as department head, allowed me the opportunity to pursue an applied geology thesis on a condensed timeline.
- Dr Claudia Adam, who taught me the joys of MATLAB and geophysical models and proposed the microgravity portion of this study.
- Dr David Steward, for allowing a geologist to take his civil engineering classes and for his unique engineering viewpoint on a geologist's research.
- Dr Sara Vero, for introducing me to my very first groundwater model.

and to my major professor,

- Dr Saugata Datta, for accepting me as his graduate student, teaching me the fundamentals of graduate research, making sure I stayed on track, and doing it all despite the busiest schedule I've ever seen.

Dedication

This research is dedicated to my wife and best friend, Ashley, whose love has endured a cycle of frequent uprooting and displacement from friends and family and whose support was instrumental in allowing me to attend K-State.

Chapter 1 - Introduction and Background

"It's not that the Arkansas River doesn't flow for most of the year. It doesn't flow most years." – Fred Jones, Water Resources Manager for Garden City, KS.

1.1 Aquifer Depletion

Extraction rates from many of the world's major aquifers are unsustainable and require reducing use, increasing recharge, or some combination of both (van der Gun, 2012). This is particularly true in arid and semi-arid regions where groundwater provides the only perennial source of fresh water. Perhaps the most extreme example is Saudi Arabia, which experimented with aquifer mining to encourage desert agriculture. The resultant aquifer depletion within just several decades led to curtailment of farming subsidies and regulation of groundwater extraction (Elhadj, 2004). In the United States, concerns about groundwater depletion during California's most recent drought led to the 2014 passage of the state's first laws regulating groundwater use (California Department of Water Resources, 2017). Closer to home, Kansas shares the Ogallala aquifer with seven other states. The high rate of withdrawal from this aquifer has led to the conclusion that sustaining current pumping rates will lead to significant impacts by 2030; in particular, increasingly scarce water will result in declining agricultural yields from this highly productive region (Steward et al, 2013).

While agricultural practices account for most groundwater withdrawals, municipal extraction for city water also contributes to depletion. Low precipitation rates and few surface water resources in much of the western United States, including parts of Kansas, mean a stable supply of groundwater is critical to the existence and growth of cities and towns. Some cities have begun artificially enhancing or recharging local aquifers to ensure future water security. Arid southwest states have taken the lead, implementing municipal scale recharge programs, but

the practice of storing water in aquifers is gaining favor in other parts of the country as well. On May 12th of 2017 the Secretary of the Interior announced $23.6 million for water reclamation and reuse projects in seven states. As part of this funding Garden City, KS, received money to study the best method to reuse effluent water (Department of the Interior, 2017). Aquifer storage may be a viable option.

Hydrogeological models can be created to estimate the effectiveness of aquifer recharge programs. Such models can simulate the physical flow of water and associated pressure heads. They can also simulate the fate and transport of contaminants within groundwater or the mixing of water with different salinities. This research applies groundwater flow models to two locations: (a) Cape Cod, Massachusetts, and (b) El Paso, Texas. Two recharge techniques are modeled at each location: (a) an infiltration basin and (b) a vadose zone well. Throughout this research, abbreviations will be used for the aquifers in El Paso and Cape Cod. In the Cape Cod study area the aquifer is known as the SLA. The abbreviation used is "SLA" for *Sagamore Lens Aquifer*. In the El Paso study area the aquifer is known as the *Hueco-Bolson Aquifer*. It will be abbreviated as "HBA" throughout the thesis.

This research simulates the use of managed aquifer recharge in an arid and lithologically complex location (HBA) to provide quantitative assessments of two aquifer recharge techniques, namely an infiltration basin and a vadose zone well. The effects of complex lithology are analyzed with a focus on how the relationship between location of low permeability layers and vadose well depth affects recharge rates. The results are contrasted with simulated aquifer recharge in a humid continental location with simple lithology (SLA). Finally, results from the first part of a microgravity survey taken at recharge facilities north of El Paso, TX, will be

analyzed in an attempt to validate or refine the models by defining the extent and location of perched layers and water mounds beneath the recharge structures.

1.2 Managed Aquifer Recharge (MAR) & Aquifer Storage and Recovery (ASR)

1.2.1 Volumes and Conversions

Managed Aquifer Recharge (MAR) research and projects typically provide water volumes values in *Acre-Feet*. One *acre-foot* is the volume of water required to cover a one acre surface with one foot of water. The term is commonly used in conjunction with a time unit to provide a rate. For example, ten acre-feet per day would imply that a water volume of ten acre-feet is changing each day within the system. *Acre-feet* is abbreviated as AF and when written as a rate is shown as AF/D or AF/Y, corresponding to *acre-feet per day* and *acre-feet per year* respectively.

Rate in *gallons per minute* (GPM) is also commonly used when discussing aquifer recharge or extraction. 1 AF/D is equivalent to 226 GPM or 1,233 m^3/d of flow. Volume in AF and rates in AF/D, AF/Y, and GPM are standard units when expressing groundwater volumes and rates. When these values are used, the SI equivalent is also given. Conversion factors between commonly used volumes and rates are provided in Appendix Q.

1.2.2 Aquifer Definitions and Fundamentals

A few definitions are required to understand MAR. Knowing which type of aquifer is targeted for recharge helps explain what infrastructure is required for MAR implementation. Aquifers come in two major and one minor type: unconfined, confined, and perched, respectively.

Unconfined, or *water table*, aquifers (Fig. 1) have a water surface that is at atmospheric pressure, meaning the water table is the upper boundary of the aquifer. A well drilled into an unconfined aquifer will have a water column surface elevation equal to the height of the regional water table (Fig. 1).

The term *aquifer matrix* is used extensively. This refers to the dominant material class forming the aquifer. In Fig. 1 the aquifer matrix is a sand. For this research, the aquifer matrix is considered to be the dominant material in both the unsaturated and saturated zones. For example, Fig. 1 would be referred to as having a *highly permeable sand matrix* with *low permeability clay horizon* forming *perched conditions.*

Interbedded low permeability layers form perched conditions. In Fig. 1 recharge occurs from a stream but recharge from an infiltration basin would have the same effect. The combination of an interbedded low permeability layer and recharge creates the minor aquifer type, a *perched aquifer*. Perched aquifers form anywhere water pools on low permeability layers above the regional water table. The *perching layer* is the low permeability layer above which the perched water is present (Wilson et al., 1995).

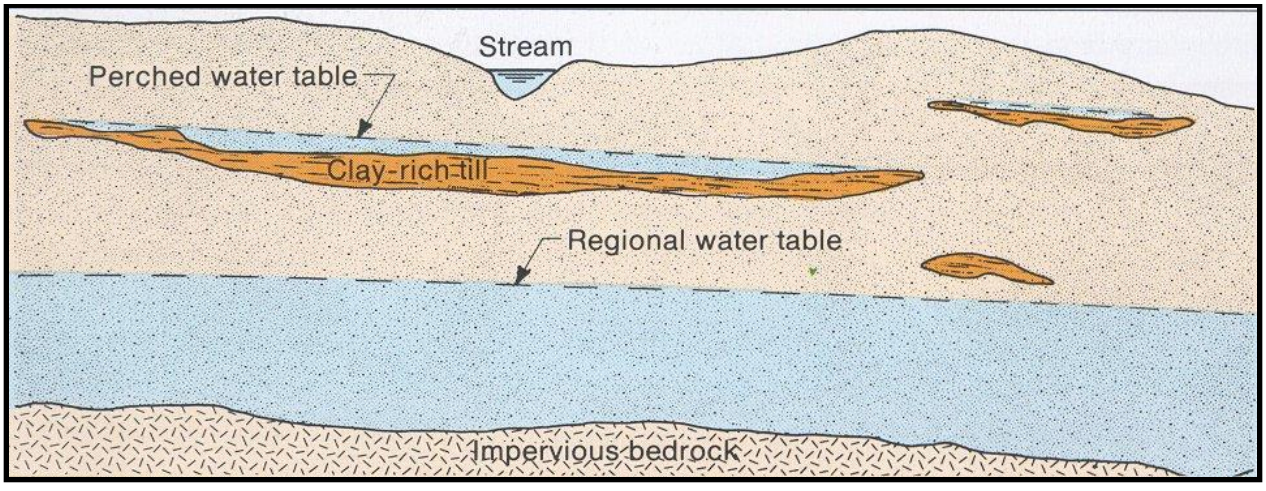

Figure 1: Parts of an unconfined aquifer (Vandike, 2014)

A *confined* aquifer has groundwater under some pressure due to low-permeability layers overlying a more permeable lithologic layer which contains water (Fig. 2). In Fig. 2 the potentiometric surface is displayed as a dashed black line. Where the water table equals the potentiometric surface the aquifer is unconfined (Far right section of Fig. 2 labeled "Bedrock recharge zone") but where the potentiometric surface is above the top of the aquifer it is confined. Confined aquifers are not discussed in this research because they cannot be recharged using infiltration methods due to the low permeability horizon above the aquifer.

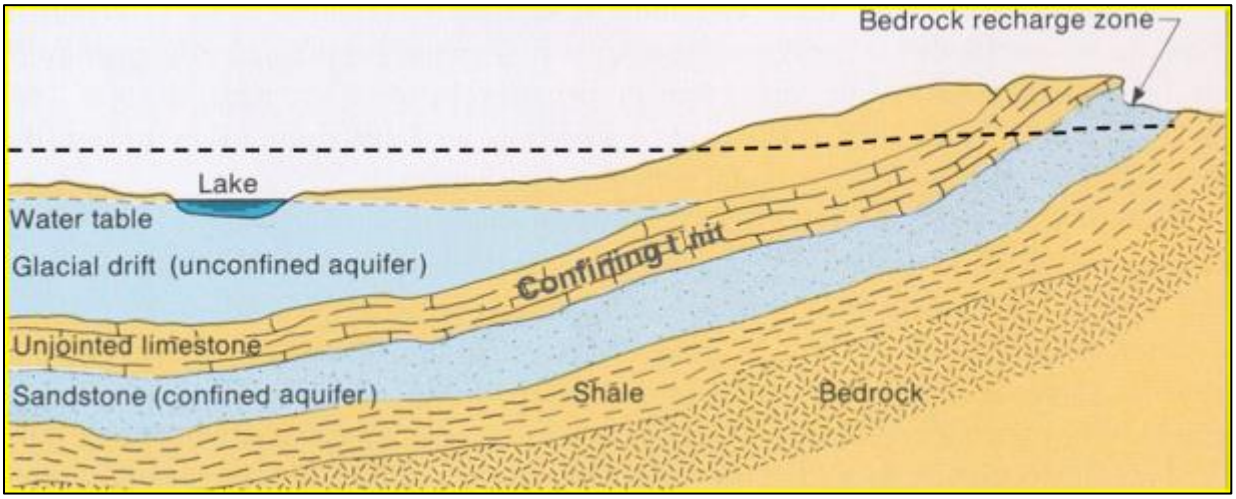

Figure 2: Parts of a confined aquifer (Vandike, 2014)

The confining unit, shown here as unjointed Limestone, overlies a more permeable Sandstone aquifer.

The term *porosity* is widely used in this research and critical to equations discussed in Chapter 3. Total porosity is the ratio of void space to total space in a volume. The term *effective porosity* is also used in hydrogeology. Effective porosity refers only to void spaces that are interconnected and allow flow. Due to lithology at the research locations, effective porosity values and total porosity are nearly identical; the term *porosity* will therefor refer to the effective porosity. Effective porosity is often misinterpreted as being equivalent to permeability, however, permeability is additionally influenced by factors such as cross section and tortuosity of capillary

passageways (Koponen et al, 1997). Distinctions are made in the research between effective porosity and permeability.

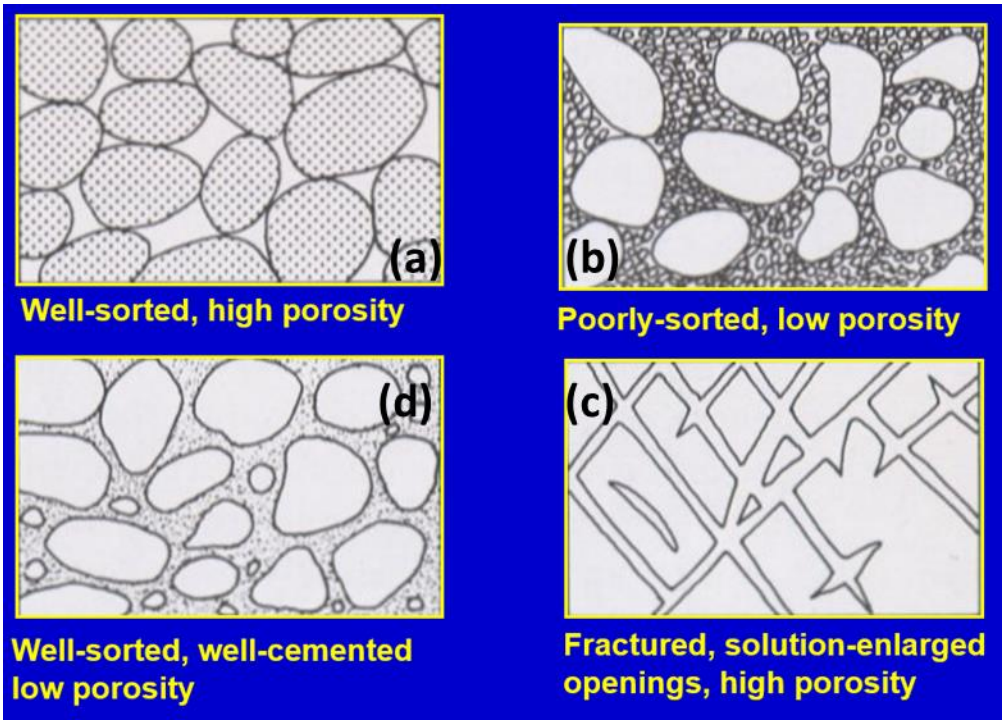

Figure 3: Descriptions of porosity for various types of soils and rock (Vandike, 2014)

Fig. 3 demonstrates various types of porosity: (a) a well sorted matrix, similar to beach sand, where all particles are roughly the same size; (b) poorly sorted matrix, such as can occur in glacial tills, in which no single particle size is dominant and small particles fill the voids between larger particles; (c) porosity caused by fractures in rocks, potentially creating high porosity; and (d) low porosity in well sorted, cemented rocks such as sandstones. Caliche is another example of well sorted desert soils with void spaces cemented by calcite, similar to Fig. 3d. Fractures like those shown in Fig. 3c may be the result of dissolution in limestones or dolomites, unloading of intrusive igneous rocks, or cooling such as occurs in columnar basalts. Tectonic actions may also cause fractures. The two sites chosen for this research have soil types that most closely resemble in the porosity shown in Fig. 3a. Porosity associated with well sorted, poorly cemented soils and sediments is very high. Published values differ depending on source, but porosity

values in gravels range from 15 - 45% and in sands from 10 - 50% (Fetter, 2005, Bell, 2006; Gangopadhyay, 2013). Both locations modeled in this research have unusually well sorted, and therefore highly porous, aquifer matrices, which suggests their porosities are on the upper extreme of these ranges.

Heterogeneity and *homogeneity* are two relevant terms describing an aquifer's degree of uniformity. A *homogeneous* aquifer refers to an aquifer that has same hydrologic properties regardless of the direction of water movement due to a uniform aquifer matrix. A *heterogeneous* aquifer has multiple types of soils or rock, or has been subject to compaction or cementation such that water will flow preferentially in one direction. Heterogeneous aquifers are the norm, especially when considering water flow in the vertical (*z)* direction to water flow in the horizontal (*x*) direction.

1.2.3 Types and Goals of Aquifer Recharge

For this research, Managed Aquifer Recharge (MAR) is defined as the recharge of treated water through engineered structures to aquifers for storage and subsequent recovery. The term MAR is sometimes used interchangeably with Aquifer Storage and Recovery (ASR), although to meet a strict definition of ASR water must be injected and recovered using the same well. Artificial recharge is expected to become increasingly necessary as growing populations require more water and greater storage capacity is needed to save water in times of surplus for use in times of shortage (Bouwer, 2002).

Regions with wet and dry seasons, such as southwest Kansas, or with cyclical droughts, such as central California, can employ MAR programs to store water during times of plenty. This water can be sourced from captured runoff or excess water rights that would otherwise be unused. Another possible water source is treated wastewater. In addition to being "drought

proof", using this water for recharge and subsequent extraction avoids the "toilet to tap" stigma associated with directly returning treated wastewater back in the potable water network. MAR recharge can even further purify infiltrated water through a process known as Soil Aquifer Treatment, or SAT. SAT is the sum of water quality benefits derived during percolation through vadose zone sediments and subsequent groundwater storage. It has been shown to significantly reduce the total organic carbon load, among other benefits (Quanrud et al, 2003).

This research focuses on two MAR techniques. Both infiltrate water through the vadose zone to recharge an unconfined aquifer. These two techniques utilize structures known as infiltration basins and vadose zone wells.

1.2.3.1 Infiltration Basin: This is the most common form of infiltration used for unconfined aquifer recharge. Infiltration basins consists of a depression that receives water and drains by gravity (Figs. 4 & 5). The top several meters of soil are typically removed, especially if they contain organics or clays, to allow water to pond over permeable soils. Infiltration basins can be various sizes depending on the volume of inflow and the rate of infiltration. El Paso has six such basins, and each is approximately 0.4 acres in surface area (Fig. 5). In contrast, infiltration basins in Arizona's Granite Reef Underground Storage Project have a combined surface area of approximately 217 acres (Salt River Project, 2017).

For the purposes of this project a 0.5 acre basin was modeled. Fig. 4 demonstrates how water drains by gravity from a surface depression. Blue arrows represent the generalized flow path of water. Such basins are not typically deep and so pressure heads that form from standing water are low.

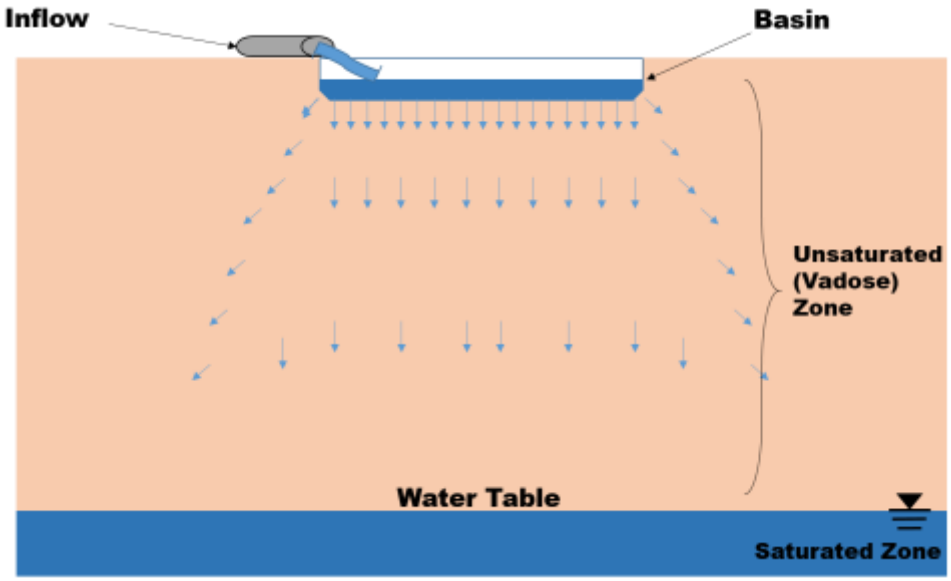

Figure 4: Cross section of an infiltration basin.

Fig. 5 shows examples of the infiltration basins at the El Paso study site and provides an example of a typical small infiltration basin. The infiltration basin in Fig. 5a receives inflow of 1.33 AF/D (300GPM). With periodic maintenance (note absence of vegetation on basin floor), infiltration rates are high enough to prevent water ponding at this inflow rate. Fig. 5b shows the infiltration basin constructed during American Water Works Association Research Foundation (AWWA) study. This basin will be referenced throughout this thesis for comparison. Fig. 5c shows the condition of one of the infiltration basins requiring maintenance. Vegetation has grown along the basin floor and infiltration rates are reduced, creating ponded water.

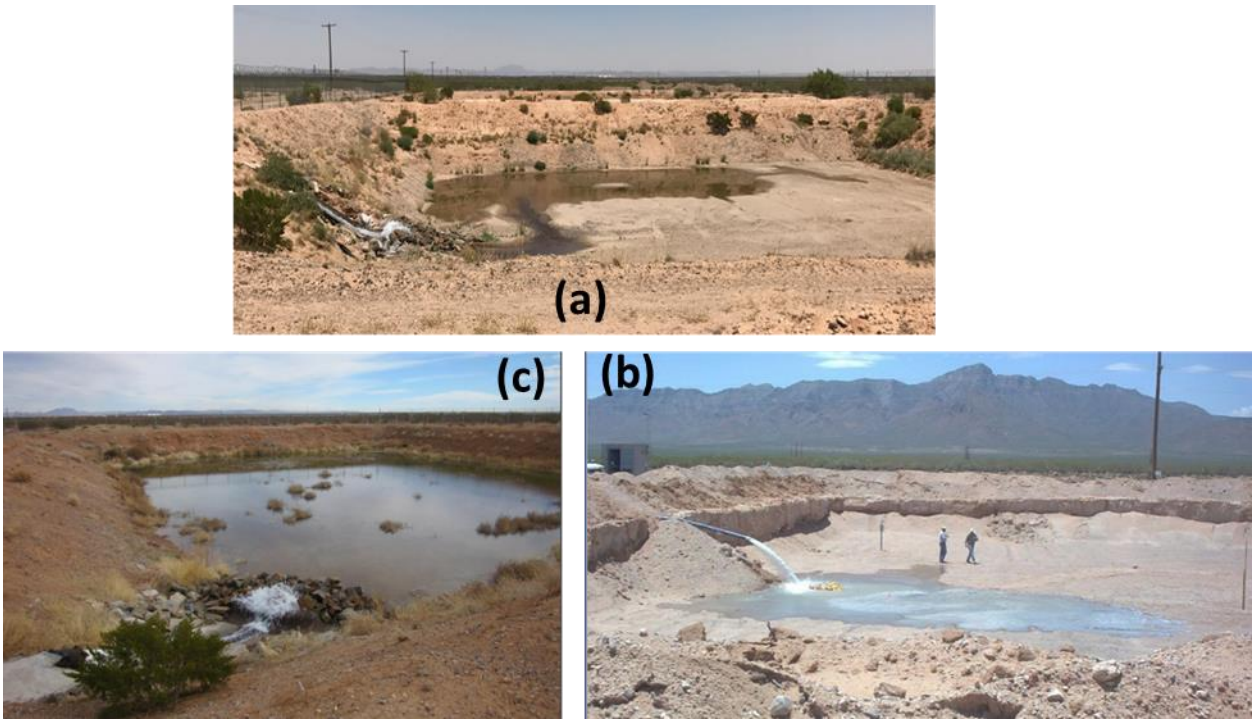

Figure 5: El Paso Water Utility (EPWU) infiltration basins.

Each basin area is approximately 1,619 m^2 (0.4 acres). (a) is a field photograph taken during this research project; (b) and (c) are from Reinert (2016)

1.2.3.2 Vadose Zone Wells: These are commonly called a dry well or recharge shaft. In their simplest form, vadose zone wells are holes drilled then backfilled with highly permeable sands and gravels (Bouwer, 2002). Water is then supplied through a small pipe in the center. This allows recharge to begin further below ground than is possible with infiltration basins since recharge starts at the bottom of the well. This has practical application when local lithology or land availability is not conducive to infiltration basins (Fig. 6). Water is supplied into the well and allowed to drain. The standing water column in the well can provide a large pressure head near the bottom of the well, helping force water into the aquifer matrix. However if poor quality water is used the water column pressure can also force small suspended solids into the aquifer matrix, potentially clogging an area around the well screen and reducing infiltration.

Goodyear, Arizona, operates a vadose zone well field to recharge their local aquifer. Each well is 33.5m below ground level. The vadose zone well modeled for this thesis is 33m deep for the El Paso site and 10m deep for the Cape Cod site. These depths correlate to 1/3 the vadose zone thickness at El Paso and 1/2 the vadose zone thickness at Cape Cod (AWWA, 2003 and Demolition Area 1 Monitoring Report, 2013).

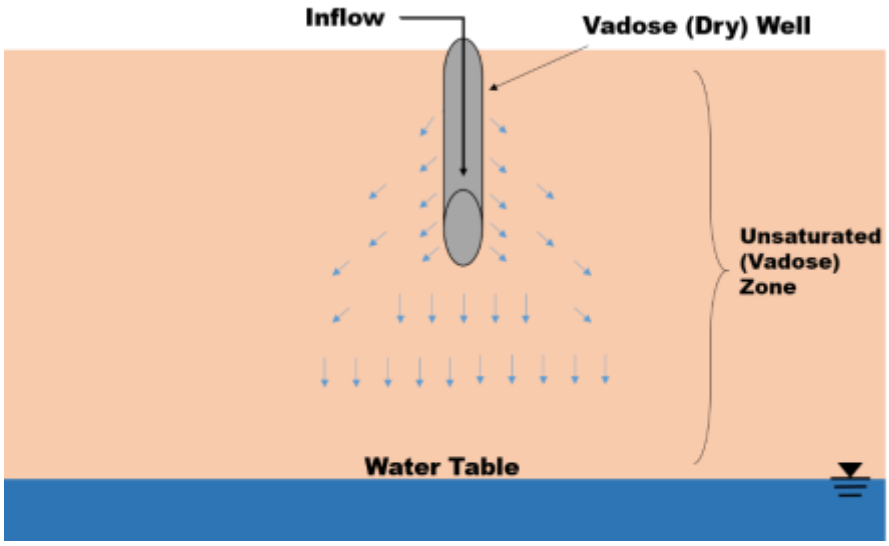

Figure 6: Cross section of a vadose well.

1.2.4 Select Examples of MAR and ASR

Table 1 lists select examples of current MAR and ASR project utilizing infiltration basins or vadose zone wells. When vadose zone wells are the infrastructure chosen to implement MAR, the cluster of resulting wells is called a *vadose zone* or *recharge* wellfield. Clusters of infiltration basins are referred to simply as infiltration basins.

El Paso, Texas. During normal years this city relies on an approximately equal amount of surface water from the Rio Grande River and groundwater from the Hueco Bolson and Mesilla Bolson aquifers. El Paso Water Utility (EPWU) is normally allocated just under 70,000 AF/Y (acre-feet per year) ($8.6*10^7$ m^3 per year) of water rights from the Rio Grande River; the amount available to pump is reduced during periods of drought (EPWU, 2016). Groundwater

makes up the difference between demand and river water availability. Years 2007-2009 averaged less than 30,000 AF/Y ($3.7*10^7$ m^3/y) of groundwater extraction due to high volumes of river water available, but for 2012-2015 over 50,000 AF/Y ($6.16*10^7$ m^3/y) of groundwater was extracted (EPWU, 2016). During a drought of record scenario, El Paso plans for a reduction in surface water withdrawals from 60,000 AF/Y ($7.4*10^7$ m^3/y) to only 10,000 AF/Y ($1.23*10^7$ m^3/y) - a reduction of 83%. In addition to being the only source of surface water, the Rio Grande only flows during irrigation releases from a dam 130 miles upstream (EPWU, 2016). The city currently recharges 5,000 AF/Y ($6.17*10^6$ m^3/y) to the Hueco Bolson Aquifer with plans to scale up by implementing enhanced arroyo recharge along dry stream beds. The idea that groundwater is viewed as a stable, drought-proof alternative to surface water for cities like El Paso is seen in Fig. 7. In response to a drought from 2011-2015, groundwater pumping was significantly increased to offset the loss of surface water available from the Rio Grande river.

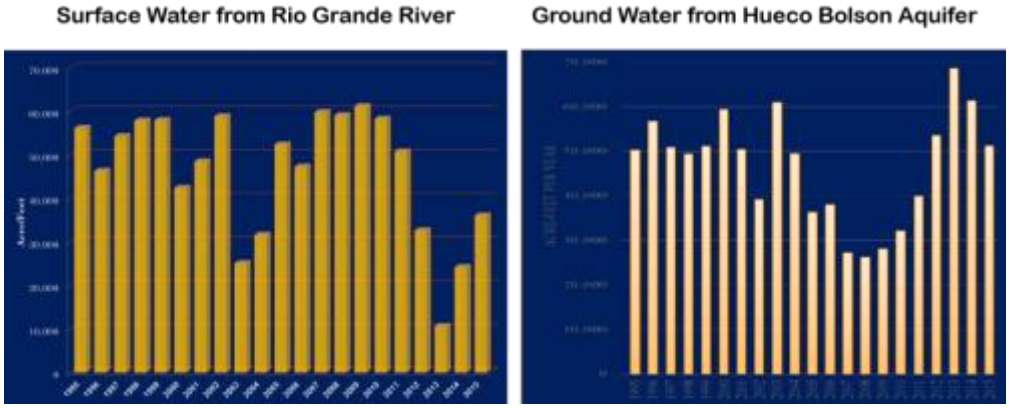

Figure 7: Historical surface and groundwater use in El Paso, Texas, 1995-2015 from Reinert (2016).

Bars represent cumulative extractions for the year.

Tucson, Arizona. A desert city, Tucson relies on the extensive Central Avra Valley Storage and Recovery Project to bank Colorado River water rights in the local aquifer. A comprehensive legal framework created in response to declining water tables encourages aquifer

recharge to prevent further declines. The city can store over 70,000 AF/Y ($8.6*10^7$ m^3/y). Tucson later recovers the water for use, for example, recovering almost 65,000 AF ($8.0*10^7$ m^3) of stored water in 2012 (Tucson Water, 2017).

Wichita, Kansas. With current sources of water supply not expected to meet demand into the 21st century, the city of Wichita decided to use the local aquifer as an additional reservoir (Ziegler et al., 2001). Water levels in the aquifer fell as much as 50 feet lower than predevelopment levels and the city's reliance on a single surface reservoir was not considered sufficient to meet future needs (Stone et al, 2016). This spurred the city to complete a project capable of infiltrating 10 acre-feet per day (AF/D) (12,334.82 m^3/d) of surface water during high river flows to help provide the 767 AF/D ($9.46e10^5$ m^3/d) peak demand the city expects by year 2050 (City of Wichita Public Works and Utilities, 2017).

Table 1: Select MAR projects in the US Southwest

Name	Location	MAR Type	MAR Structure Size	Target Volume Recharged
Infiltration Basins				
Hueco Bolson Aquifer Recharge	El Paso, Texas	Infiltration Basin	6x 0.4 acre basins (2.4 acres total)	5,000 AF/Y
Granite Reef Underground Storage Project	Mesa, Arizona	Infiltration Basin	7x basins (217 acres total)	93,000 AF/Y
New River-Agua Fria River Underground Storage Project	Pheonix, Arizona	Infiltration Basin	6x basins (125 acres total)	75,000 AF/Y
Sweetwater Recharge Facility	Tuscon, Arizona	Infiltration Basin	8x 0.75 acre basins (6 acres total)	6,500 AF/Y
Equus Beds Aquifer Recharge	Wichita, Kansas	Combination	Wells, Basins, and Trenches	112,014 AF/Y *
Vadose Zone Wells				
Scottsdale Water Campus	Scottsdale, Arizona	Vadose Wells	27x standard wells 28x backup wells	19,602 AF/Y*
Goodyear Vadose Injection Project	Goodyear, Arizona	Combination	15x wells *planned* 4x basins (14 acres)	8,300 AF/Y *wells only*
North Regional Wastewater Treatment Plant	Lake Havasu City, Arizona	Vadose Wells	5x wells *installed* 32x wells *planned*	3,921 AF/Y
South Plant Water Reclaimation Facility	Surprise, Arizona	Vadose Wells	20x vadose wells	8,049 AF/Y
**theoretical maximum recharge. Actual recharge is constrained by available water volume and work/rest cycle of basins*				

Chapter 2 - Research Rationale

"The occurrence of water in the rocks of any region is therefore determined by the character, distribution, and structure of the rocks it contains- this is by the geology of the region"- Oscar Meinzer, The Father of Modern Groundwater Hydrology.

2.1 Literature Review

2.1.1 Vadose Zone Well Recharge

Various studies and projects have considered the effectiveness of vadose zone wells as compared to infiltration basins. Infiltration rates of 7,000 m^3/d, 354 m^3/d, and 146 m^3/d were achieved in widely different conditions and using widely varying vadose zone well types in Tampere, Finland; Styria, Austria; and Kansas, USA, respectively (Handel et al, 2014 and 2016; Jokela and Kallio, 2014). In addition to experimental research, vadose wells have been constructed as integral parts of municipal water supply systems in parts of the U.S. Southwest. The city of Scottsdale, Arizona, has 27 standard vadose zone wells with a design infiltration flow of 2,453 m^3/d each and 28 emergency vadose zone wells with an average infiltration of 1,635 m^3/d.

The studies above generally simplified the effects of complex, heterogeneous lithology. This research considers the effects of vadose zone well recharge in both a complex, heterogeneous, thick vadose zone and a shallow, homogenous vadose zone to determine vadose well and infiltration basin performance. The previously listed projects were also tested physically by building vadose wells and actual infiltration rates were measured. This work measures expected infiltration rate through vadose zone wells at two locations where infiltration basins, not vadose wells, are functioning.

2.1.2 Infiltration Basin Recharge

Much work has been done on determining infiltration rates through the vadose zone from surface recharge (Green and Ampt, 1911; Bouwer, 1969; Bouwer, 2002; Hantush, 1967; Marino, 1975a, b). Green and Ampt (1911) presented one of the first equations for quantifying infiltration in one dimension. Infiltration as applied to MAR has been looked at in more recent times, perhaps most prolifically by Herman Bouwer (Bouwer, 2002). Prominent publications on ASR include Brown (2006) and Bloetscher et al. (2014). Brown's study included 50 ASR projects from across the world, whereas Bloetscher et al. included 204 sites from within the United States to draw out lessons learned from their design, construction and operation. These publications, while not focused on infiltration basins, provided a general overview on ASR operation. Finally, numerous studies have been conducted on individual sites to determine effectiveness of infiltration basins. These studies were reviewed for this research and included both papers and presentation given at professional gatherings, including Dillon et al. (2006), Izbicki et al. (2008), Bekele et al. (2013), Mawer et al. (2016). The studies often included a numerical model portion to interpret observed conditions.

Literature review combined with review of current MAR projects (El Paso, TX; Goodyear, AZ; Surprise, AZ; Wichita, KS; Scottsdale, AZ; Las Vegas, NV; others), informed certain parameters used in modeling. These include the following:

- Size of infiltration basin: set at 0.5 acre (2,023m^2) in both models to represent basins used at El Paso, TX
- Depth of vadose zone wells: set at 33m (100ft) to represent a well penetrating 1/3 of the vadose zone. Vadose zone well depth did not commonly exceed 55m (180ft) during the

review of current projects in similar geologic settings. This depth is based in part by the preferred drilling method and is not an absolute limit.

- Depth of vadose zone well at Cape Cod: set at 10m (33ft) to represent a well penetrating 1/2 of the vadose zone. This is similar in depth to a numerical study that simulated a vadose well 12m deep (Handel et al., 2014) and a field study that used a shallow partially-penetration well screened from 4.6m to 18.3m (Gaisheng et al., 2016).

2.2 Hypothesis

Based on the above literature and project references, the following hypotheses are proposed.

- A 33m (100 ft- El Paso) and 10m (33 ft- Cape Cod) deep vadose zone will recharging more water in a set period of time than a 2,023m^2 (1/2 acre) surface basin, based on estimates of similar models by Händel et al. (2014) and field tests of similar scenario by Liu et al. (2016).
- A 33m (100 ft- El Paso) and 10m (33 ft- Cape Cod) deep vadose zone well will deliver more total volume of water than a 2,023m^2 (1/2 acre) surface basin to a production well located 402m (1/4 mile) down gradient due to less lateral dispersion during infiltration.

The vadose well is hypothesized to outperform the infiltration basin for three reasons: (1) infiltration begins at some depth in the vadose zone, so water has less distance to travel before recharging at the water table; (2) perched conditions are less likely to form in vadose well models because infiltration begins below some or all of the low permeability layers; and (3) the weight of a standing water column in a vadose well (the *pressure head*) will enhance flow from the well, a situation which does not occur in infiltration basins where water is ponded only to shallow depths.

Vadose zone well depths were chosen to be 1/3 the distance from surface to water table at the El Paso site and 1/2 the distance from surface to water table at the Cape Cod site. These depths are hypothesized to provide a strong contrast with the infiltration basin while ensuring the wells remain above any water table mounding that may occur during modeling.

Size for the infiltration basin was chosen at 1/2 acre. While there is no standard size for infiltration basins in ASR projects and many projects use much larger basin sizes, 1/2 acres was chosen to match the test basin constructed at El Paso during an AWWA study (AWWA, 2003). This AWWA study constructed both an infiltration basin and vadose well in the HBA to test effectiveness of each structure at recharging the alluvial aquifer.

A distance of 1/4 mile (402 meters) between the infiltration location and the target well was chosen to show any lateral dispersion in the models output. By measuring water table rise at this location in both locations and with both infiltration methods, the volume of water resulting from recharge at this point can be determined.

2.3 Objectives

Objectives of the study include:

- Determine infiltration rates of a 1/2 acre basin (2,023 m^2) and groundwater flow rate from the basin to a monitoring well located 1/4 mile (402m) away in two different geologic settings, i.e. the HBA near El Paso, TX and the SLA in Cape Cod, MA.
- Determine infiltration rates of a vadose zone well set at a depth of (a) 33m in the HBA and (b) 10m in the SLA and establish the groundwater flow rate from the wells to a 1/4 mile (402m) distance monitoring well.

- Determine the relationship between the number of vadose-zone wells required to match the performance of the infiltration basin with respect to volume of water infiltrated and water table rise at a monitoring well 1/4 mile (402m) downgradient for both sites.

2.3.1 Benefits of Studying Two Sites

This research considers two different sites to gain an understanding of infiltration basin and vadose well recharge in aquifers with differing geologic characteristics. Both aquifers are unconfined, which is a requirement if surface recharge is to be considered, and both aquifers are highly permeable, which makes recharge more practical. In other respects, the aquifers are quite different. These differences are summarized in Table 2.

Table 2: Comparison of sites selected for modeling

	Location	Average Precipitation	Aquifer Matrix	Depth to Water Table	Dominant Geologic Facies	Heterogeneity	Groundwater Age
Hueco-Bolson Aquifer (HBA)	El Paso, TX	24.6 cm/yr	Sand	~107 meters	Fluvial and Alluvial Fan	Highly	12,100-25,500
Sagamore Lens Aquifer (SLA)	Cape Cod, MA	119 cm/yr	Gravel and Sand	~21 meters	Glaciofluvial	None-very slight	<100 years

Apart from answering the thesis hypothesis, additional advantages of modeling two sites:

- Interpret the effect (if any) of widely different lithology on basin and vadose well recharge
- Interpret the effect (if any) of widely different vadose zone thickness on infiltration rates from both vadose wells and infiltration basins.
- Interpret the effect (if any) of isotropy on infiltration rates from both vadose wells and infiltration basins

2.4 Model Selection

This study uses two models to determine (a) infiltration rates and dispersion direction from a vadose zone well and a 1/2 acre infiltration basin and (b) water mounding, flow, and residence time in the saturated zone from the point of infiltration to a target well 1/4 mile distant. Within the vadose zone the program VS2DTI (Healy and Essaid, 2012) was used. Within the saturated zone, MODFLOW-2005 is used (Harbaugh, 2005). This workflow is shown graphically in Fig. 8. In each aquifer, literature review will supply hydrologic and geologic parameters used in modeling and current infiltration rates from existing structures or precipitation. Each aquifer will be duplicated with all parameters identical except for the infiltration method, which will be basin infiltration in one scenario and vadose well infiltration in a second scenario. These inputs will be used in two sequential models to simulate flow through the vadose zone (using VS2DTI) and subsequent changes to the water table caused by a rise in the saturated zone (using MODFLOW-2005). Results from the models will indicate the volume of flow from each infiltration method and measure subsequent water volume increase at a target monitoring well distant from the infiltration site. In addition to these two models, the vadose zone model Hydrus 1D was also initially used but was discontinued after VS2DTI was determined to be more applicable to this project. The programs are described in detail in the next chapter.

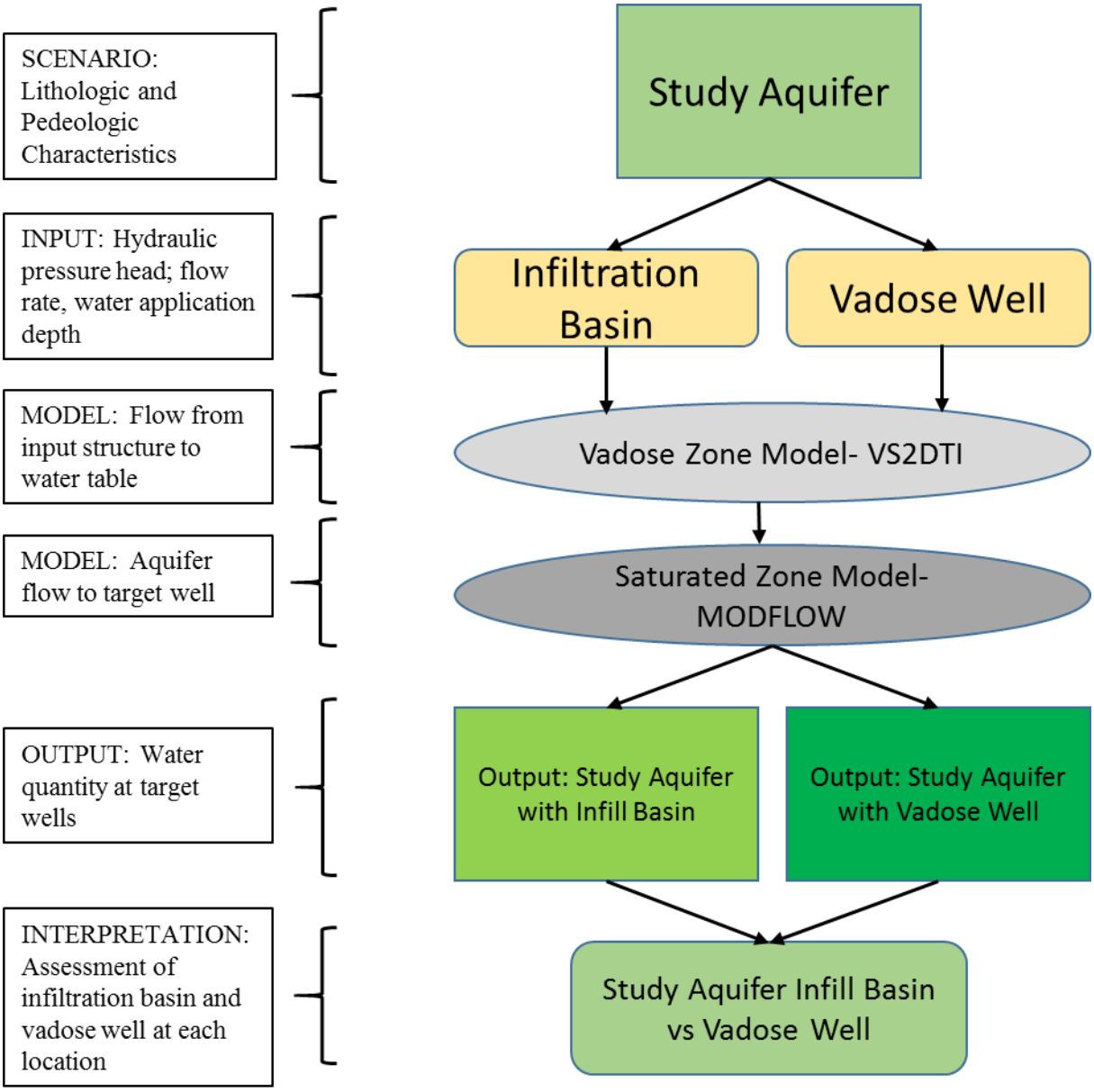

Figure 8: Study Flow Chart.

One additional model, RETC (van Genuchten, M. et al, 1991), was used in conjunction with VS2DTI. RETC is a transform function program that uses soil inputs such as particle size characteristics and water retention parameters to estimate the van Genuchten variables required in vadose zone modeling. Both Hydrus 1D and VS2DTI can automatically input van Genuchten variables from several generic classes of soil, but these generic classes may not be representative of the soils at the site being modeled. To ensure that soils simulated in the models were as close

to real world conditions as possible, generic soil classes were not used for modeling the aquifer matrix at either location. At the HBA location, data on soil water retention versus various pressure heads from a USGS publication (Abeyta et al., 1999) was run through RETC to calculate van Genuchten parameters required to accurately model water flow in the vadose zone. For the SLA location, literature review informed the selection of these parameters (Hess et al, 1992; Masterson and Walter, 2009; Moench et al, 2004; Mace et al, 1998; Grimestad, 2002; El-Kadi, 2005).

Combining water quantities infiltrated through the vadose zone using VS2DTI with groundwater movement in MODFLOW results in an assessment of how much water arrives at the target well in any given time period. VS2DTI model parameters will then be changed to simulate an infiltration basin or vadose zone well. The output from the model simulating an infiltration basin will be compared to the model simulating a vadose zone well to contrast water quantity flow at the target well (Fig. 9). The upper image in Fig. 9 shows an infiltration basin and heterogeneous aquifer cross section. Water flow from the basin follows a stair step path across low permeability layers as it travels to the aquifer. Ultimate recharge at the water table is spread out over a large area. Bottom image shows a vadose well in the same aquifer. Recharge occurs partially below the upper clay layer, resulting in ultimate recharge at the water table across a smaller area.

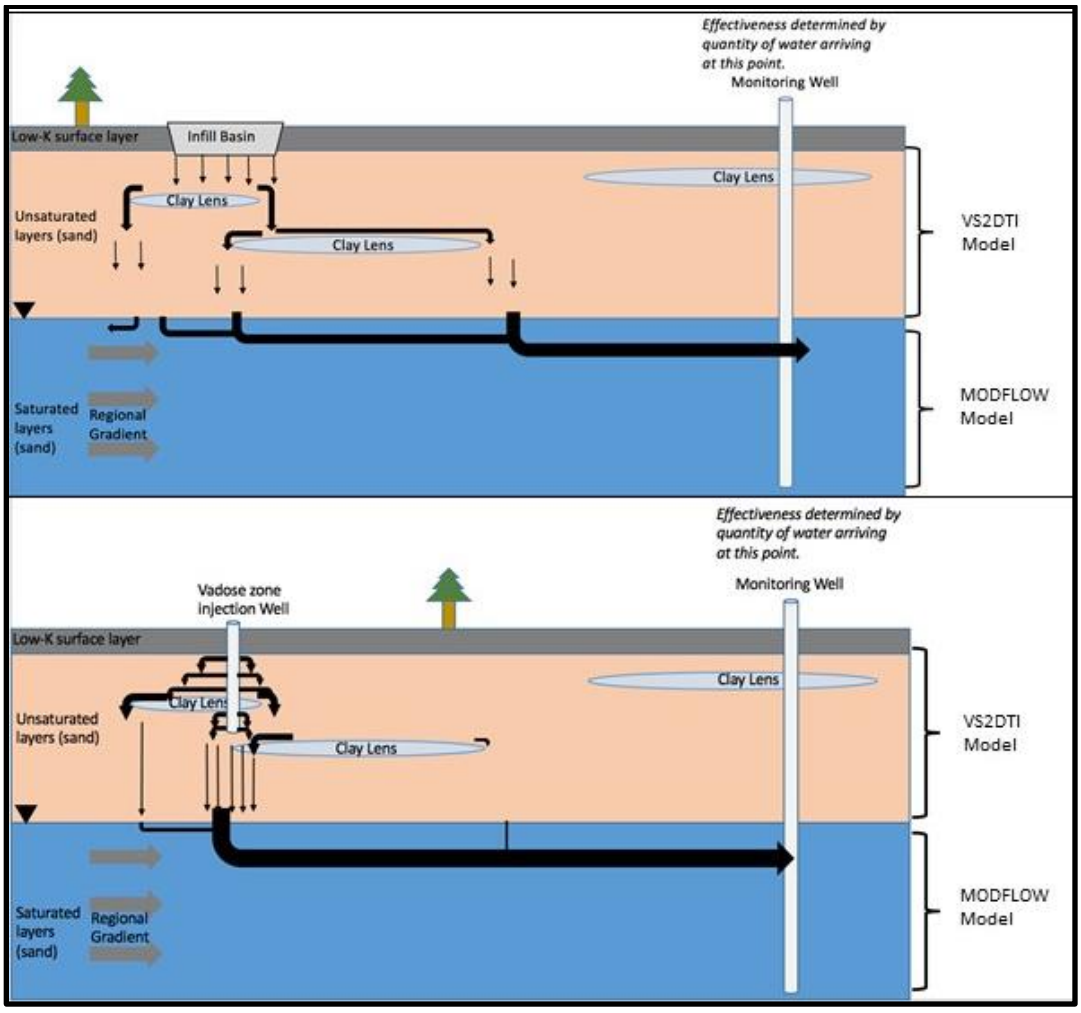

Figure 9: Conceptual model of basin and vadose well recharge.

Chapter 3 - Geologic and Hydrogeology Setting

"I never realized what beauty water added to a river until I saw the Rio Grande." – Mark Twain

3.1 Sagamore Lens Aquifer, Cape Cod, Massachusetts

3.1.1 Geologic Setting and History: SLA

The Sagamore Lens Aquifer (SLA) is the largest and western-most of the seven fresh water lenses that define the Cape Cod Alluvial Aquifer. Located on the Upper Cape, it discharges to the ocean in all directions: North to Cape Cod bay, South, Southwest, and East to Nantucket Sound, and Northwest to the Cape Cod Canal (Fig. 10). Topography in the SLA area takes the shape of a low hill with highest elevation in the center, furthest from the coast. Groundwater gradients generally follow elevation contours (LeBlanc et al, 1996). Aquifers on Cape Cod provide the only source for drinking water and most other domestic, industrial, and agricultural fresh water uses on the Cape (Barbaro et al., 2014).

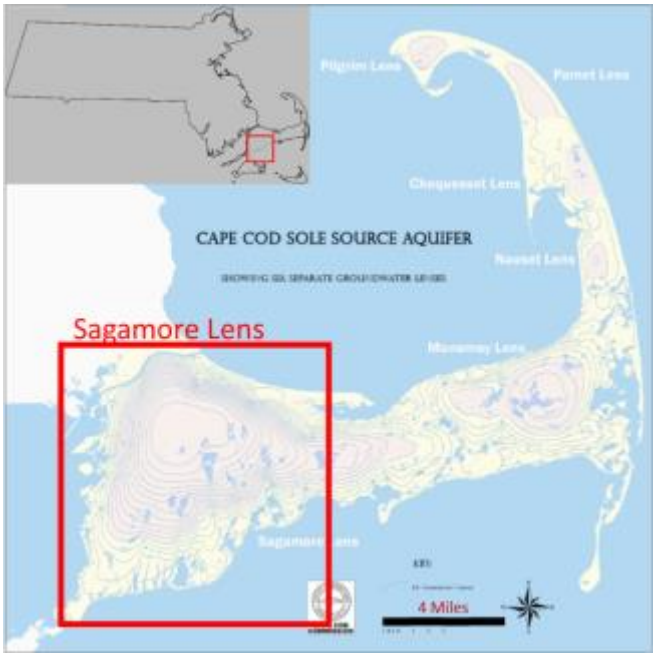

Figure 10: Location of SLA, Cape Cod, MA (modified from Masterson and Walter, 2009)

Bedrock type underlying the unconsolidated sediments of the SLA is believed to consist primarily of granitoids and orthogneisses, along with minor basalt, diabase and amphibolite (Oldale and Barlow, 1986; Hallett et al., 2004). There is some weak deformation and regional metamorphism thought to have occurred in the Proterozoic and/or during the Permian Alleghenian orogeny. The highest metamorphic grade in the study area is believed to be lower amphibolite facies (Hallett et al, 2004). A bedrock elevation map was created in 2013 using borehole data and passive seismic techniques and is available in Appendix M (Fairchild et al., 2013). Regionally, bedrock dips in the southeast direction. Highest bedrock elevation is 23m below sea level in the northwest corner of the study area and the lowest recorded bedrock elevation, just offshore in the southeast corner, is 129m below sea level. Dip angle decreases in the northwest resulting in the bedrock morphology being called a monocline in one paper (Uchupi and Mulligan, 2005); the location chosen to model recharge is on the flattened upper part of this monocline. Bedrock in the study area is 45m below sea level (about 92m BGL, although exact depth BGL depends on surface topography).

Cape Cod's topography and surficial geology were created during the Wisconsin glaciation when the Laurentide ice sheet reached maximum extent south of Cape Cod approximately 20,000 years ago. The ice sheet then began a slow retreat across the Cape, uncovering the southern shore about 19,000 years ago and departing the Cape completely by retreat northward around 17,000 years ago (Fig. 11) (Uchupi and Mulligan, 2005). Outwash plains associated with Cape Cod's glacial history are responsible for high degree of particle sorting, creating grain size homogeneity in the aquifer.

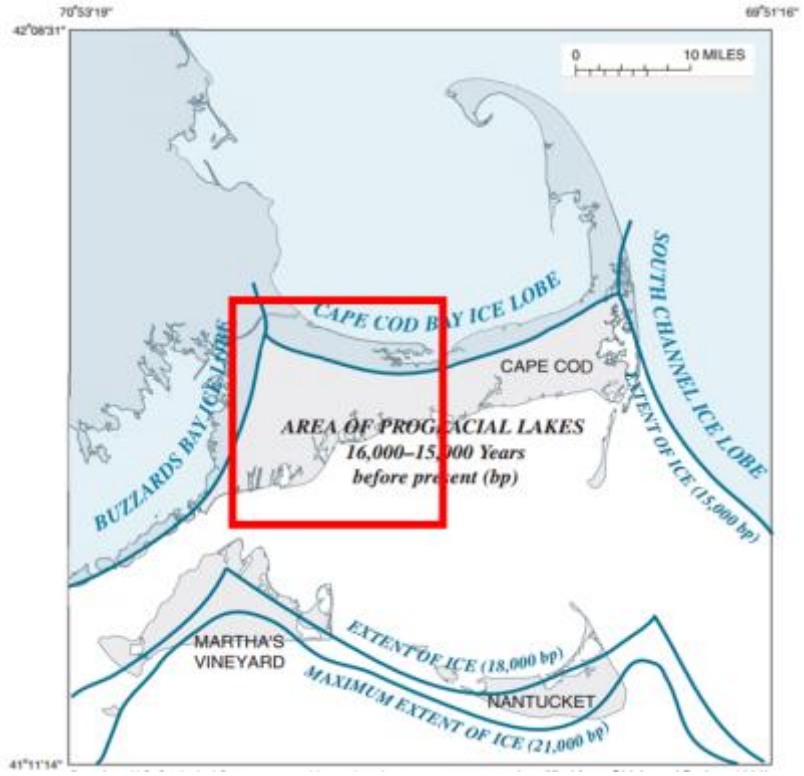

Figure 11: Pleistocene epoch glaciation in SLA study area (Walter and Whealan, 2004)
Red box encloses the Sagamore Lens area.

The highly permeable glacial outwash portion of the aquifer is classified as glaciofluvial deposition. In most areas glaciofluvial deposits overlie a less permeable but also unconsolidated layer of glaciolacustrine sediments consisting of fine to medium silts and sands (Fig. 12). The study area appears towards the left of Fig. 12 where "Otis A.F.B." is annotated. According to Fairchild et al. (2013), "the study area overlies unconsolidated glacial drift deposits that consist of medium-to-coarse-grained glaciofluvial sand and gravel outwash overlying find-to-medium-grained glaciolacustrine sand and silt". Appendix C shows a cross section of the SLA area with glaciofluvial, glaciolacustrine, and bedrock annotated.

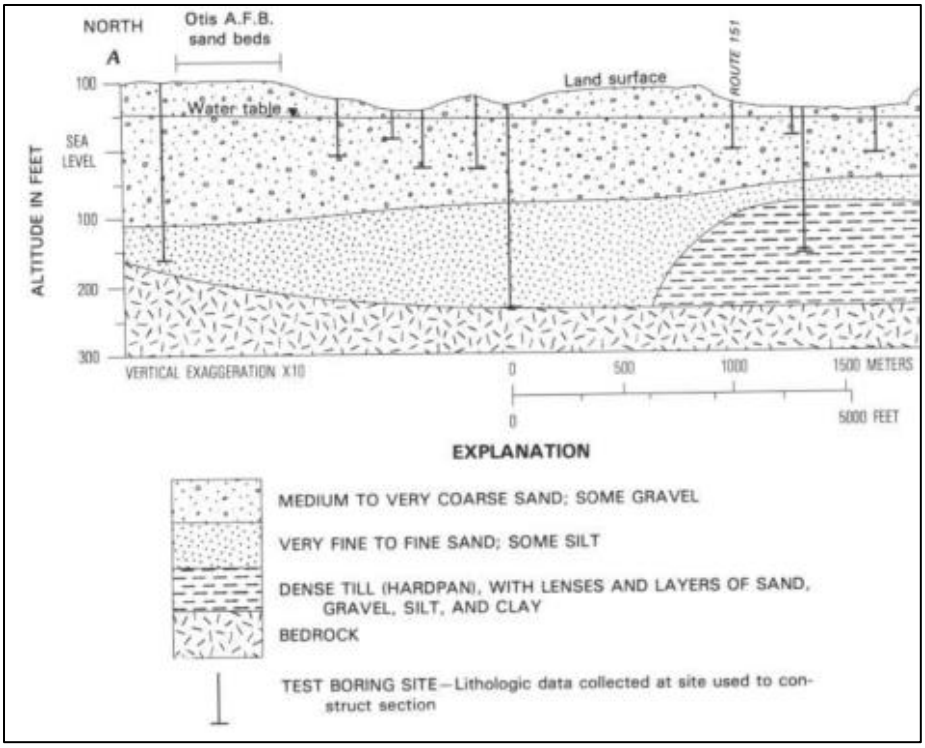

Figure 12: Lithologic cross section representative of the SLA study area (LeBlanc 1984)

3.1.2 Hydrogeological Setting: SLA

The unconfined aquifer matrix is glacial outwash consisting of clean, medium to coarse sand and gravels with less than 1% clay and silt (Hess et al., 1992). It was described as having "remarkably homogeneous flow" by Moench (2002), who conducted aquifer tests in the SLA and wrote "The aquifer is only mildly heterogeneous, i.e. the horizontal and vertical correlation scales are small in comparison with the scale of the aquifer test."

The sole source of fresh water recharge to all aquifers on Cape Cod is precipitation. Precipitation averages ~119 cm/year, with 68.5 cm/yr of that precipitation recharging the aquifer. Around 70% of groundwater discharges into streams and ultimately the ocean. Another 25% discharges directly to the ocean without entering a stream, especially if recharge occurs towards the center of the groundwater divide (Fig. 13). This flow path is generally deeper than the flow path taken by groundwater discharging into streams. The remaining 5% of groundwater

discharges to wells (Fig. 13) (Carlson et al., 2015). Flows closer to ground surface typically contain younger water and spend less time between recharge and discharge. Deeper flows are typically older. The continual recharge of fresh water forms a barrier which prevents salt water from encroaching into the aquifer. In the SLA, the constant replenishment and short time between recharge and discharge stands in contrast to the situation in the HBA discussed in the next section.

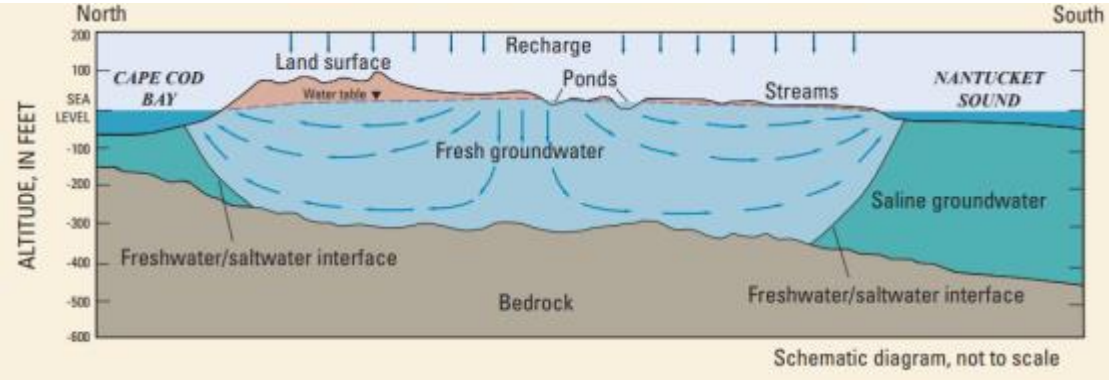

Figure 13: Conceptual model of groundwater flow in the SLA (Masterson and Walter, 2009)

Flow lines show the direction of water movement.

The highest water table elevation occurs approximately 21 m above sea level (Fig. 14) (Fairchild et al., 2013; USACE NAE, 2016). Water table height varies seasonally and annually due to fluctuations in precipitation and is generally highest in the spring and lowest in the fall (Masterson and Walter, 2009). Above the water table, the SLA area of Cape Cod is home to Joint Base Cape Cod (JBCC), a United States military installation. Training over the past 100 years has resulted in soil and groundwater contamination that is undergoing remediation by the US Army Corp of Engineers (USACE). Data provided by USACE includes an enormous array of aquifer test results and local geologic conditions. Groundwater within known contamination plumes, the result of past fuel spills, training, disposals, and associated military activity in the area, are pumped out of the aquifer through purpose built water wells, treated to remove the

contamination, and reinjected into the aquifer (US Army Environmental Command, 2011). The large number of monitoring wells installed in the study area to sample contamination and the extensive groundwater modeling chosen to locate and treat leachate plumes provides a wealth of data to facilitate vadose zone and groundwater models (JBCC IAGSP document repository, first accessed 2016). USGS has also created groundwater flow models (Fig. 14) in addition to researching unsaturated flow characteristics for the Cape Cod aquifer (Stevens, 1994).

Figure 14: Groundwater contours in SLA (US Army Corp of Engineers, 2016)
Blue contours are 2ft intervals above mean sea level; flow direction is perpendicular to contours. Red box indicates study area.

Monitoring well #255 was chosen as the upgradient starting point for a representative section of the overall sand and gravel aquifer at Cape Cod (red box, Fig. 14). Depth to water

table in the SLA at monitoring well #255 is 20.7m (AMEC, 2003 & US Army Corp of Engineers, 2013). Well #255 is located in proximity to a treatment system and injection well #1D-IW-1, which injects treated water at a rate of 250 GPM (0.94 m^3/min) into the aquifer. The lithology of the subsurface at this location is almost exclusively sand with layers differing only in small variations to grain size and sorting characteristics. A cross section of this area is available in Appendix A.

3.2 Hueco Bolson Aquifer, El Paso, Texas

3.2.1 Geologic Setting and History

The Hueco Bolson Aquifer (HBA) is an alluvial, unconfined aquifer located in far-west Texas, south-central New Mexico, and the Mexican state of Chihuahua (Fig. 15). The aquifer forms in the down-dropped basin (a graben) between the Franklin Mountains to the west and the Hueco mountains to the east (horst features), roughly forming a lopsided V-shape (Fig. 15) with the deepest point (the bottom of the V) located on the west side close to the Franklin mountains (White et al., 1997). This V-shaped trough has a total length of approximately 200 miles north-south and an average of 25 miles east-west (Sheng and Devere, 2005). The sediments forming this aquifer matrix consists of between 0 and 2,700m of unconsolidated to slightly consolidated, highly permeable alluvial and alluvial fan facies with interbedded layers of lower permeability lacustrine deposits (Druhan et al., 2003; Sheng and Devere, 2005). Current deposition in the basin is from weathering of the surrounding mountains and, to a much lesser extent, aeolian transport. Historically, sediments were also fluvially transported when the Rio Grande ran east of the Franklin Mountains.

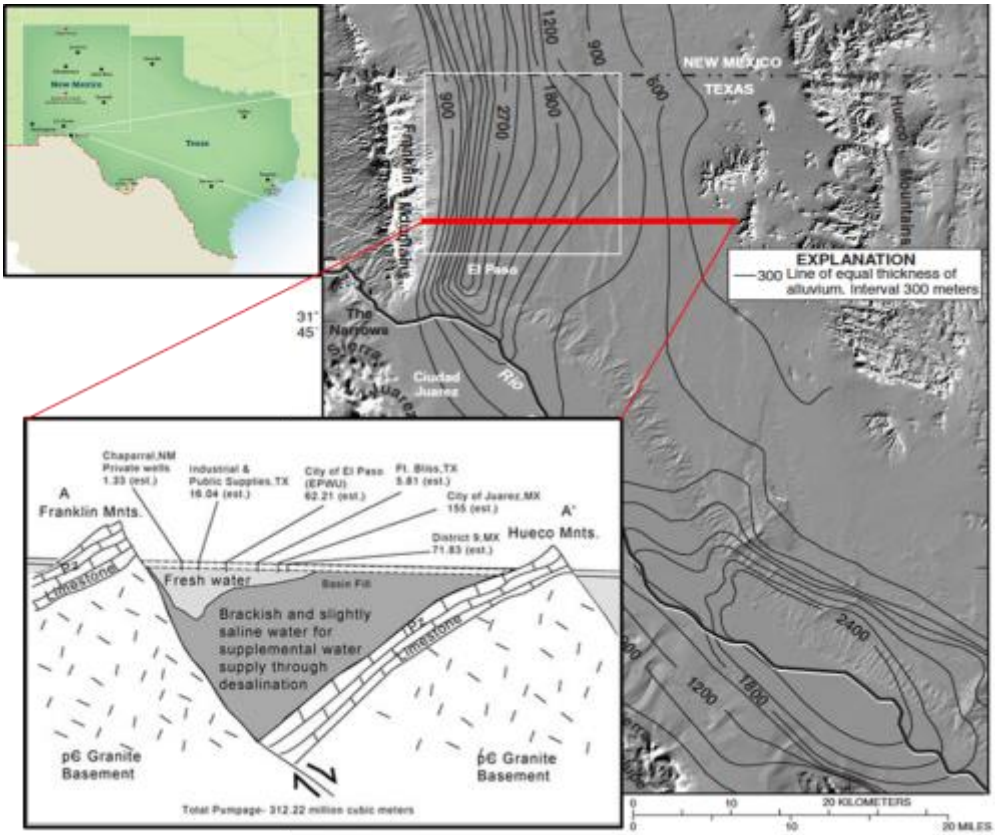

Figure 15: Hueco-Bolson aquifer and HBA study area (modified from Heywood and Yager, 2003 and Sheng, 2005)

Contours shown in the plan view are sediment fill depth in meters.

These weathered materials form several laterally continuous horizons of sand and gravel or silt and clay, both frequently containing smaller, less continuous interbedded layers of the other type. The formation of layered sediments is the result of alluvial fan deposition from the Franklin Mountains and deposition from the ancestral Rio Grande River, which flowed east of the Franklin Mountains. Deposition of thinner discontinuous horizons formed from fluvial processes, including silts and clays in the playa lakes that still occasionally form on the basin floor (Buszka et al., 1994).

More detailed description of the facies forming the HBA in the study area is provided by Heywood and Yager (2003) and Sheng and Dever (2005), who describe the aquifer as formed

from four hydrogeological facies based on depositional environment: fluvial, alluvial fan, lacustrine-playa, and alluvial.

- The fluvial facies formed when the ancestral Rio Grande meandered along the east side of the Franklin Mountains. During this time a thick sequence of fluvial sediments consisting of fine- to coarse-grained channel sand was deposited. Silt and clay overbank deposits also formed during this time when the river periodically flooded its banks. On average, low permeability deposits account for 1/3 of the fluvial facies with high permeability sand comprising the remaining 2/3. This facies is Tertiary to Quaternary in age.
- Alluvial fan deposits formed by weathering of the surrounding Organ, Franklin and Sierra Juarez mountains. Deposition of this facies interfingers with the fluvial facies and formed contemporaneously with them.
- A thick clay and silt deposit is found below the fluvial and alluvial facies, interpreted to be a mid-Cenozoic age lake or similar low-energy environment, classified as lacustrine-playa facies. Smaller and less continuous layers of silts and clays have been deposited as playa lakes
- Recent alluvial sediments were deposited south of the study area beginning 0.67 m.y. ago when the Rio Grande River changed course to flow west of the Franklin Mountains.

Lithology at the recharge location reflects this complex layering (Fig. 16). Borehole logging in the study area uncovered 54 distinct layers from surface to a depth of 129.5m BGL (AWWA, 2003). Layers ranged from highly permeable gravels and sands to low permeability clays and caliche. Hydraulic conductivity values for these layers determined at an comparable site 5 miles

away range from $2.3*10^{-2}$ cm/sec (0.023 cm/sec) for upper sand and gravel layers to $9.5*10^{-10}$ cm/sec (0.00000000095 cm/sec) for a thick clay lens at 79m BGL (Abeyta et al., 1999).

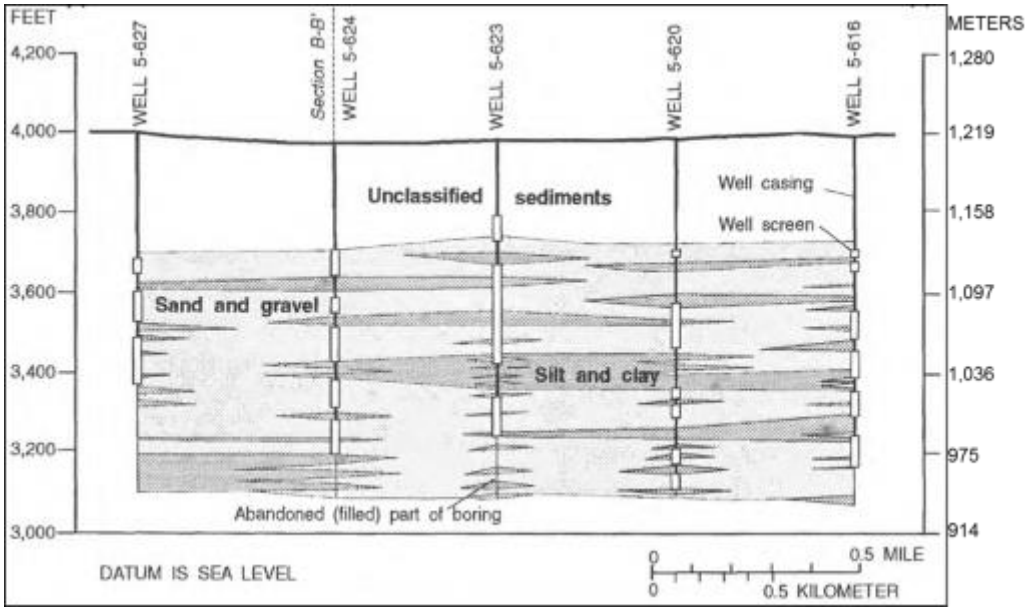

Figure 16: Cross section of interbedded lithology at the HBA study site (Buszka et al, 1994)

3.2.2 Hydrogeological Setting

To understand why the basin holds water, why much of that water is brackish or saline, and why the aquifer is being depleted requires some knowledge of the region's geologic history. The basin and surrounding geologic features are part of the Rio Grande Rift and considered the eastern-most extent of the Basin and Range Province in the USA (National Parks Service, 2017). Similar to other areas in the Basin and Range, the basin and surrounding mountains in the El Paso area formed from uplift and extensional stresses beginning around 35 m.y. ago. Through periodic faulting, some of which continues today, the Franklin (west) and Hueco (east) mountains rose along the sides of the basin, which is filled with alluvium eroded off the uplifted horst blocks (White et al., 1997). This alluvial material is deposited in some places as well sorted sand, silts, or clays, but in many others as much more heterogeneous mixtures of clayey or silty sands (White et al., 1997).

Water sampled from 137-152m BGL (22m below water table) at a well approximately 4 km north of the study area was tested using carbon-14 dating (Anderholm and Heywood, 2003). It returned an apparent age of 14,100 years. Other wells tested a similar distances west and south returned ages between 12,100 and 25,500 years. Local production wells for the City of El Paso's water supply are typically screened deeper than this (Texas Water Development Board, 2017) and so pump even older water! The groundwater withdrawn from these wells originated during the Pleistocene epoch and is not a sustainable resource in the long term.

The low average annual precipitation of 22.1 cm/year (National Weather Service Forecast Office, 2017) in the center of the basin and high evapotranspiration potential of 175.3 cm/year (Texas Water Development Board, 2016) result in minimal precipitation recharge to the aquifer. Precipitation typically arrives with summer monsoon storms that produce localized flash floods but are ineffective at recharging the aquifer (Heywood et al., 2003).

The Rio Grande River flows along the southern border of the HBA. Prior to widespread pumping, which began in early 1900's, the regional groundwater gradient in the HBA trended south and southeast to the river, which was at that time a gaining stream. Pumping in the El Paso area has reversed this gradient and the Rio Grande is now a losing stream (Fig. 17). Due to damming and diversions, it also no longer flows for significant portions of the year (White et al., 1997). On the left of Fig. 17 is groundwater flow direction in 1903 before widespread groundwater development. On the right of Fig. 17 is groundwater flow 99 years later after widespread groundwater extraction (El Paso Water Utility, 2016). The changes in groundwater flow are anthropogenic and unsustainable.

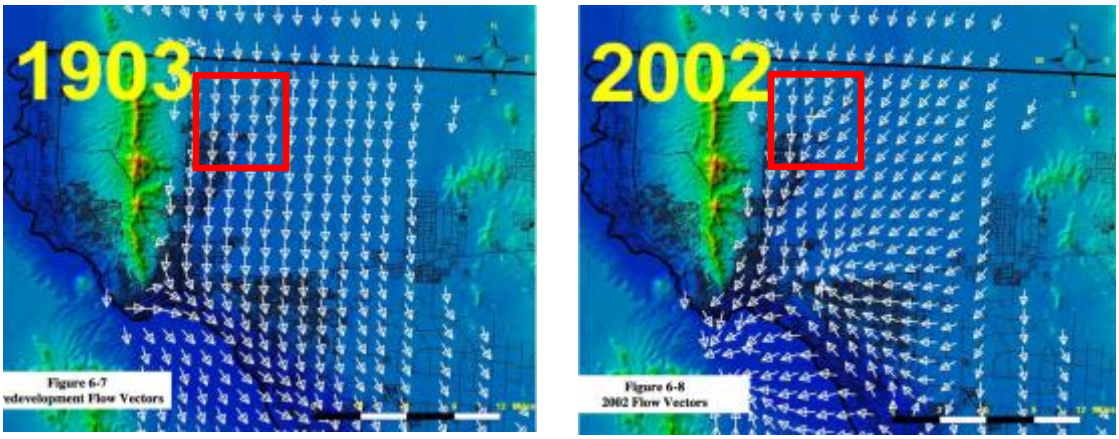

Figure 17: El Paso Water Utility model of flow path changes, 1903 and 2002 (El Paso Water Utility, 2016)

Arrows indicate the direction of groundwater flow. Red box indicates current study area.

Aquifer management is complicated by the transboundary nature of the aquifer as it is shared by the United States and Mexico. The Mexican city of Ciudad Juarez, located just across the border from El Paso, uses groundwater for 100% of its drinking water (Sheng and Devere, 2005). In addition to aquifer level decline and changing flow direction, management is complicated by saline water intrusion that is a consequence of groundwater extraction in the HBA. Although groundwater near the study area has been dated to as young as 12,100 years old, groundwater age increases to 25,500 years towards the center of the basin (Anderholm and Heywood, 2003). This older groundwater has been in contact with soils longer and results in an increase in total dissolved solids (TDS). The advanced age of groundwater in the HBA means that only a thin upper lens of fresh water near mountain front recharge areas is potable without treatment (lower left insert of Fig. 15). The basin fill is mostly saturated, but the majority of the water is brackish or saline, a consequence of the age of the water and chemistry of the basin fill sediments. In the El Paso area, 16.4 million acre-feet (AF) are estimated to have chloride concentrations of less than 500mg/l ("fresh"), whereas 29.1 million AF are above 500mg/l ("brackish" or "saline") (Hutchison, 2004). Just north of the study area in New Mexico,

groundwater tends to have TDS concentrations above 1,000 mg/L. East of the study area groundwater becomes brackish to saline with TDS concentrations of 1,000 to 3,000 mg/L. South of the study area, along the Rio Grande River, groundwater is also slightly saline or brackish, although this is a generalized statement, as individual locations are affected by recharge from the river and pollution from a variety of sources near El Paso and Ciudad Juarez (Sheng and Devere, 2005).

As fresh water is pumped, a cone of depression in the fresh water portion of the aquifer is formed by lowering hydraulic head, and saline water flows both vertically up and horizontally west, reducing the overall water quality by mixing with the fresh water. This pumping-induced gradient reversal has increasingly brought brackish water towards the city, necessitating the construction of the world's largest inland desalinization plant (El Paso Water Utility, 2017; Sheng, 2005). The challenges facing El Paso are both a non-renewable supply of fresh groundwater and the encroachment of brackish water. As the brackish water mixes with the limited volumes of fresh water, more groundwater becomes non potable and the problem expands.

Chapter 4 - Methods

"When the well is dry, we know the worth of water." – Benjamin Franklin

4.1 Vadose Zone Models

4.1.1 Theory of Unsaturated Flow

Flow in saturated porous media can be considered using Darcy's law (Freeze, 1994; others) which is discussed in "Theory of Saturated Flow" section. The governing equation for steady unsaturated flow is a variation on the familiar Darcy's law equation (Hornberger et al., 1998). If increasing depth is in the positive *z* direction:

$$q_z = -K(\theta)(\frac{\delta\psi}{\delta z} + 1)$$

Equation 1: Steady Unsaturated Flow

Where q_z is the specific discharge, $K(\theta)$ is the unsaturated hydraulic conductivity, and ψ is the capillary pressure head. ψ Increases as soil dries and decreases as soil gains water. When plotted on a graph this relationship between the value of ψ and the moisture content of the soil is known as the moisture characteristic curve (Hornberger et al, 1998). Each soil has a different moisture-to-ψ relationship depending on physical properties such as grain size, porosity, and pore shape. A soil's hydraulic conductivity is also influenced by these factors. Specific discharge in the unsaturated zone for any given soil type is a function of moisture content *and* hydraulic conductivity.

Since specific discharge q_z depends on $K(\theta)$ and ψ, Equation 1 can be written as a function of moisture content θ in a form called the *Richard's Equation* (Healy et al, 2012; Hornberger et al, 1998; Botros et al., 2011; others):

$$\frac{\partial \theta}{\partial t} = \frac{\partial}{\partial z}\left[\mathrm{K}(\theta)\left(\frac{\partial \psi}{\partial z} + 1\right)\right] + \frac{\partial}{\partial x}\left[\mathrm{K}(\theta)\left(\frac{\partial \psi}{\partial x}\right)\right]$$

Equation 2: 2D Richard's Equation for Unsaturated Flow

When flow is steady, the derivative of moisture content with respect to time is zero and the specific discharge (q_z) replaces the value of $\frac{\partial \theta}{\partial t}$ causing *Equation 2* to revert back to *Equation 1*.

Equation 2 describes the relationship between θ, ψ, and K (Hornberger et al, 1998). The left-hand side of the equation describes the moisture content (θ). The right side describes the hydraulic conductivity (*K*) in terms of moisture content and describes ψ, the capillary pressure head. Using the Richard's equation, unsaturated zone flow may be summarized by stating that hydraulic conductivity is dependent on degree of saturation and changes in capillary pressure head.

4.1.1.1 Soil-Water Retention Curves

The two most widely used expressions for estimating soil water retention are the Brooks-Corey and van Genuchten functions. The van Genuchten expression was used in this research.

An equation for flow in the unsaturated zone was developed by van Genuchten in 1980 (Van Genuchten, 1980) that relates hydraulic conductivity to saturation for a given soil type, allowing *K* to be determined as moisture content changes. Such conditions apply when artificial recharge occurs through the vadose zone. Van Genuchten's equation takes the following form:

$$\theta = \theta_r + \frac{\theta_s - \theta_r}{[1 + (\alpha|h|^n)]^m}$$

Equation 3: van Genuchten Equation for Describing Relative Moisture Content

Where θ is the moisture content, h is the matric potential, and $\alpha, n,$ and m are empirical parameters derived from the soil moisture curve and therefor unique to a particular soil (Ghanbarian-Alavijeh, et al., 2010). Given a known moisture content θ, the relative hydraulic

conductivity of the partially saturated soil can be found with the equation (Van Genuchten, 1980; Neto, et al, 2011):

$$K_r(\theta) = \theta^{\frac{1}{2}}[1 - \left(1 - \theta^{\frac{1}{m}}\right)^m]^2$$

Equation 4: van Genuchten Equation for Unsaturated Hydraulic Conductivity

$K_r(\theta)$ is the relative hydraulic conductivity of a soil at moisture content (θ). The equation is derived from Mualem's equation for predicting the relative hydraulic conductivity from a soil water retention curve (Leiji et al., 1989; others).

The two vadose zone models used in this thesis (Hydrus 1D and VS2DTI) both calculate the value of θ_r and $K_r(\theta)$ using soil water retention characteristics to determine input values for the van Genuchten equation. Both Hydrus 1D and VS2DTI have a catalog of van Genuchten parameters for various soil types ranging from medium sands to clays based on experimentally determined water retention curves. The values for these catalog soil types are generic and not necessarily indicative of the study area. To create an accurate, site specific model for the SLA study area, values for van Genuchten variables were chosen from publications (Mace et al., 1998; Hess et al, 1992; others). For the HBA model, RETC and published data from USGS report #99-271 (Abeyta and Frenzel, 1999) was used to select van Genuchten values. Some differences were found between published and calculated values; these are available in Appendix F. Catalog values from VS2DTI were used for low permeability layers in the HBA model.

4.1.2 Hydrus 1D

The numerical model Hydrus 1D was first used to simulated vadose zone flow at the HBA site. It was not used in to simulate flow at the SLA site. Hydrus 1D uses the Richard's equation to simulate one-dimensional flow in variably saturated media and allows changes in the media's hydraulic properties with respect to location in the simulation- meaning multiple discrete

layers each of a different soil type may be simulated (Simunek et al., 2009). The objective was to determine if horizontal layers in the HBA were effecting the downward migration of water through the unsaturated zone. Using a matrix of sand, ten discrete horizon were modeled in one dimension to determine which horizons retarded the water flow by preventing the water from moving vertically or slowing the water migration. This was accomplished by placing observation nodes above and below each horizon and recording the time when nodes reflected changes to the soil moisture content.

The initial ten horizons simulated were selected based on data published by the USGS at the Fort Bliss landfill facility (Frenzel and Abeyta, 1999), located in the HBA and expected to have similar lithology to the El Paso recharge site. The report also provided detailed hydraulic parameters for each of the soil layers at the site which were then used in the Hydrus model. The simulation returned a water migration time through the vadose zone of over 668,000 days- almost 1,830 years! The know travel time from the surface to water table at the HBA study site is 28 days (AWWA, 2003)

The very large value given by Hydrus 1D was due to water flow being constrained to the vertical direction and hydraulic conductivity for each layer only reflecting primary porosity. For example, Abeyta and Frenzel published the hydraulic conductivity value for a 2.1m thick clay layer at 20m (65ft) as $7.26*10^{-7}$ m/d (Frenzel and Abeyta, 1999). The value is laboratory-derived and does not consider the possibility of secondary porosity and assumes the entire 2.1m thickness has a uniform hydraulic conductivity. Because Hydrus 1D is a 1D model it has no mechanism for water flow horizontally around low permeability layers. Values used in the ten layer Hydrus model are given in Table 3 and the modeled profile is shown in Fig. 18. These values were selected from USGS Water Resources Investigations Report 97-4036 from among

23 samples tested at a site analogous to the HBA study area (Frenzel and Abeyta, 1999). The samples were tested for porosity, dry bulk density, saturated hydraulic conductivity, and moisture retention percentages at various suction heads to calculate van Genuchten values.

In summary, the value of 1,830 years assumes water must go through each of the discrete lithologic horizons in the unsaturated zone and does not permeate through cracks (secondary porosity) or flow over edges (non-infinite lateral extent).

Table 3: Measured hydraulic parameters in HBA (Abeyta and Frenzel, 1999)

	Profile #	Qr	Qs	Alpha	n	Ks (m/day)	Ks (cm/s)
Sand with pebbles	45	0.039	0.261	0.039	4.923	21.6	0.025
Clayey silty sand	72	0.091	0.466	0.001	1.155	1.382E-06	0.000000002
Silty sand with clay	81	0.057	0.350	0.002	1.127	0.00013824	0.00000016
Sand	93	0.081	0.351	0.015	1.830	0.05616	0.000065
Clay	164	0.061	0.380	0.001	1.236	2.419E-06	0.000000003
Sand	199	0.047	0.345	0.025	1.822	3.8016	0.0044
Silty clay	220	0.101	0.480	0	1.341	4.061E-06	0.000000005
Sand	236	0.050	0.384	0.008	1.356	0.4752	0.00055
Clay	259	0.068	0.380	0.008	1.090	8.21E-07	0.000000001
Sand	289	0.045	0.367	0.020	5.450	1.6416	0.0019

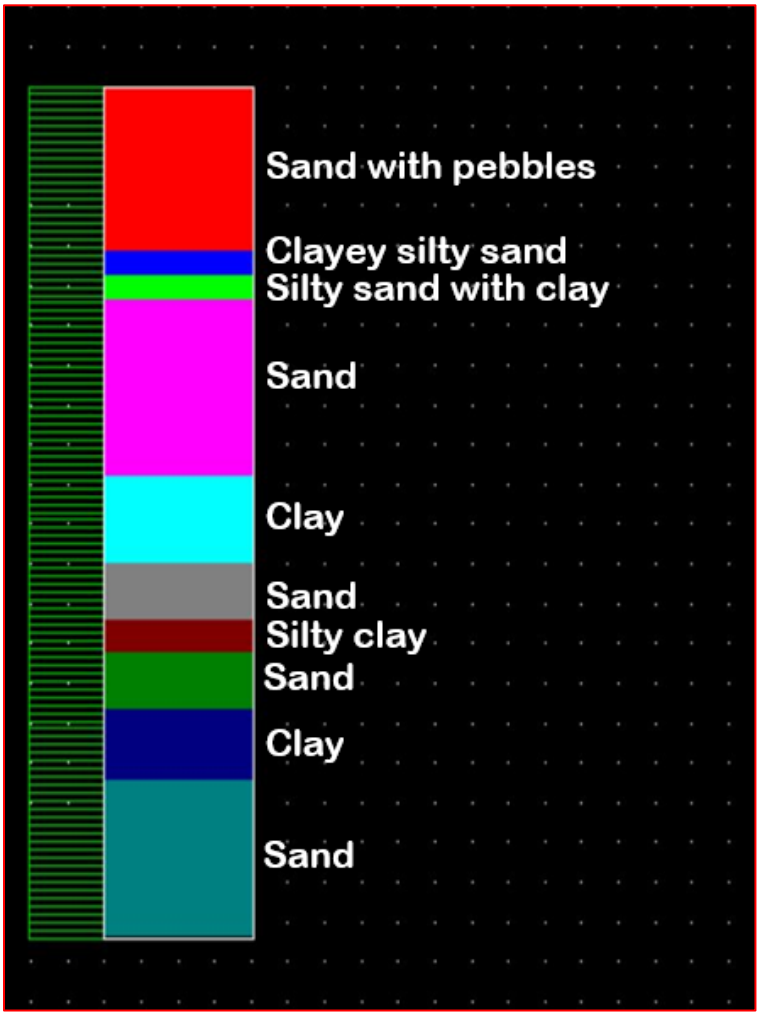

Figure 18: 1D View of soil profile in Hydrus model, HBA.

Initial Hydrus 1D input showing discretization (green lines, left side) and modeled horizons (thick colored blocks).

After simulating the ten most prominent horizons, Hydrus was again run with horizons selected to represent only layers observed to cause perching during the AWWA pilot project. These horizons are visually shown in Fig. 19. Only profiles hypothesized to create perched conditions based on field observations (AWWA 2003) and therefor have a significant influence on water travel time were used. Profile 2 (center) had a travel time of ~50 days, and Profile 3 (right) had a travel time of ~30 days. Under these revised inputs it was possible to get a simulated travel time of approximately 28 days but only by unrealistically manipulating layer thickness and hydraulic

conductivity values beyond what the author considers realistic. Ultimately, the Hydrus 1D program provided a starting point for understanding water behavior in a complex vadose zone consisting of highly permeable aquifer matrix and interbedded low permeability horizons.

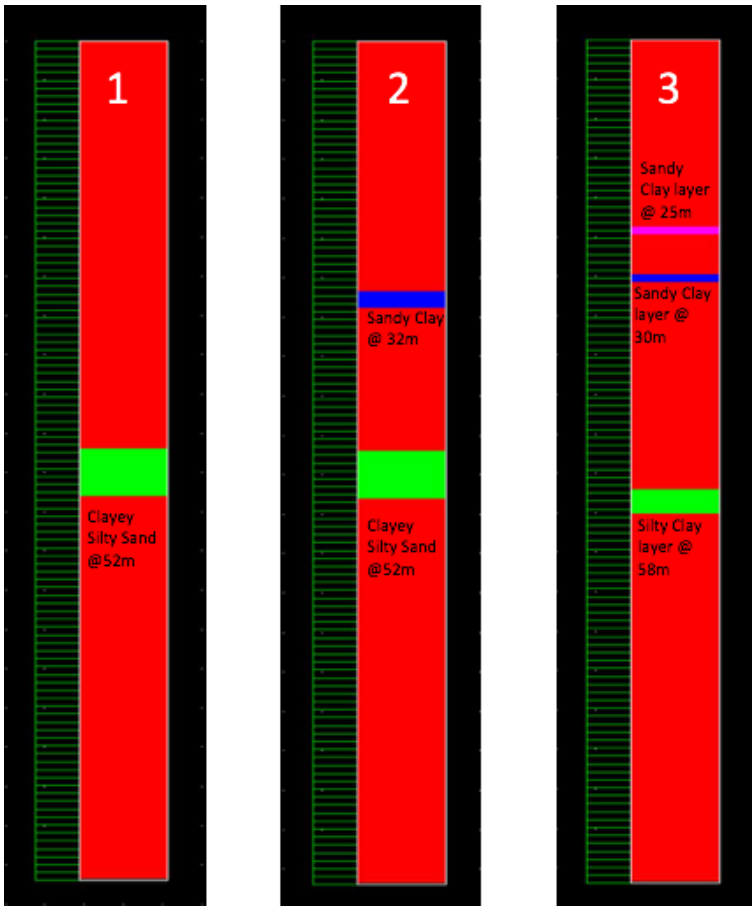

Figure 19: Three Hydrus soil profiles

Refined Hydrus 1D model input showing two soil types (left column, sand in red and single clay layer in green); three soils types (middle column, sand, clay, and sandy clay in blue); and four soil types (right column, with the addition of a purple sandy clay layer).

4.1.3 VS2DTI

This program simulates two-dimensional water flow and solute transport in variably saturated porous media by solving the Richard's equation in a finite-difference model (Hsieh et al., 2000). The same types of values used in the Hydrus 1D program are required as input in VS2DTI along with the addition of Cartesian or radial coordinates for each soil horizon to

creating the second dimension. Outputs can be visualized as two dimensional contours of pressure head, moisture content, degree of saturation, and velocity. Numerical values for the same can also be obtained at any time step desired. For this project the primary outputs considered were values for flux and rate of flux into and out of the model because these correlated to recharge.

Solver parameters used in VS2DTI model are given in Table 4. Since VS2DTI solves partial differential equations (such as the Richard's equation) using an iterative method, these parameters provide guidance to the model on how to decide if a particular iteration has converged on an answer.

Table 4: VS2DTI values chosen for modeling vadose infiltration

Physical Properties

	x-direction (m)	z-direction (m)	Water table Elevation (m BGL)	Length Unit	Time Unit
SLA	600	30	20.7	Meters	Hours
HBA	800	110	107	Meters	Days

Model Solver Properties

	Relaxation Parameter	Minimum Iterations / Time Step	Maximum Iterations / Time Step	Max # of Time Steps	Closure Criterion
SLA	1	3	4000	2.00E+03	0.001
HBA	0.7	1	400	2.00E+05	0.05

Hydrologic characteristics of each modeled horizon are required. VS2DTI allows the user to choose between van Genuchten, Brooks-Corey, Haverkamp, or data points to represent hydraulic characteristics (Hsieh, et al., 2000); van Genuchten's equation was used. Van Genuchten parameters provide a prediction of unsaturated conductivity based on fitted to observed data using the following equation:

$$S_e = \frac{1}{[1 + (\alpha h)^n]^m}$$

Equation 5: van Genucthen Equation for Describing Relative Moisture Content

Where S_e is the effective saturation calculated by $\frac{\theta-\theta_r}{\theta_s-\theta_r}$, θ is the water content, $\theta_r$is the residual water content, θ_s is the saturated water content, *h* is the matric potential in kPa, *m* is given by the equation $m = 1 - \frac{1}{n}$, and α and *n* are empirical parameters dependent on the particular soil (Ghanbarian-Alavijeh, et al, 2010). Note that this equation is mathematically equivalent to *Equation #1*.

4.2 Saturated Zone Models

4.2.1 Theory of Saturated Zone Flow

Saturated flow is described by the Darcy equation, discovered by Henry Darcy in 1856 (Darcy, 1856). Simplified it is:

$$Q = KiA \text{ or } q=Ki$$

Equation 6: Darcy Law Equation

Where *Q* is the volume flow rate, *q* is specific discharge, *A* is the area of the medium (referred to in this research as the "aquifer matrix") normal to the flow direction, *i* is the hydraulic gradient calculated as $\frac{\Delta head}{\Delta distance}$, and *K* is the hydraulic conductivity. Hydraulic conductivity is an intrinsic property of the soil or rock forming the aquifer matrix (Brown, 2002). For this project, *Q* is generally described in terms of m^3/d, *K* in terms of m/d, and *A* in terms of m^2. *q* is also called the Darcy flux and has units of m/d.

To calculate flow velocity it is necessary to relate the Darcy flux to soil porosity to obtain the actual speed at which water flows between soil particles. This is done by dividing *q* by the porosity:

$$v=\frac{q}{n}$$

This step is required because flow only occurs in the void spaces between particles.

By building on Darcy's equation the movement of water in three dimensions can be described by the partial differential equation:

$$\frac{d}{dx}\left(K_{xx}\frac{dh}{dx}\right)+\frac{d}{dy}\left(K_{yy}\frac{dh}{dy}\right)+\frac{d}{dz}\left(K_{zz}\frac{dh}{dz}\right)+W=S_s\frac{dh}{dt}$$

Equation 7: Darcy Law in Three Dimensions as Utilized in MODFLOW 2005

W is the volumetric flux per unit volume; S_s is the specific storage of the aquifer; *h* is the hydraulic head value; and *t* is time (Harbaugh, 2005). This equation generally cannot be solved using analytical solutions and so requires a numerical method to obtain an approximate solution. MODFLOW-2005 does this using the finite-difference method to discretize the volume being studied and applying linear algebraic equations to solve for hydraulic head. These discretized volumes are called cells. Once the area is discretized by applying the finite-difference method, the continuity equation (mass of water into a cell equals mass of water out of a cell plus change in storage) is applied to give the following equation:

$$\sum Q_i = SS\frac{\Delta h}{\Delta t}\Delta V$$

Equation 8: Continuity Equation for Saturated Flow in a Discretized 3D Model

Where Q_i is the flow into a discretized cell; *SS* is the volume of water that can be injected into a cell per change in head (equal to S_s in confined aquifers and S_y in unconfined aquifers), and ΔV is the volume of the discretized cell (Harbaugh, 2005).

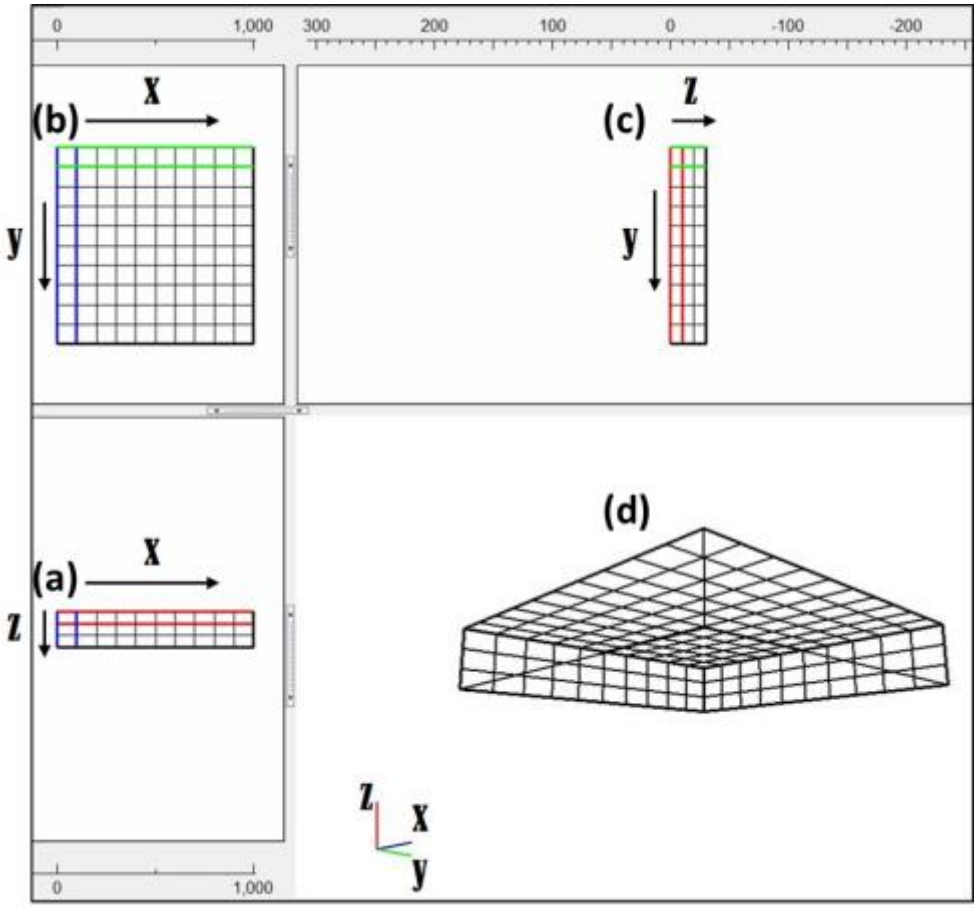

Figure 20: Example of 3D discretization

(a) Side View showing x and z direction; (b) Plan View showing x and y directions; (c) Side View showing y and z directions; (d) 3D view showing discretization into rectangular cells.

For the above equations, water is assumed to be incompressible. Steady state is achieved when flow into all cells equals flow out of all cells with no change in hydraulic head. When hydraulic head is not in equilibrium or when *Q* increases or decreases, flow occurs to establish a new equilibrium in accordance with *equations 7* and *8*.

4.2.2 MODFLOW-2005

The second modeling effort undertaken in this research simulates water movement in the saturated zone. This was accomplished with MODFLOW 2005 (Harbough, 2005). Pre- and Post-processing was done using ModelMuse (Winston, 2009). MODFLOW is the calculation program that solves the equations previously described. ModelMuse is the graphical user

interface (GUI) designed to visualize and create the plain text and binary files used to run MODFLOW. ModelMuse also interprets the plain text and binary file outputs of a MODFLOW simulation, essentially taking the numerical solutions created in MODFLOW and displaying it in a visual manner that can be manipulated and studied.

(The following section draws exclusively and extensively from Harbough, 2005, who published the user and technical manuals for MODFLOW 2005 and many of its packages and programs). MODFLOW discretizes a simulated aquifer into cells by dividing the volume into columns on the *x* axis, rows on the *y* axis, and layers along the *z* axis. The resulting cells can be inactivated to simulate no flow areas such as crystalline bedrock. Time periods are referred to as stress periods, within which variable inputs such as hydraulic head at boundary conditions or recharge fluxes are constant. For example, imagine in a ten day period a well does no pumping for the first three days, pumps for two days, and turns off for another three before finally running again for the last two. Modeling this scenario would require at least four stress periods since there are four periods during which a flux (the pumping) is constant. The first stress period would be three days, the second two days, the third would be three days, and the fourth stress period, two days.

MODFLOW's layer-property flow (LPF) package was chosen to model groundwater flow in saturated conditions. The LPF is one of two packages that MODFLOW uses to simulate internal flow; it was chosen for the ability to simulate an unconfined aquifer and because it is the package with which the author is most familiar. Details on values chosen as model inputs for the LPF package are described in subsequent sections. Head values at each cell are known at the beginning of each stress period, either because they are equal to initial inputs or are outputs from

the previous period. The linear algebraic equation described previously (*equation 7*) is then applied in an iterative manner to solve new head values for each cell.

In order to solve more complex problems, stress packages are used. Mathematically these packages add terms to the previously discussed flow equations. They simulate various types of boundary conditions. In this research only the Well Package (WEL) and the Time-Variant Specified-Head (CHD) packages were used. The well package is used to simulate constant rate addition or extraction of water from the aquifer during a stress period. To simulate an infiltration basin the WEL package was used by creating a two dimensional object placed on the surface of the model (z=0) and spread over a 2,025m^2 area of model ($x=y=45m$). To simulate a vadose zone well a three dimensional point object was placed in a single cell with z direction depth of 0 to -33m in the HBA model and 0 to -10m in the SLA model.

The Time-Variant Specified-Head package (CHD) was used to simulate the natural water table gradient in the study areas. This package allows the user to define the beginning and ending head values for each stress period for any selected cells in a model. Head values may rise or fall over a stress period using this package if instructed to do so but otherwise are not influenced by anything in the model. For example, suppose a head of "10" was chosen for the start of a stress period on day one and a head of "1" was chosen for the end of that period on day one hundred. On day fifty the head value for the object would be "5". For this thesis the CHD package was used a slightly different way. At the up gradient and down gradient limits of the study area the water table height was determined using historical monitoring well records. These heights were converted from their given values (generally "feet above sea level") to an appropriate head value for the model (generally "meters below datum", with datum being ground surface=0). This value was then assigned as the fixed value for head at the model's boundary

conditions and did not change across any stress periods. Since the up gradient values were slightly higher than the down gradient values, a simulated flow from the higher head boundary to the lower head boundary formed in the model.

4.3 Cape Cod, MA Modeling Considerations

The aquifer matrix of the Sagamore Lens Aquifer (SLA) is composed of a homogenous glaciofluvial sediment consisting of sands and gravels.

Table 5: References chosen to obtain hydraulic parameters, SLA

Author and Report	Aquifer Property Described
Hess et al., *Large Scale Natural Gradient Tracer Test in Sand and Gravel, Cape Cod, MA*	Measurements of hydraulic conductivity using flowmeters and permeameters. Includes longitudinal dispersivity analysis.
Masterson and Walter, *USGS Circular 1388*	Discussion of hydrogeology and groundwater resources of the area including information on soil deposition.
Moench et al., *Importance of the Vadose Zone in Analysis of Unconfined Aquifer Tests*	Values for specific storage, specific yield, hydraulic conductivity and aquifer thickness.
Mace et al, *Suitability of Parametric Models to Describe the Hydraulic Properties of an Unsaturated Coarse Sand and Gravel*	Van Genuchten parameters for modeling vadose zone flows.
Grimestad, *A Reassessment of Ground Water Flow Conditions and Specific Yield at Borden and Cape Cod*	Values of specific yield and hydraulic conductivity.
El-Kadi, *Validity of the Generalized Richards Equation for the Analysis of Pumping Test Data for a Coarse-Material Aquifer*	Reinterpreted van Genuchten parameters including a summary of Moench, Mace, and Hess's interpretations.

4.3.1 Values Required for Saturated Flow Modeling

Physical characteristics of the aquifer matrix were described or inferred from Moench (Moench et al., 2004) and Mace (Mace et al., 1998) (Table 5). Coarse materials, such as the aquifer matrix of the SLA, can pose challenges to equations derived from soil water retention

models such as the van Genuchten equation used in this research. Mace describes measuring the relationship between degree of saturation and hydraulic conductivity using laboratory analysis of SLA soil samples and comparing the findings to results from four soil-water retention curve models, including the van Genuchten model. Values published by Mace and used in simulating the SLA during this research were the van Genuchten parameter α=0.242, porosity n=0.298, and residual moisture content θ_r=0.034. Specific storage was set at $4.28*10^{-5}$ based on aquifer tests done by Moench. Moench also estimated the value of saturated hydraulic conductivity in the SLA area as ~0.118 cm/s (101.9 m/d).

The most comprehensive testing of hydraulic conductivity in the SLA was done by Hess (Hess et al., 1992). Hess and colleagues tested 16 wells and cores from the SLA area for information on hydraulic conductivity using several methods. Their most accurate method was determined to be flowmeter testing resulting in a mean *Kx* measurement of 0.11 cm/s (95.04 m/d). Grimestad reevaluated previously published pumping data from the SLA to evaluate errors in the data cause by inflows from sources other than aquifer storage. His work evaluated the average *Kx* value of the SLA to be 102.2 m/d and the specific yield of the aquifer to be 0.19-0.20 (Grimestad, 2002).

Saturated hydraulic conductivity used in this research was chosen as 95.04 m/d (0.12 cm/s), the value determined by Hess (Hess et al., 1992). This value was checked against a wide range of other published values for the hydraulic conductivity of SLA glacial outwash sediments and found to be in good agreement with USGS published values which ranged from 60.96 m^3/d to 106.68 m^3/d (Walter and Whealan, 2005, and Masterson and Walter, 2009). It was also similar to the 97.42 m/d average of *Kx* values published by El-Kadi (El-Kadi, 2005).

The ratio of vertical to horizontal conductivity for this aquifer as reported by Hess is between 1:2 and 1:5 (Hess, 1992). Hydrogeologists working in the study area on Joint Base Cape Cod reported a value of 1:5 used in their modeling (USACE New England District, personal communications, 2016). However the value of 1:5 (vertical:horizontal) was used for saturated zone flow models. The values of *Kv* and *Kx* provided in El-Kadi, 2005, result in a ratio of .676:1. In view of the wide ranging values published for *Kv* to *Kx* ratio, 1:1.48 (0.676) was chosen since this value is from the most recent work published.

Due to the relatively rapid movement of water through the unsaturated zone, early simulations using *days* as the time unit showed water movement occurring too quickly for accurate interpretation. The models time units were switched to *hours*, although for consistency this thesis continues to provide most information in terms of *days*.

4.3.1.1 Boundary Conditions, Grid Discretization, and Recharge

Two versions of the saturated zone model were constructed, one simulating an infiltration basin and the second simulating a 10m deep vadose zone well. Aquifer hydrogeological values such as specific yield and hydraulic conductivity were kept the same those used in the unsaturated model and can be found in Table 6:

Table 6: Saturated zone model inputs, SLA

SLA Setup: Datum = Ground level = 0					
# Columns	200	Column Thickness(m)	5	X-Direction Total Length (m)	1000
# Rows	200	Row Thickness (m)	5	Y-Directions Total Length (m)	1000
# Layers	1	Layer Thickness (m)	61	Plan View Area (km)	1
SLA Hydrogeological Setup					
East CHD Boundary (m)	-17.53	Kx (m/h)	3.96	Initial Water table @ Recharge Location (m)	20.7

West CHD Boundary (m)	-19.21	Kz (m/h)	2.68		
Specific Storage	0.0000428	Specific Yield	0.264		

Boundary conditions were set to simulate the natural groundwater gradient in the study area. Groundwater flow is from east to west. The base of the aquifer was used as the datum, so model surface elevation is -61m. The eastern boundary of the model was created using the time-variant specified head (CHD) package as -17.53 which was held constant during all times steps in the model. -17.53 simulated a water table of 19.21m below the surface of the model along the eastern boundary. The west boundary was set using a CHD value of -19.21. This created an east-west hydraulic gradient of 0.168% ([19.21m-17.53m] / 1000m x 100 = 0.168). The bottom of the model was set as a no-flow boundary *z* direction to simulate bedrock. The north and south boundary conditions were also no-flow.

In the center of the model the grid was refined so each column and row was no more than 2.5m wide. Recharge structures were simulated in the exact center of the model. This allowed the infiltration basin to be modeled as an object with a width and length of 45m each, or 1/2 acre of surface area. The infiltration basin was created as a two dimensional object on the surface of the model and having no depth in the *z* direction. The vadose zone well was created as a three dimensional point object with a depth of -10m BGL in the *z* direction. Point objects have no provided *x* or *y* lengths but appear as determined by grid discretization. Model area excluding the central refined grid area was a square with sides of 1,000m created by using 200 columns and 200 rows each 5m wide.

Three stress periods were used to study saturated flow. The first stress period received no recharge in either infiltration basin or vadose well model. It was run from hours -1 to day 0 as

"steady state" and was used to set the pre-recharge groundwater flow by calculating the head values in every cell using only the boundary conditions defined at the west and east edges of the model. Effectively this created a water table with a drop of 1.67m over a lateral distance of 1,000m. Values chosen to create this aquifer gradient were taken from the Corps of Engineer's Impact Area Groundwater Study Program (USACE NAE, 2013). The second stress period was run from hours 0 to 240 with a step length of 60 in order to model recharge over ten days with outputs every 2.5 days. Infiltration into the basin and vadose zone well were constant for this period. The third stress period maintained the constant infiltration rate but started on hour 240 and ended on hour 720 using a step length of 120. This allowed a full month to be simulated with outputs on day 15, 20, 25, and 30 (Table 7).

Table 7: Saturated model time discretization, SLA

Stress Period	Starting Time	Ending Time	Length (hours)	Max First Time Step Length	Multiplier	Steady State or Transient	Number of Steps
1	-1	0	1	1	1	Steady State	1
2	0	240	240	60	1	Transient	4
3	240	720	480	120	1	Transient	4

4.3.2 Values Required for Unsaturated Flow Modeling

Relatively little work has been done on applying the van Genuchten equation to describe water movement for coarse-grained, highly permeable aquifer matrix. A consequence of this lack of study is the absence of a default coarse sand or sandy gravel soil type in either the VS2DTI or RETC programs. Literature review turned up only a handful of publications applying the van Genuchten equation in gravel aquifers. Fortunately, of the few such studies available, Mace and El-Kadi both used the SLA area (Mace et al, 1998 and El-Kadi, 2005). Van Genuchten values used for the SLA area are taken from their work.

Mace obtained the empirical values needed to solve soil water retention properties for the coarse sand and gravel outwash in the SLA area by laboratory analysis on six cores, ultimately

obtaining forty two measured values for the relationship between $K_r(\theta)$ and $\theta(h)$ (Mace et al., 1998). His van Genuchten variables were determined during a study of parametric model performance and are used in this researches' SLA model. Physical properties such as porosity and specific storage are shown in Fig. 23 and Table 7.

Model	#Data Sets Converged	Mean SSQ ($\times 10^5$)	Mean r^2	Mean α	Mean n
VG, MU	42	25.0	0.993	0.242	2.758
VG, BU	42	27.6	0.992	0.296	3.378

Figure 21: Published van Genuchten values, SLA (Mace et al, 1998)

Table 8: van Genuchten values used in VS2DTI model, SLA

	Vertical to Horizontal *K* Ratio	Saturated Conductivity *K*	Specific Storage	Porosity	Residual Moisture Content	Alpha	Beta
JBCC Matrix	0.2	3.96 m/h	4.28E-05	0.298	0.034	0.242	2.758

4.3.2.1 Boundary Conditions, Grid Discretization, and Recharge

Six model variations of the SLA area were run with VS2DTI using the hydrogeological parameter described in *Methods* and either an infiltration basin or vadose zone well providing recharge. The infiltration basin was chosen first.

There are two possible methods to simulate basin inflow. One method is to use injection values from the Demo Area 1 Monitoring Report (USACE NAE, 2013). These values come from two saturated zone wells in the vicinity of the study area each capable of injecting 250 GPM of treated water directly into the aquifer. These injection wells are currently in use as part of the areas ongoing groundwater cleanup efforts. Using this value of 56.78 m^3/h (250 GPM) was the first option tested. The advantage of using this value is that it represents an influx of water known to be accepted by the aquifer, whereas a higher value may work well in a model but exceed the actual acceptance capacity of the aquifer. Using this value in a 0.5 acre basin (45m x

45m) translates to a flow value of 0.028 m/h in a two-dimensional model with a length of 45m (units of L/T are often used for measuring precipitation, and is used here in the same way). This can easily be simulated as infiltration basin recharge by applying the value to the model surface using a flux boundary condition, similar to how precipitation is simulated.

A problem with using this value arises because VS2DTI cannot simulate a known quantity of well recharge. That means this value of inflow is not easily simulated using a vadose well and so makes comparison between infiltration basin and vadose well impossible. To understand why, consider the example of a 10m deep dry well. A given volumetric rate can be modeled against a vertical boundary created by the well screen but the program considers the influx rate to be equal in magnitude at all points along that vertical boundary. In the case of our 10m deep dry well the volume of water simulated to flow across the well screen in the upper 1m of the well would be the same as the volume simulated to flow across the well screen in the bottom 1m. This is not realistic- the weight of the water column (the pressure head) increases flow at the bottom of the well where pressures are greatest (Fig. 5).

An additional problem prevents modeling a constant influx rate for vadose wells using VS2DTI. For relatively small rates of influx into highly permeable soils (such as 56 m^3/h into the SLA matrix) the water column would not extend the entire depth of the well- the water would flow out of the well too quickly to form a tall water column. Simulating a known influx rate through a vertical well screen is not practical using VS2DTI.

Instead of using a known influx rate, a known total head can used by assuming that sufficient water is available to create ponded conditions in the infiltration basin or a steady-state water column height in the wells. This assumption allows the use of VS2DTI's total head boundary conditions instead of the flux boundary conditions. To understand the total head

boundary condition again consider the example of a 10m deep dry well. To simulate a water column of 9m in the well, the boundary condition in VS2DTI would be set to "Total Head -1". This means there is a total head at any point along the boundary condition equals the depth (+*z* direction) of that point minus 1m. At the bottom of our 10m dry well, this would be simulated as a total head of 10m – 1m = 9m. This is correct because we are simulating a 9m tall water column. At a point on the boundary condition 1m below the surface the total head would be 1m – 1m = 0m, or the top of the water column in the well with no pressure head exerted across the boundary. This is correct again because a 9m water column would have a surface elevation of 1m BGS in a 10m deep well. By recalling that the boundary condition is used to simulate the well screen it is possible to understand how this boundary condition was used to simulate water column.

Fig. 22 visually demonstrates how the "total head" boundary condition was used in the project. The figure shows a 10m deep vadose zone well in the SLA study area with color contours of pressure head and black lines of flow velocity. Note that the colors do NOT represent water content or saturation, which is related to pressure head but not shown in Fig. 22. The boundary conditions- the left and right sides of the well- were set as "Total Head -1" to simulate a 9m water column in the 10m deep well. The image on the left is the well condition ~1 minute after recharge began while the right shows the same well after 5 hours. The higher pressures created at the bottom of the well from a standing water column result in greater pressure head and subsequently faster water flow.

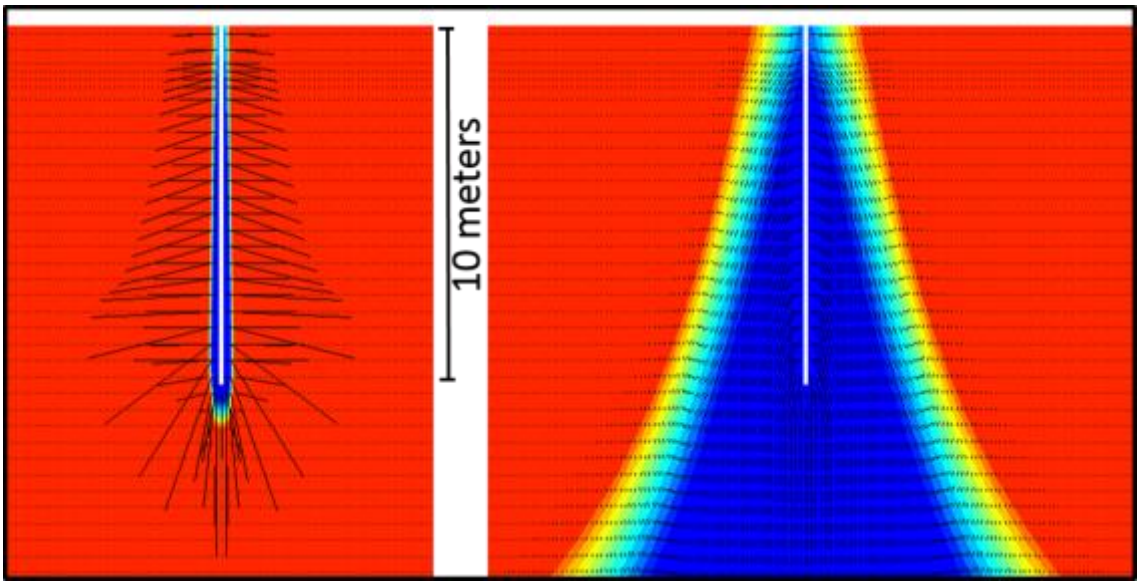

Figure 22: Pressure head (colors) and Flow velocity (lines) in 10m deep well, SLA.

Red areas are low pressure head. Dark blue areas are high pressure head. The length of the black lines indicates the magnitude of flow.

Model boundary conditions must also be defined for the top, sides, and bottom of the model. The top and bottom were both set as "no-flow" boundaries, the top because it simulated ground level and the bottom because it simulated bedrock. The side boundary conditions were set as no flow below 20.7m in the *z* direction and "possible seepage face" above 20.7m BGL to allow water flow out of the model. This maintained the water table at the desired height.

Vertical grid discretization was finer at the bottom of the basin and constant below 1.5m. Grid discretization was constant in the *x* direction with each column width set to 1 meter. In the vadose well model this created a simulated well of 1m diameter with a left side at x=299m and a right side at x=300m.

4.3.2.2 Additional SLA Modeling Considerations

The highly permeable aquifer matrix combined with the relatively small distance from land surface to water table is expected to create model boundary condition challenges. Specifically, the left and right model boundary conditions which are set as "possible seepage

face" may influence the resulting shape of the water mound. This boundary condition effectively holds the water table at a given elevation along the left and right limits of the model. If these boundary conditions do influence the shape of water mounding at the water table, infiltration rates could be expected to be influenced also because (Bouwer 2002, 2008).

To determine what, if any, effect the unsaturated zone model discretization has on infiltration rates, SLA models were also run using the same parameters described above but with a horizontal distance varying between 600 and 2,500m. Using the 2,000m long model boundaries, the depth to water was tested at 20.7m (observed conditions at the site, and the condition considered for the previously described model) and at depths of 40, 60, 80, 100, and 120m for the infiltration basin model.

4.4 El Paso, TX Modeling Considerations

4.4.1 Values Required for Saturated Flow Modeling

The model was constructed by creating a homogenous, anisotropic aquifer matrix of fine sand and then adding discrete lithologic horizons between 20-45m and 50-70m. The decision to use a homogenous fine sand as the aquifer matrix was based on these publications (Table 9):

Table 9: References chosen to obtain hydraulic parameters, HBA

Report Name	Description of Materials
AWWA-RF, 2003	Primarily fine sand based on laboratory test results from samples taken at the recharge pilot project (page 62)
USGS Water Resources Investigation Report 97-4036	The aquifer was determined to consist of 86% sand horizons (page 10)
USGS Water Resources Investigation Report 02-4108	The aquifer was determined to consist of four hydrogeological facies, with three (Fluvial, alluvial fan, and recent alluvial fan) consisting primarily of sand and gravel, accounting for ~67% of the fill (page 5)

Well logs confirm the dominance of sand horizons compared to low permeability silts and clays. Appendix A.5.1 shows lithology of six wells along a 800-meter transect that were used to construct the VS2DTI model as well as the lithology recorded during drilling the AWWA test well.

Anisotropy was simulated in the aquifer matrix using a K*z*/K*x* value of 0.1 to create a 1:10 vertical to horizontal hydraulic conductivity. A 1:10 ratio was chosen because it was the smallest K*x* to K*z* difference used in the USGS Report 2004-5197 (Huff, 2005). Huff eventually reached a calibrated ratio of 1:10,000 to 1:100,000, however, this ratio is a average of the effects of all layers in the saturated and unsaturated zones including low permeability silts and clays that strongly limit the downward movement of water. The HBA model created for this research consider low permeability layers as separate from the aquifer matrix and their effect on the anisotropic ration is not part of the fine sand matrix. The maximum observed ratio of vertial to horizontal flow in HBA models was 56m vertical to 285m horizontal, or approximately 1:5 horizontal to vertical. This occurred just before day 17 of the infiltration basin models. Larger ratios occurred during the first several days of model run time before the wetting front encountered low permeability layers, and much smaller ratios occurred while the wetting front moved along the surface of the low permeability layers. This leads to the conclusion that the controlling factor for horizontal to vertical permeability in the vadose zone is the extent of the low-*K* layers, not the horizontal to vertical ratio for the aquifer matrix. With this in mind, the thin low-*K* layers were all modeled using 1:1 vertical to horizontal hydraulic conductivity.

After creating the aquifer matrix as a homogenous, anisotropic fine sand, low permeability (low-*K*) layers that create the heterogenaity within the aquifer had to be included. There are 54 discrete layers listed in the AWWA report (Appendix S) but not all of these layers

influenced the downward migration of the recharge wetting front. Furthermore modeling each individual layer as displayed in the AWWA well log would have resulted in a complex and inaccurate model. The complexity arises from including layers represented in the well log that do not actually retard downward movement of water. It's important to remember a well log represents a 1-dimentional view of subsurface lithology. A layer on the well log, such as "Clay, red-brown, stiff, damp" at 77.6m BGL on the AWWA log, might represent a layer of clay with very limited lateral extent. Water would hardly perch above this layer before spilling off the sides and the effect on slowing the overall wetting front velocity would be negligable. A 2-dimensional model was required to consider how lateral extent of low-*K* layers influence the movement of water in the subsurface. Additionally, secondary porosity can greatly increase the hydraulic conductivity of layers such as the clay at 66.7m which was noted to possibly contain paleoroots (AWWA, 2003). This secondary porosity would allow water to travel through cracks in the soil much more quickly than if the water was limited to traveling through the effective porosity of the soil itself.

The AWWA report contained information regarding which layers influence downward migration of water (AWWA, 2003). During years 2001-2002, El Paso Water Utility infiltrated water through a 1/2 acre basin and monitored the subsequent groundwater movement through two monitoring wells adjacent to the basin. Data showed two significant perched layers formed at 31.7m and 51.8m BGL (AWWA, 2003). The report's well log clearly shows the positive neutron log deflection associated with the buildup of a saturated horizon formed by perched layers (Appendix D).

This high quality data shows the horizons that influence downward migration of water at the El Paso study location. Equally pertinent to this research, it also shows which layers do not

influence the downward migration of water. Between 32m and 52m are two clays horizons and one silt horizon that resulted in no perched water. Between 58m and the water table there are an additional four clay horizons that also did not create perched conditions. These horizons must have been limited in lateral extent or had significant secondary porosity not reflected in well logging, although which is the correct case is impossible to tell without additional boreholes.

4.4.1.1 Saturated Model Boundary Conditions, Discretization, and Recharge

Outputs from VS2DTI, especially infiltration rate, were used as inputs to the saturated zone beneath the recharge area. These model inputs are given in Table 10:

Table 10: Saturated model inputs, HBA

HBA Area Setup: Datum = Ground Surface = 0					
# Columns	200	Column Thickness	10	X-Direction Total Length	2000
# Rows	200	Row Thickness (m)	10	Y-Direction Total Length	2000
#Layers	1	Layer Thickness (m)	-400	Plan View Area (km)	4
HBA Hydrogeologic Setup					
East CHD Boundary (m)	-104	Kxx (m/d)	21	Initial Water Table at Recharge Location (m)	-107
West CHD Boundary (m)	-110	Kzz (m/d)	2.1		
Specific Storage	0.0001	Specific Yield	0.305		

In the center of the model where the recharge structures were simulated the grid was refined so each column and row was 5m thick. This allowed the infiltration basin to be modeled as an object with a width and length of 45m each, or 1/2 acre of surface area. The infiltration basin was created as a two dimensional object on the surface of the model with no depth in the *z* direction. The vadose zone well was created as a three dimensional point object with a depth of -33m BGL in the *z* direction. Point objects have no provided *x* or *y* lengths but appear as determined by grid discretization.

Three stress periods were used to study saturated flow (Table 11). The first stress period received no recharge in either model. It was run from day -1 to day 0 as “steady state” and was used to simulate the pre-recharge groundwater flow by calculating head values in every cell

using only the boundary conditions defined at the west and east edges of the model. Effectively this created a water table with an elevation drop of 8m over a distance of 2,000m which is a good approximation of the local water gradient based on 2014 well data (TWDB, 2017). The second stress period was from day 0 to day 30 with a step length of three and a constant recharge. This effectively allowed the first month of recharge values to be output every three days. The third stress period did not include changes to recharge rates- they stayed constant- but started on day 30 and ended on day 90 with a step length of ten. This allowed the second and third month's recharge to be calculated every ten days.

Table 11: Saturated model time discretization, HBA

Stress Period	Starting Time	Ending Time	Length (hours)	Max First Time Step Length	Multiplier	Steady State or Transient	Number of Steps
1	-1	0	1	1	1	Steady State	1
2	0	30	30	3	1	Transient	10
3	30	90	60	10	1	Transient	6

The model was run in two iterations. The first iteration (a) used the same recharge rate for both the infiltration basin and the recharge well in order to determine if the geometry and depth of the recharge structure influence water mounding or movement. The second iteration (b) used the recharge values calculated from VS2DTI as the rate of recharge for the recharge structure. The first iteration was useful for comparing the two structure's effect on water mounding shape while the second iteration was intended to answer the second part of the thesis questions.

4.4.2 Values Required for Unsaturated Flow Modeling

To satisfy the van Genuchten equation and input all required parameters into VS2DTI, references from USGS Report 99-271 were used (Abeyta, et al. 1999). This report contained van Genuchten values experimentally derived from cores taken from a landfill location 7.5km away from the study area (Appendix E). Given the limited lateral extent of the many low-*K* layers in

the study area, these van Genuchten values were only used to provide reference. The lithologic horizons they represent may not be continuous between the two sites. The author independently determined van Genuchten values through curve fitting using pressure head and moisture content values from the report and running these values through the RETC program. The RETC output was compared to the published values. While not mentioned again in this thesis, a summary of these findings appears in Appendix F.

Final van Genuchten values for layers in the model were chosen as (Table 12):

Table 12: van Genuchten parameters, HBA

	Color	$\frac{K_z}{K_h}$	K_h	Ss	Porosity	Residual Moisture Content	α	β
HBA Matrix	Yellow	0.1	21 m/d	1.00E-04	0.377	0.072	1.04	6.9
Clay	Black	1	0.048 m/d	1.00E-04	0.38	0.068	0.8	1.09
Silty Clay	Grey	1	0.005 m/d	1.00E-04	0.36	0.07	0.5	1.09
Sandy Clay	Turquoise	1	0.029 m/d	1.00E-04	0.38	0.1	2.7	1.23
Loamy Sand	Green	1	3.5 m/d	1.00E-04	0.41	0.057	12..4	2.28

Values used to create horizons in the HBA unsaturated zone model.

Four of these parameters (clay, silty clay, sandy clay, and loamy sand) are generic values taken from the VS2DTI catalog. Values for the fine sand matrix were modified from VS2DTI generic values to better fit site-specific conditions. A comparison between the values used and values determined in USGS report 99-271 and RETC program shows these differences (Table 13):

Table 13: van Genuchten value comparison, HBA

	Porosity	Theta R	Alpha	beta	% difference (Porosity)
Clay (value used)	0.380	0.068	0.800	0	22.50
USGS value (220ft profile)	0.506	0.121	0.006		
RETC Calculated	0.480	0.101	0.006	1.341	

Silty Clay (used)	0.360	0.070	0.500	1.090	15.090
USGS value (147ft profile)	0.424	0.098	0.009		
RETC Calculated	0.391	0.071	0.012	1.297	
Sandy Clay (used)	0.380	0.100	2.700	1.090	-7.650
USGS value (81ft profile)	0.353	0.070	0.760		
RETC Calculated	0.349	0.057	0.207	1.127	
Loamy Sand* (used)	0.410	0.057	12.400	2.280	-4.060
USGS value (92ft profile)	0.394	0.032	0.014		
RETC Calculated	0.395	0.150	0.009	1.785	
Fine Sand** (value used)	0.377	0.072	1.040	6.900	3.220
USGS value (318ft profile)	0.389	0.073	1.727	6.092	
RETC Calculated	0.397	0.013	1.638		

*Loamy Sand chosen as the closest approximation of Sandy Silt available in VS2DTI
**Fine Sand values based on data interpretation, not VS2DTI default values

Within the timeframes used in this research the fine sand matrix has the greatest impact on vertical wetting front travel because significant quantities of water don't pass vertically through any other layer. This implies that accurately representing the first four soil types is less critical than getting values used for the fine sand matrix as calibrated as possible. The hydrologic parameter values for the fine sand matrix were adjusted during calibration of the model to ensure the wetting front reached the water table in the expected amount of time (subsequently described in "validation of model").

4.4.2.1 Vadose Model Boundary Conditions, Grid Discretization, and Recharge

Like the SLA model, boundary conditions in the HBA model along the bottom of a one meter deep infiltration basin were set as a known total head. Three values were used: (a) 0

representing a full basin with 1m of ponded water, (b) -0.5 to simulate a half-full basin with 0.5m of ponded water, and (c) -0.787 to simulate a basin with 0.213m (8 inches) of ponded water. Side and bottom boundary conditions were set as possible seepage faces. For the vadose well model the left and right sides of the well was set as total head boundary conditions with values adjusted to simulate changes in water level. For example, when the boundary conditions were set as "-23" they simulated a water column at 23m BGL. The actual height of this water column for boundary condition "-23" varied according to the bottom depth of the well. For example, in a well with bottom depth of 33m the water column in the well is simulated to be 10m high. If the same well had a boundary condition "-10" then the water column would be simulated as 23m high.

The HBA study area is a heterogeneous mix of multiple horizontal soil layers. After resolving which layers control water migration rates (see "methods"), setting those layer's lateral extent was required to create a model of the unsaturated zone. Multiple closely spaced well logs along a single transect were required in close proximity to the study area. Six monitoring wells on an 800m long east-west transect were chosen from a location 4.5km from the infiltration basins.

Grid discretization represents a balance between precision and computational time. Finer spaced discretization provides more precise results but takes much more computational effort while more widely spaced discretization has the opposite effect. Columns in the *x* direction were designed to become more refined towards the center of the model. These columns started with a width of 3.62m at the left edge and gradually reduced to 1.64m spacing in the center of the model before increasing again to 3.62m on the right edge. The effect created a pattern of columns widening from the model's *x*-axis center. Because perching layers are hypothesized to

occur in the upper 78m of the vadose zone, row width in the *z* direction was held constant at 1m from model surface to 78m BGL, then increased to 2m width. Appendix G provides a visual example sketch of the grid discretization. Data provided by the Texas Water Development Board, shown in Appendix H, delineates the location of six monitoring wells chosen to create the 2D model.

4.5 Gravity Measurements

4.5.1 Theory of Aquifer Measurements Using Microgravity Readings

Microgravity instruments measure lateral density variation and can therefore measure water volume change in aquifers. Microgravity or gravity studies and have been applied to measure water table change due to both natural and artificial recharge (Pool 2008, Howle et al. 2003, Bonneville et al. 2015). These instruments have a sensitivity of +/- 1 μGal; a Gal is equivalent to $1cm/s^2$. When such precision is not required, the earth's gravity field is generally considered to have a mean value of 981 Gal. A relatively new concept in hydrogeology, microgravity surveys of aquifers can provide porosity and specific yield values for an aquifer without the cost of pumping tests and monitoring wells (Pool, 2008). Repeated temporally at the same locations, measurements can be used to evaluate the loss or gain of water in an unconfined aquifer.

Microgravity measurements across an aquifer do not directly record water. Rather, microgravity readings are a measurement of subsurface lateral density variations. Higher density results in greater gravitational pull as defined in Newton's Law of Gravitation (Adam, personal communications, 2017). In an unconfined aquifer, an influx of water (density of 1000 kg/m^3) displaces air or gasses (density assumed ~0 kg/m^3) in pore spaces. Pore space volumes therefore experience an increase in density.

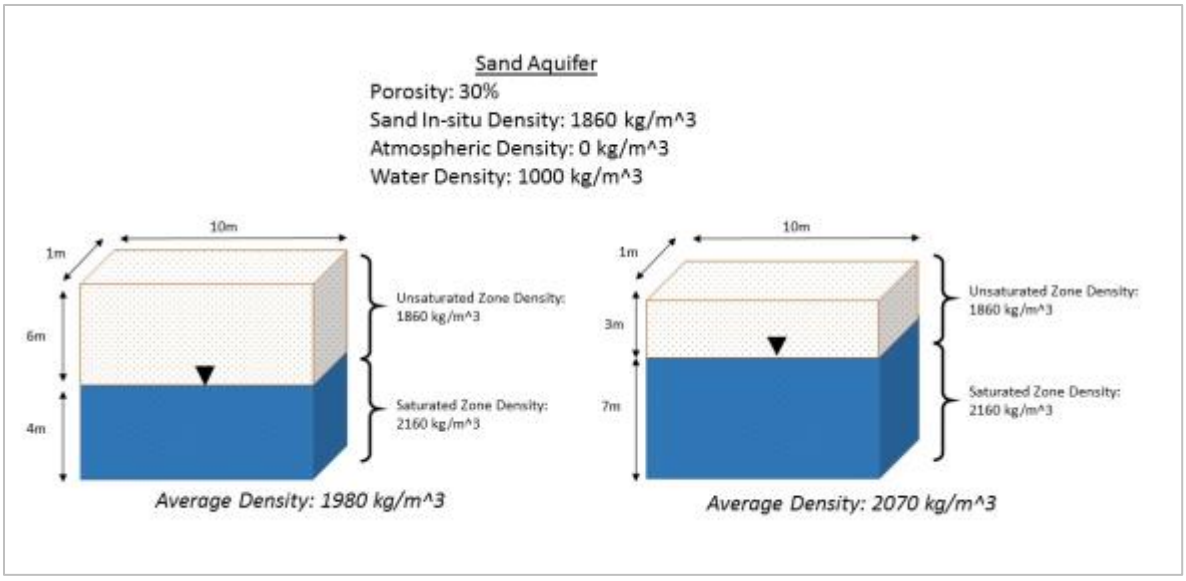

Figure 23: Effects of water table on average aquifer density.

Fig. 23 demonstrates how an aquifer's porosity affects density values change with water table rise or fall. The gravitational reading taken above each cube will be higher for the cube on the right because the density of that cube is greater. The hypothetical aquifer in Fig. 23 has a porosity of 30% so single cubic meter of aquifer could hold 300 kg of water. The difference between a "dry" cubic meter of aquifer (1860 kg/m^3) and a saturated cubic meter (2160 kg/m^3) is the weight of the additional water.

To measure aquifer changes with microgravity, measurements are made at different times from the same points along a survey line. Sometime referred to as four-dimensional or time-lapse microgravity (Koth and Long, 2012), the measurements track the temporal change of gravity at the microGal scale by observing changes in density distribution cause by migration of water (Bonneville et al, 2015). During measurement interpretation, corrections for changes in elevation are made using a Trimble NetR9 GNSS Reference Receiver differential GPS (dGPS) (Trimble, 2010) to account for any change between points and corrections for instrument drift are done by repeatedly visiting a reference station during the course of the survey. After

applying these corrections any changes in gravitational force measured between the first and second survey are representative of changes in the mass of water in the subsurface.

Work done by Pool exemplifies of the use of microgravity in measuring unconfined aquifer changes. Pool measured aquifer water table changes and estimated specific yield for an aquifer in Arizona (with similar lithology to the HBA in Texas) by application of the infinite slab equation (Pool, 2008):

$$\Delta g(\mu Gal) = 41.9\left(\frac{\mu Gal}{m}\right) x\ \Delta\sigma\ x\ \Delta T(m)$$

Equation 9: Gravitational Equation of an Infinite Slab

Where Δg is the change in gravity between the survey at time 1 and the survey at time 2 in microGals, $\Delta\sigma$ is the dimensionless change in specific gravity over the time interval, and ΔT is the change in thickness of the slab, which in this case equals the rise in the aquifer's water table. There is therefore a positive linear correlation between increasing gravity and increasing water levels.

Measuring the water table at point-source recharge locations like MAR structures requires considering the shape of density anomalies. The infinite slab equation cannot be easily applied when calculating the gravitational difference caused by a saturated zone water slope, a condition that is expected below recharge structures. To accurately gauge aquifer properties a recharge locations, measurements are made at closely spaced intervals along the survey line. After applying free air, drift, and terrain correction, the difference in the magnitude of gravity readings between measurement locations indicates the presence of higher (or lower) density saturated (or dry) area. Ideally these plot as a bell or Gaussian shaped curve along the survey line. The measurement made at the recharge structure would be directly over the high-density anomaly and has the highest magnitude. The shape of the curve is influenced by the geometry of

the density anomaly while the magnitude of the curve is influenced by the anomaly's depth (Musset and Khan, 2009). Fig. 24 demonstrates two high density anomalies with simple geometries at three different depths and how the corresponding gravity measurement curve would plot. The figure shows a buried sphere shaped (left) and cylinder shaped (right) gravity anomaly and graph of the associated gravity measurements taken along a surface transect. As shown in this figure, the depth to the gravity anomaly (*z* in fig 24) strongly influences the magnitude of the measurement. Shallow high-density anomalies have measurements of greater magnitude.

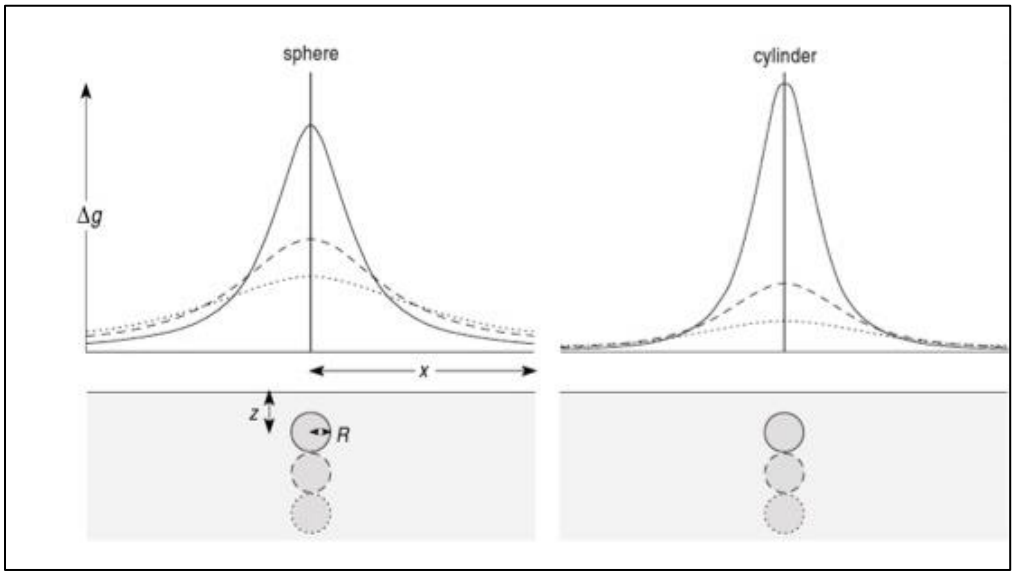

Figure 24: Gravity anomaly curves created by two geometric shapes (Musset and Khan, 2009)

Gravity anomalies in complex lithology such as the recharge basins in the HBA are not simple. The curve created by plotting gravity measurements along a transect may appear as more squiggle than a bell curve. This is because the gravity reading of every point is the sum of the gravity pull from every density anomaly in the subsurface. In the HBA this includes perching layers above the main water table and lithologic horizons with variable soil (and therefore density) composition. Fig. 26 provides an example of what such a curve can look like.

4.5.1.1 Theoretical Gravity Curves Utilizing MATLAB Script

The gravity anomaly, Δg, created by a density anomaly Δρ, is found with equation 10:

$$\Delta g = \sum_{i,j} \frac{G * \Delta\rho(j,i) * \Delta x * \Delta y * \Delta z * H}{d(j,i)^3}$$

Equation 10: Change in gravity at any point in a 2D model

In this equation the gravity anomaly is situated at a distance d from the measure point and scales as the mass anomaly (i.e. the density anomaly in kg m^{-3}, Δρ, multiplied by the volume, Δx* Δy* Δz), multiplied by the depth between the measure point and the anomaly (*H*), and multiplied by the gravitational constant, *G*, divided by the cube of *d*(i,j).

To obtain the density anomaly at a given point on the surface, we make the sum of all the density anomalies in the subsurface. This equation has been applied to a density 2D model. This prediction was then compared with field observation to assist with field data interpretation. An advantage to using a theoretical model for comparison is the relative ease of evaluating different lithology at varying depths. For example, Fig. 25 shows a theoretical aquifer with two positive density anomalies at 38-40m BGS and 55-60m BGS. The density anomalies are shown in yellow as laterally non-continuous layers. The positive density anomaly was created by using the density of water (1000 kg/m^3) instead of air (~0 kg/m^3) in the yellow layers and multiplying it by the aquifer porosity to calculate a mass of water, then adding this to the dry density mass of the aquifer. In the field this is similar to conditions created by perched water above a low permeability layer.

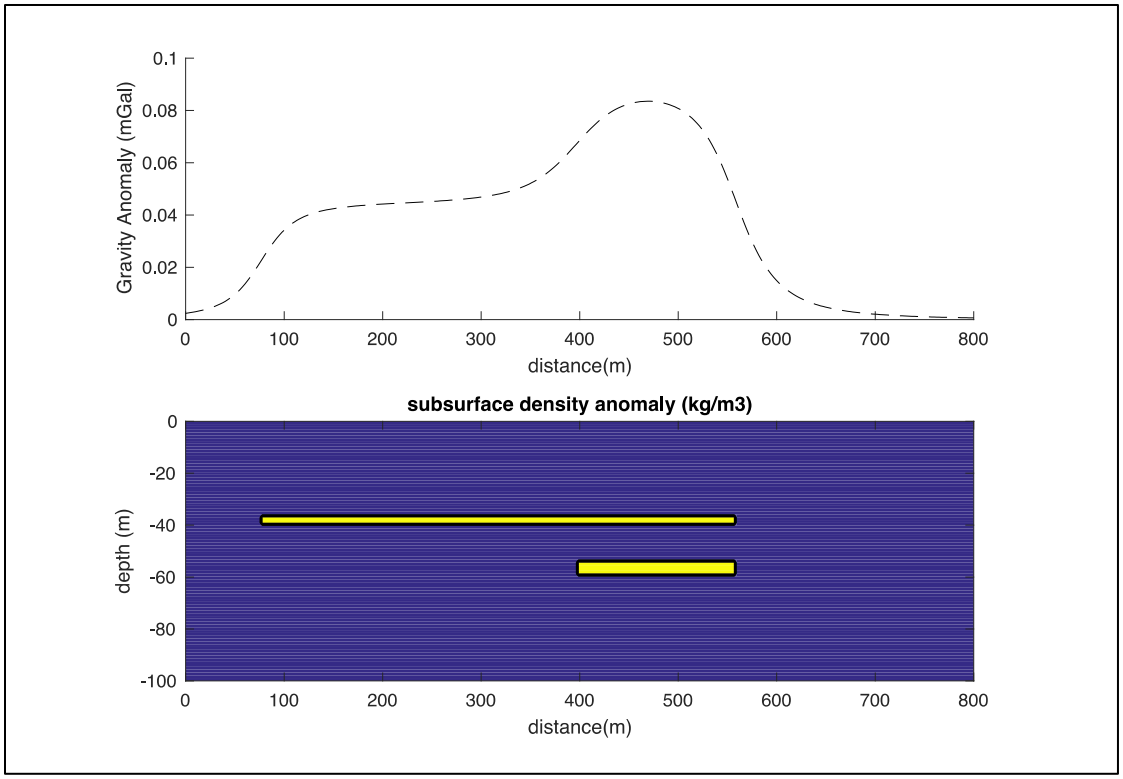

Figure 25: Theoretical density difference, $\Delta\rho$ (kg/m^3), and associated gravitational curve.

We developed a Matlab script to integrate *equation 10* in this subsurface structure. The resulting gravity anomaly is shown in Fig. 25. Peak relative gravity is shown between 400-500 meters, corresponding to the location in Fig. 25 directly above both layers. Because the density anomalies are not identically shaped, the curve is bimodal, corresponding to the number of density anomalies.

4.5.1.2 Using Model Outputs to Anticipate Microgravity Survey Results

Output from numerical modeling can be used to predict microgravity measurements. A high correlation between the anticipated measurements from model data and actual measurements from the field can confirm a model's validity; conversely, low correlation can provide information required to refine the model's accuracy.

Theoretical gravity measurements were computed using the beginning and ending moisture contents from VS2DTI and textural class codes describing different lithology (Table 14

and Fig. 26). These outputs from VS2DTI were used as inputs in the computer program MATLAB (MathWorks, 2016). The model began as completely dry with initial moisture content values equal to the residual moisture contents chosen in model setup. These textural classes were then assigned a density based on Das's Table of dry unit weight for various soils (Das, 2010) and the author's interpretation of well logs. Code for assigning density values was developed in house. This created a matrix with density values for at each point in the model according to a dry condition.

Table 14: Dry density used for gravity calculation. (modified from Das, 2010)

Soil Horizon	Density (kg/m^3)
Sand (aquifer matrix)	1610
Loamy Sand	1986
Sandy Clay	1561
Silty Clay	1561
Clay	1297

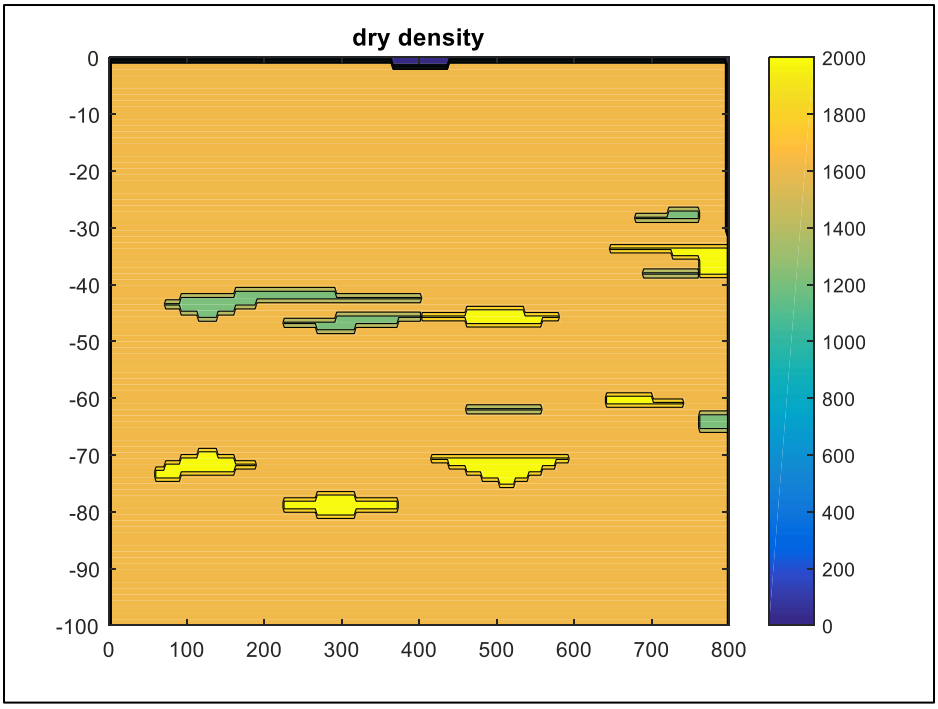

Figure 26: Dry density profile of HBA model.

Density in kg/m^3.

The theoretical gravity curve at model startup using a dry aquifer can be seen in the blue line on Fig. 27. The model was then run for 30 days. Subsequent output from VS2DTI now included a higher moisture content resulting from 30 days of water infiltration. The density value of water (1000 kg/m^3) was assigned to this moisture content and the MATLAB script was again run to determine the change in gravity. There is a clear increase in gravity potential in the areas nearest the infiltration, as is seen in the red line in Fig. 27.

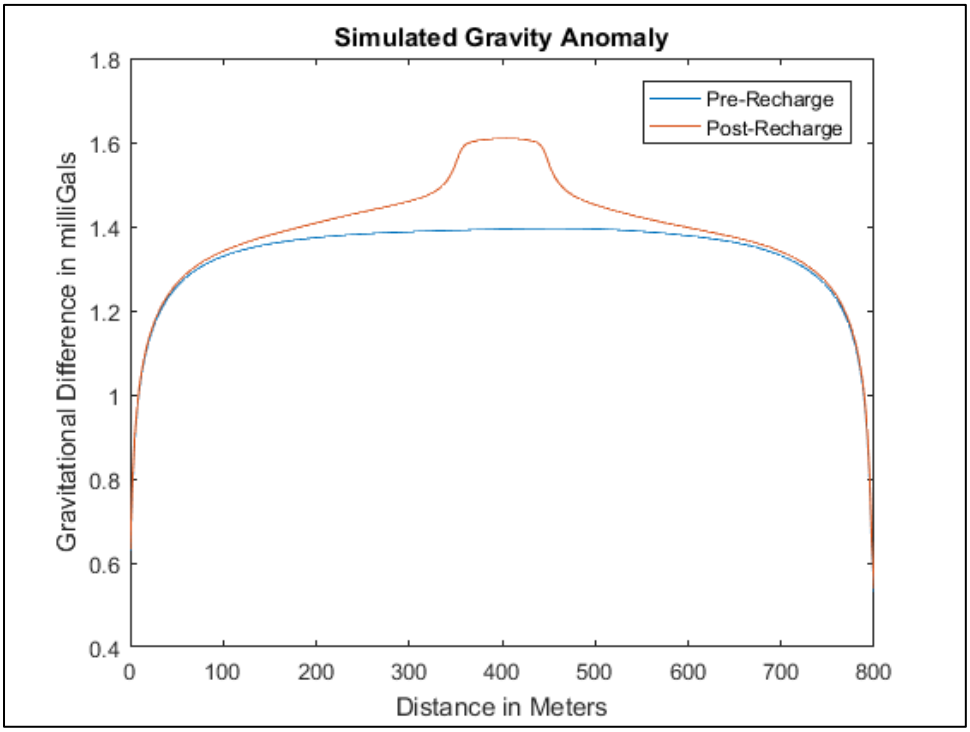

Figure 27: Simulated gravity curve, pre- and post-recharge

4.5.1.3 Survey Methods

A microgravity survey was conducted at the HBA site in June 2017. A LaCoste and Romberg Model D microgravimeter was used to take measurements. The instrument was first calibrated to the El Paso area, a process known as "re-ranging", in accordance to the Model D user manual (LaCoste & Romberg, 2004).

A Trimble dGPS receiver and antenna were used to record elevation changes at each measured point. This was required to find the vertical difference between base station and measurement points and subsequently correct for vertical displacement. The primary survey line ran east-west along EPWU's dirt access road, beginning at the eastern edge with the intersection of access road and McComb Street and ending where the access road made a "T" and stopped heading west. An additional north-south survey line which centered on the basins and ran into open desert to the north and south. Survey lines were walked and measurement positions located and marked by spray painting a rock or local feature that would assist with subsequently locating the position.

The east-west survey line was approximately 1,500km long. Collection points are shown as purple markers in Fig. 28. Measurement spacing was approximately 30m except for the five most westerly points, which were spaced approximately 100m apart. 31 measurements were taken along this transect. The north-south survey line was approximately 800m long. Collection points are shown as green markers in Fig. 28. Measurement spacing was progressively coarser with greater distance from the basins. Fifteen measurements were taken along this transect.

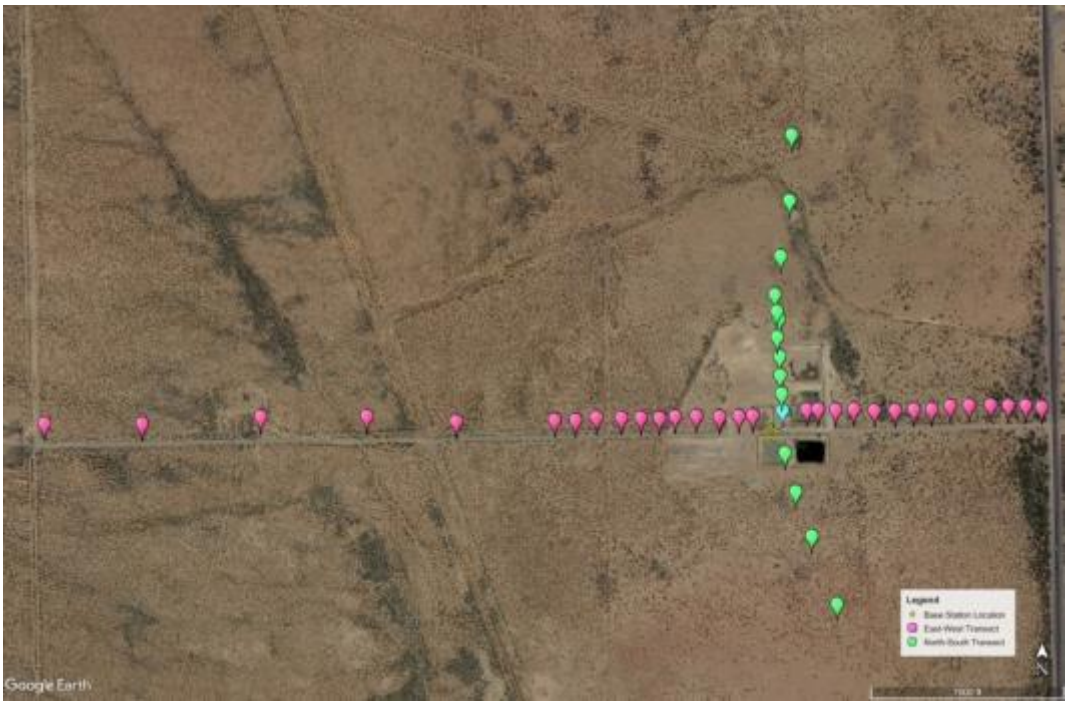

Figure 28: Locations of June microgravity survey

Yellow star represents the base station; Blue point was used for both transects.

A reference station was established on a concrete pad near the intersection of the north-south and east-west survey lines. The concrete pad provided a flat, immovable object for consistent, repeated measurements across two days. This reference station was revisited at the start of each day, the end of each day, and every hour during survey to account for instrument drift in later processing. The dGPS base station was established at this reference point. The dGPS rover was placed at each measurement point for at least 20 minutes after taking microgravity measurements. The obtained accuracy in the altitude are in the order of the cm (Leigh). This allowed us to correct for the topography variations, known as the Bouguer correction. We also corrected the data for the instrumental drift.

4.6 Soil Measurements

Collecting soil samples was not planned and the opportunity to collect the sample was provided only once when EPWU personnel initially escorted us through the site, so tools to

collect samples were limited to a shovel and a one-gallon plastic bag. The sample was taken from the southwest infiltration basin. This produced a disturbed soil sample that does not have the same density characteristics as *in situ* soils. No equipment on hand to test *in situ* soil density or compaction. However, grain size analysis and permeability tests were still conducted to check against previously published literature. Grain size was not anticipated to change between disturbed and *in situ* samples and permeability testing took place according to ASTM 2434 which assumes a disturbed sample.

4.6.1 Grain Size Analysis

Grain size analysis was made with a Malvern Mastersizer 3000, nicknamed "Sandy". This machine consists of a mixing component that looks like a miniature Keurig coffee machine with a beaker (Foreground, Fig. 29) and a silver box that houses electronics and lasers (background, Fig. 29) where measurement takes place. Samples are mixed in the beaker and drawn into the machine for measurement.

Sandy was run twice, once using operating parameters for silt/clay particles and once using operating parameters for sand sized particles. Each run included three separate experiments using the given parameters. It was immediately apparent that a significant fraction of the grains were larger than the 1mm upper limit defined in the silt/clay parameter. Therefore, only results obtained using the sand operating parameters will be discussed.

The sample was removed from a one-gallon plastic bag 18 hours prior to measurement and oven dried at 90^{oC} for 60 minutes. Prior to oven drying the sample, the bag had remained sealed and moisture content in the sample was assumed to have remained the same as when the sample was taken from the infiltration basin. Once removed from the oven the sample was allowed to cool and placed in two 1-quart plastic bags until measurement. No pretreatment, such

as heating or hydrogen peroxide wash, was required due to the very low organic content (effectively zero) in the sample. Small amounts of gravels in the sample were removed prior to running the instrument.

After degassing and ensuring water clarity, small (approximately 1/4 teaspoon) volumes of sample were added directly to the 500mL sample beaker filled with deionized water that serves as the Mastersizer 3000's reservoir. These volumes were added one at a time with the instrument mixing the sample at a velocity sufficient to keep the sample grains in suspension within the beaker. Samples were added until turbidity measured within the 10-15% range required for the instrument to operate. Turbidity readings fluctuated as the machine ran but generally fell within a range of 11-12%.

The Mastersizer conducted three independent tests of grain size using light scattering as a mechanism to determine grain size. Results were interpreted using the Unified Soil Classification (USC) System. This system is widely used by the Corp of Engineers and the American Society for Testing and Materials. According to this system *Sand* is defined as >50% of a sample passing the No.4 (4.75mm) sieve but <50% passing the No.200 (0.074mm) sieve (Das, 2010). The Wentworth scale was used to further refine the types of sand grains in the sample. According to the Wentworth scale sand is defined as: Very Fine Sand (.0625 to .125mm); Fine Sand (.125-.250mm); Medium Sand (.250-.500mm); Coarse Sand (.500-1mm); and Very Coarse Sand (1-2mm). Unlike the USC system, the Wentworth system classifies particles between 2-4mm as very fine gravel, not sand.

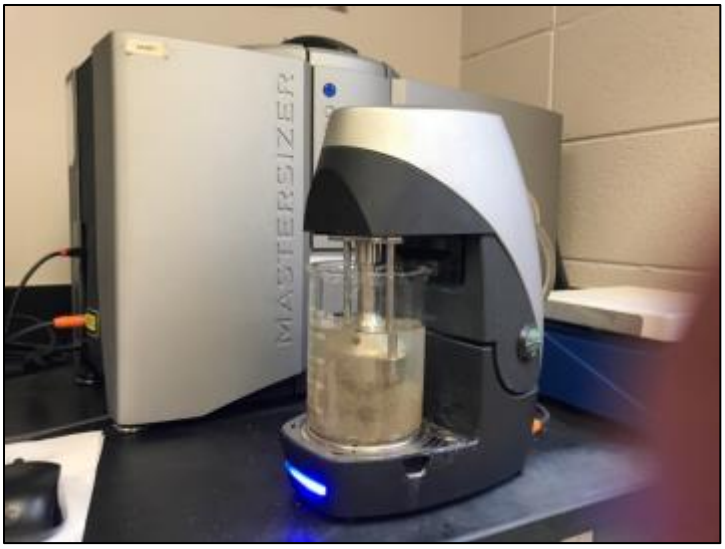

Figure 29: "Sandy" the KSU Mastersizer.

4.6.2 Permeability Analysis

Constant head permeability tests were conducted to determine the saturated hydrologic conductivity of HBA soils taken from the approximately 0.15m BGS in the southwest infiltration basins. Testing was done in accordance with ASTM D 2434 Standard Test Method for Permeability of Granular Soils (Constant Head) with one variation- due to equipment limitations compaction was done by hand instead of tamping or using a compaction hammer.

The sample was placed in a Humboldt 2.5 inch permeameter cell. Tap water was supplied through flexible clear tubing at a steady rate to a Humboldt constant head tank. The constant head tank provided flow into the top of the permeameter cell with overflow from the tank returned to a sink. Outflow from the permeameter was returned to a sink. Head measurements were made from the upper and lower side ports on the permeameter cell using a free standing Humboldt manometer. The manometer was positioned on a chair adjacent to the permeameter so that the upper pressure head reading was approximately in the middle of the manometer's range of measurements.

Chapter 5 - Results- SLA, Cape Cod, Massachusetts

The Cape Cod Aquifer is one of the most productive groundwater systems in New England and provides 100% of the Cape's drinking water. – Cape Cod Commission

5.1 Unsaturated Zone Modeling

5.1.1 Three Dimensional Scaling Factor

One of the challenge of using a 2D program like VS2DTI to compare infiltration basin recharge with well recharge is the problem of inferring total recharge in three dimensions from model outputs in two. Actual infiltration basins have a surface area normal to the depth (z) direction, so simulated in two dimensions, the resulting recharge values are for a "slice" of the basin. It is useful to consider the example of a theoretical recharge basin 10m long by 10m wide for a total recharge area of 100 m^2. A recharge rate of 0.1m/h is applied across the entire basin. A one-dimensional point in this basin therefor has a recharge of 0.1m/h. A two-dimensional cross section has a total recharge of $1m^2/h$ because 0.1m/h (recharge) x 10m (length) x 1m (width) = $1m^2/h$. A *unit width* cross section has a total recharge of $1m^3/h$ because 0.1m/h (recharge) x 10m (length) x 1m (unit width) = $1m^3/h$. The total basin recharge is 0.1m/h (recharge) x 10m (length) x 10m (width), or $10m^3/h$ (Fig. 30).

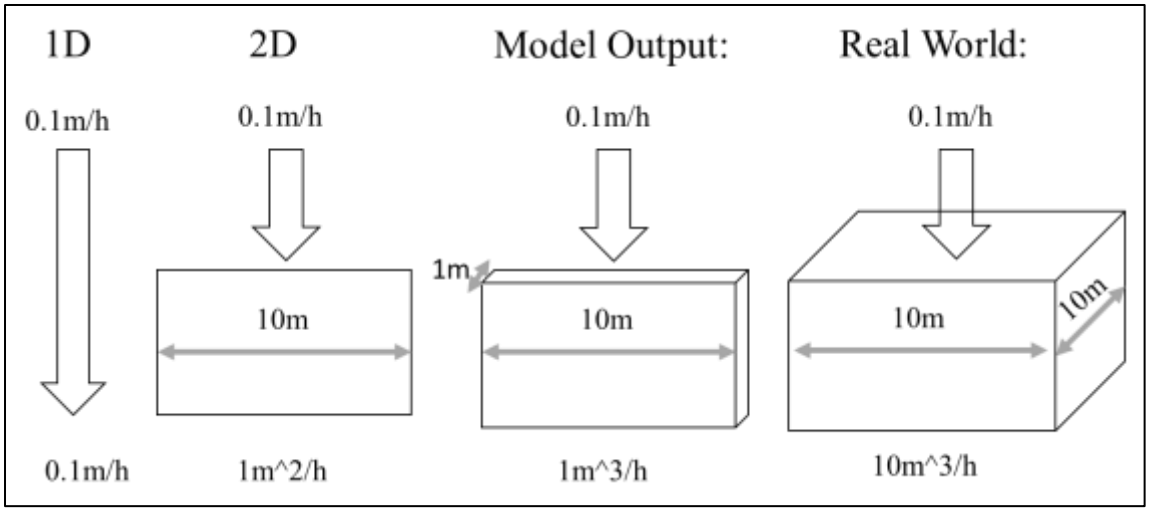

Figure 30: 1D to 3D interpretation

For an infiltration basin with square geometry, such as the 45m x 45m basin used in this thesis, scaling up to three dimensions as described above is simple. For a well screen of circular geometry the problem is harder and some simplifying assumptions were made. All wells were modeled with a diameter of 1m to assist with making calculations easier. This is not an unusual diameter for recharge wells- 4ft and 6ft boreholes are typical (Mr. Meyar, Torrent Resources, personal conversation). A 10m deep well of 1m diameter would therefore have a screen area of 31.429m^2 [10m x (2*π*0.5m) = 31.429m^2]. This is the area of the surface of a cylinder minus the area of its top and bottom, as seen in equation 12.

$$A = Length\ of\ Screened\ Area * (2 * \pi * r)$$

Equation 11: Area of Well Screen

Extending this example to a model, each side of the well in the *y* direction is unit width- it may be helpful to refer back to Fig. 30 and Fig. 31. Although the model is considered "2D", the output is in terms of m^3/d. This is the same as stating m^2/d *per meter width*. A 10m deep well has two sides that extend 1m into the model and can be thought of as forming a square-shaped well. The recharge value from the model accounts of 20m^2 of screen length (Fig 31). To infer the actual three-dimensional recharge value, the total recharge must be multiplied by 1.57

to account for the "missing" sections of screen area that are absent in the model output. 1.57 is a scaling factor that converts modeled screen area to a 3D circular screen area (equation 13). It is found by dividing the screen area of a circular well (right side, Fig. 31) by the modeled screen area (left side, Fig. 31).

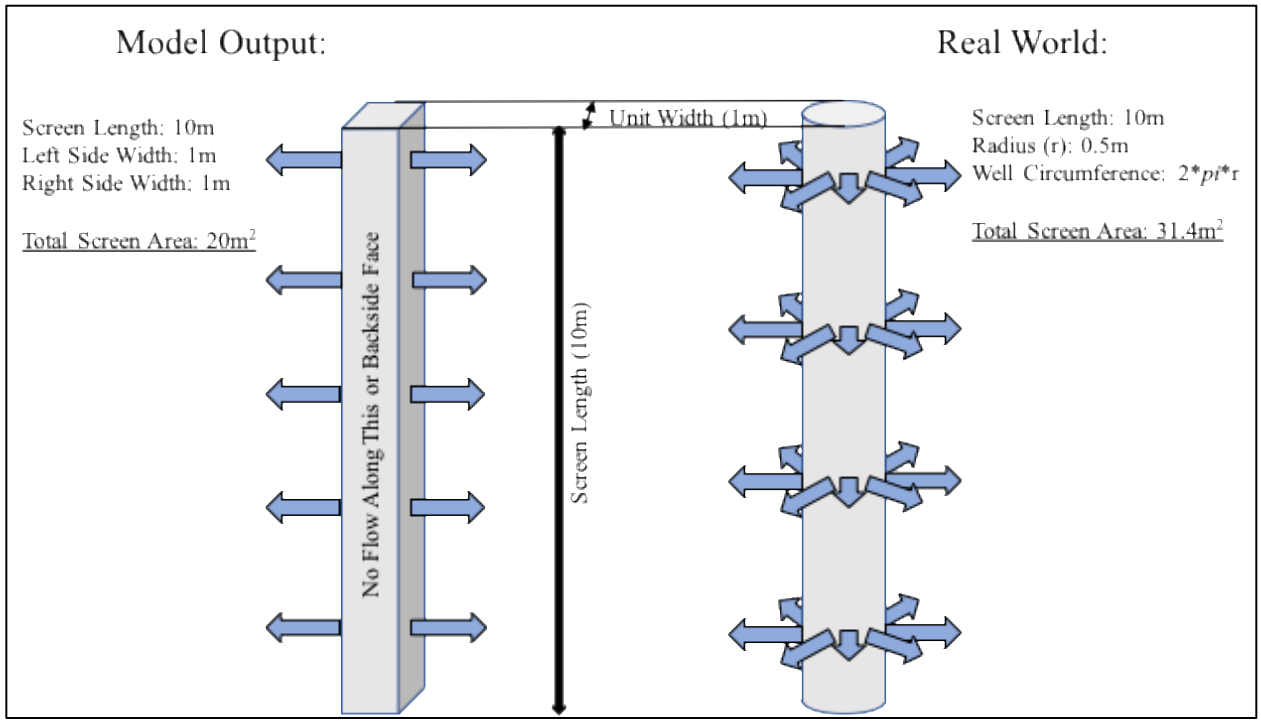

Figure 31: Model output to 3D

The scaling factor equation to go from model output (left side, Fig. 31) to a 3D circular well screen (right side, Fig. 31) is (equation 13):

$$\mathbf{2}(\boldsymbol{L} * \boldsymbol{w_y}) * \boldsymbol{C} = \boldsymbol{L} * (\mathbf{2} * \pi * \boldsymbol{r})$$

Equation 12: Model output to 3D output using scaling factor *C*

Where *L* is the length of the well screen in meters BGS, $\boldsymbol{w_y}$ is the unit width of the model (1m in this research), *C* is the scaling factor, and $(\mathbf{2} * \pi * \boldsymbol{r})$ is the circumference of the well.

5.1.2 Unsaturated Zone Results

Results for SLA modeling are given in Table 15. All wells were modeled with a water column height 1m BGL. Modeling this way assumes sufficient water is available for injection into the well to maintain a constant water column height regardless of infiltration rate. This may or may not be true, depending on site specific conditions, but allows an equivalent comparison between each well.

Five wells and one infiltration basin were modeled. For each well the simulated water column is 1m less than the well depth, i.e. for the 10m deep well there was a simulated water column of 9m. 9m of water column was chosen instead of 10m to avoid water flow against the top horizontal- i.e. ground level- boundary in the model by starting recharge 1m below this boundary, which was set as "no flow".

Table 15: Modeling results, SLA

	Modeled (2D) Infill Rate @ 4 Days m^3/d	**3D Infill Rate @ 4 Days m^3/d**
Basin @1cm	284.88	12819.6
6m Deep Well	269.28	422.77
8m Deep Well	271.44	426.16
10m Deep Well*	273.36	429.18
12m Deep Well	275.52	432.57
15m Deep Well	277.68	435.96
*Depth from thesis proposal hypothesis		

Results proved surprising- model output for all wells approached a steady state infiltration rate of about 11.5 m^3/h (276 m^3/d) after four days. This is likely due to a combination of factors. First, the aquifer is sufficiently permeable that water was able to quickly saturate the area below the wells or basin and form a mound on the water table. For the infiltration rates simulated, the mounding shape is a function of vadose zone hydrogeological characteristics and depth to water table. All simulated vadose wells provided enough infiltration to form a similar

mounding shape. As the water mound grows vertically and soil voids are saturated the head difference between the water column in the wells and the soil water pressure in the adjacent soil is reduced, slowing flow. The recharge advantage of longer screen length in the deeper wells is negated because the infiltration rate in the deeper parts of the well screen is reduced towards zero as the water mound builds (this is discussed further in *Discussion* section).

The mounding shape is also influenced by the boundary conditions at the left and right vertical limits of the model. Flow across the boundary above 20.7m (set as "possible seepage face", *see Chapter 4*) occurred at a rate related to pressure along that boundary and so outflow across the left and right model boundary "keeps pace" with the building water table mound. This prevented the water mound from growing wider than 600m at the water table surface. This leads to the conclusion that, at steady state, modeled recharge at the SLA site is controlled by *horizontal* flow, not *vertical* flow, and a conclusion that is in agreement with work done by Bouwer (1969). It also creates a condition that is unlikely to represent the actual aquifer. *The importance of considering boundary condition effects on infiltration rates must be stressed*. The large volumes and high velocity of modeled recharge at this site are unlikely to occur in real world settings. This discrepancy is discussed further in chapter 7 of this report, and results comparison between the vadose well model and infiltration basin model in this chapter are continued using the values shown in Table 15.

To validate the steady state recharge rate, the 6m well, 10m well, and infiltration basin were re-run to simulate 10 days recharge (240 hours) instead of 4 days. Results showed a slight infiltration rate decrease after 4 days, ultimately steadying around 10.45 m^3/h (250.8m^3/d) at day #10 (Fig. 32).

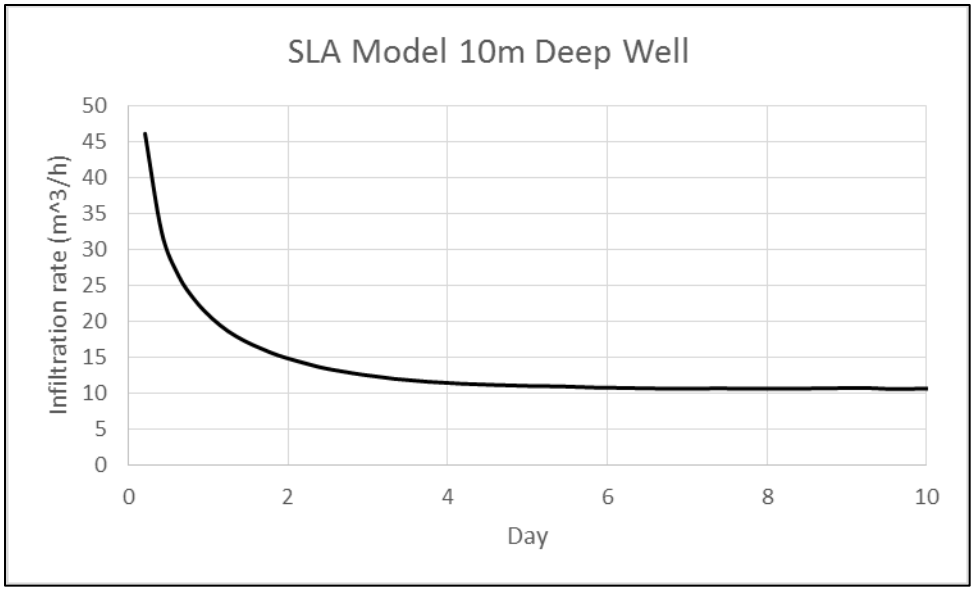

Figure 32: Infiltration rates vs time, SLA

5.1.3 Three Dimensional Interpretation

Three dimensional infiltration rates can be inferred from the two dimensional model results. The scaled rates are given in Table 15. The highly permeable, homogenous aquifer shows a large rate of infiltration through the vadose zone. A half acre infiltration basin has a simulated maximum infiltration rate of over 10.39 AF/D at just a single centimeter of ponded! This is much higher than the 2.21 AF/D (500 GPM) currently injected at the two injection well locations in the study area. The model results show large volumes of water infiltrating across relatively small areas is possible in sand and gravel soils.

To make a direct comparison between vadose well and infiltration basin recharge the scaled (3D) recharge rates and the 10m deep well model was used. Steady state recharge rate from the basin was 12,819.6 m^3/d (2,352 GPM) and recharge rate from the vadose well was 429.18 m^3/d (78.74 GPM) (Table 15). For reference, a common fire hydrant with a green colored cap has a rated capacity between 1,000 and 1,499 GPM (McCulloch, 2011), so the infiltration basin modeled would be able to infiltrate the combined flow of two opened fire

hydrants without ponding above 1cm of water. **Thirty vadose wells would be required to match the infiltration rate of a single basin, however, changes to the model's boundary conditions can affect this.** The number of vadose wells to reach infiltration equivalency with a half-acre basin is revisited in chapter 7 during discussion about model boundaries.

5.2 Saturated Zone Modeling

Infiltration rates calculated from VS2DTI modeling were used as the recharge inputs for saturated zone modeling. For the infiltration basin this was 534.15 m^3/h (12,819.60 m^3/d); for the vadose zone well it was 17.88m^3/h (429.18 m^3/d). Prior to recharge the system is in steady state with gradient contours aligned north-south perpendicular to the regional flow direction (Fig. 33).

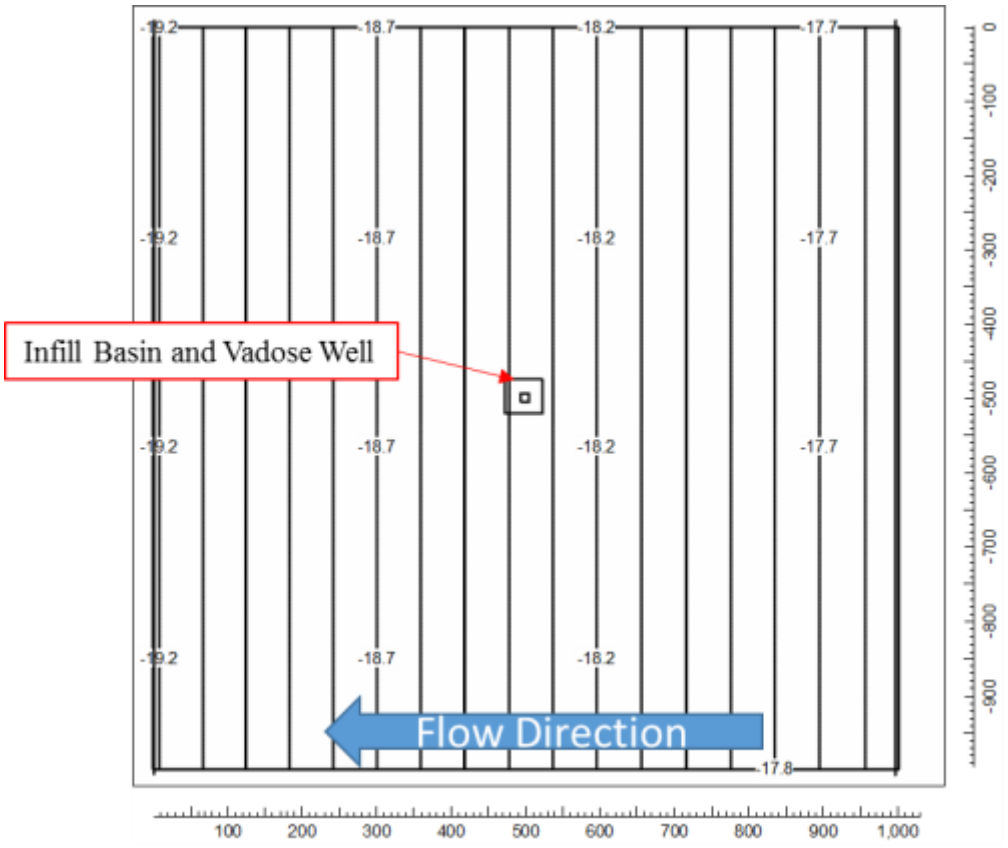

Figure 33: Steady state flow model, SLA

Contour interval is 10cm and represents depth to water BGS.

5.2.1 Saturated Zone Results

The saturated zone model used the VS2DTI calculated values for infiltration as recharge values. The vadose zone well model used the rate of 429.18 m^3/d for a 10m deep well with 9m water column. The infiltration basin used the rate calculated for 1cm deep ponding conditions of 12,819.6 m^3/d.

Results show a large increase in water table elevation in the infiltration basin model and a modest increase in water table elevation in the vadose well model (Fig 34). This was expected given the much larger infiltration rate used with the basin model. Even though it is clear more water infiltrates in the basin model, storage values must be considered for a complete understanding of recharge volumes. MODFLOW calculates storage in unconfined aquifers (such as this one) as the volume of water taken up or released by a cell given a change in head (Harbough, 2005). For unconfined aquifer models, change in head is synonymous with water table change. A good analogue is to think of a 10-gallon bucket that is half full of water. This bucket has a "storage" of 5 gallons. If one gallon of recharge is added to the bucket, it then has a "storage" of six gallons. Each cell in MODFLOW can be thought of as an individual bucket that "stores" water in a similar manner.

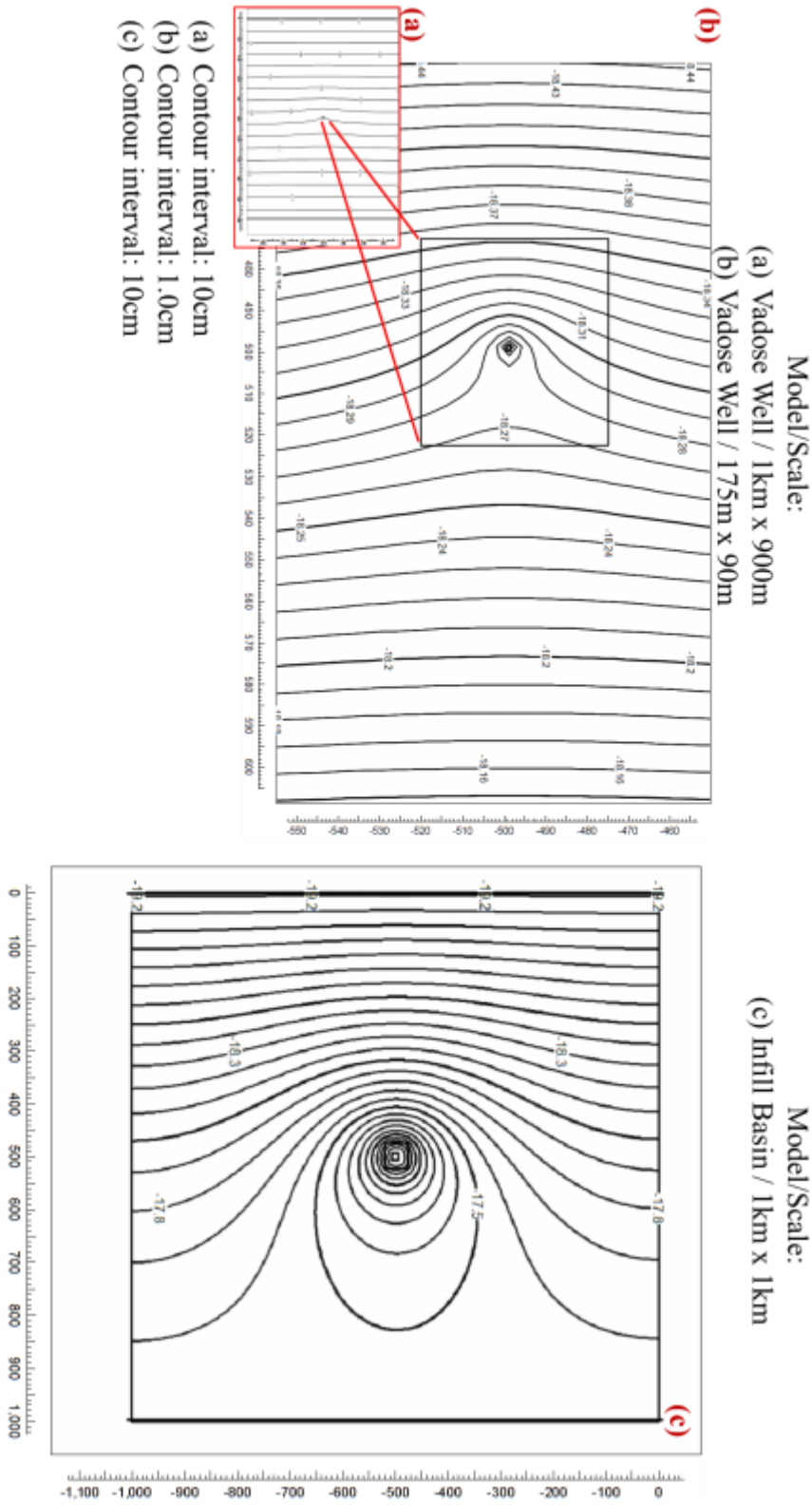

Figure 34: Water table rise, SLA

Storage values are the volume of water retained in the model's cells as the water table rises due to recharge. Recharge began only after the simulation was in steady state, so once it began recharge changes the balance of the model from a system in equilibrium to a system in transition. One might plausibly think that cumulative recharge and storage should then be the same- after all, recharge volume causes the water table rise which in turn causes the increase in storage. If the model had no-flow boundary conditions on all sides this would be true but in the SLA area groundwater naturally discharges. Establishing fixed head values along the east and west boundaries of the model created a gradient and water discharges across the downgradient boundary. Water volumes that flow across this boundary "disappears" from the model. Only water that does not cross the boundaries but is retained in the model area contributes to an increase in storage. Storage values are the volumes of recharge remaining within the model boundaries. Table 16 provides values for cumulative recharge and storage for the SLA models, while Fig. 35 displays the difference between water table rise between the vadose well model and the infiltration basin model.

Table 16: Saturated model outputs, SLA

	Day 2.5		
	Basin	**Well**	**Difference**
Cumulative Recharge (m^3)	31,906.89	1,072.80	30,834.09
Water in Storage (m^3)	26,873.96	904.61	25,969.35
	Day 10		
Cumulative Recharge (m^3)	127,627.59	4,291.20	123,336.39
Water in Storage (m^3)	73,600.44	2,482.86	71,117.58
	Day 30		
Cumulative Recharge (m^3)	382,882.75	12,873.60	370,009.15
Water in Storage (m^3)	99,258.41	3,356.55	95,901.86

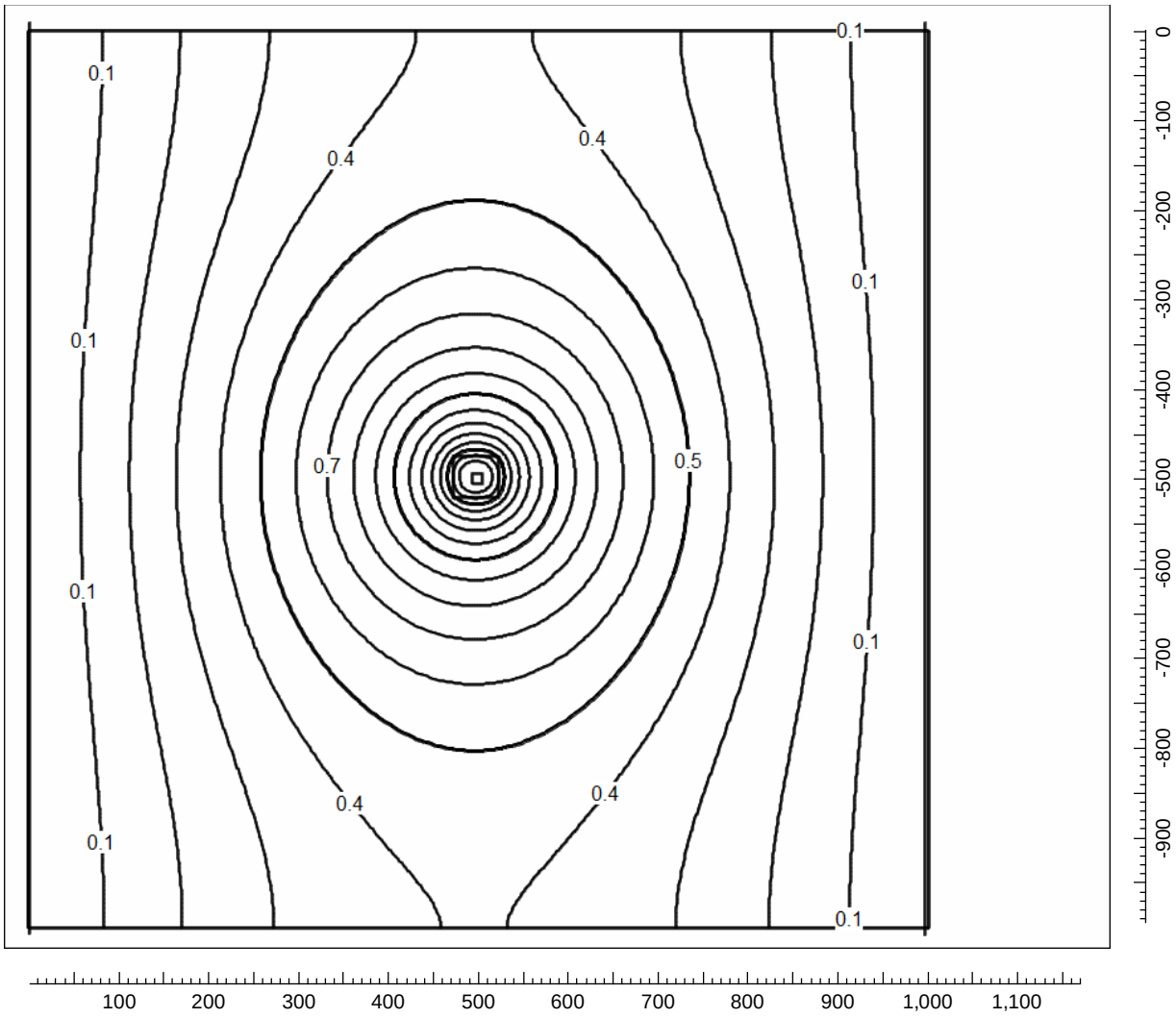

Figure 35: Water table elevation difference, basin vs well model, SLA

Contours are water level difference between infiltration basin and vadose well models in cm. Contours at 10cm intervals.

Results from the saturated zone model provide a very definitive answer to the SLA hypothesis. That answer is no- it is clear that **an infiltration basin is capable of a much greater volume of recharge over a given period of time, and that this greater recharge ultimately creates a higher water table 402m away from the recharge structure.**

Chapter 6 - Results- HBA, El Paso, Texas

"The Rio Grande is the only river I ever saw that needed irrigation." – Will Rogers

6.1 Unsaturated Zone Modeling

The infiltration basin model was run using three different recharge values: 1m of ponded water, 0.5ms of ponded water, and 0.213m (~8 in) of ponded water. Eight vadose zone well models were run to simulate five different water column heights in a well 33m deep and to simulate 20m, 45m, and 50m deep wells with 10m water columns to better understand the effects of the vadose zone perched layers on well recharge. Results from the 33m deep well with 10m water column height were used as the standard to compare effects of recharge across different well simulations (Fig. 36). *[During modeling this well was referred to as "Well #8" since it was the eight iteration, and this "well 8" nomenclature remains in several of the Figures when referring to this well.]* Fig. 37 shows fully saturated conditions as "blue" and zero moisture content as "red", so water-rich areas in the model are displayed with cooler colors that progress towards blue once all pore spaces are saturated. On day #1, lithologic horizons containing higher proportions of clays and silts- and therefore less permeable- are easily observed in Fig. 36 due to their higher residual moisture content and corresponding greater degree of saturation. Fully saturated conditions (dark blue) are observed to increase with time as recharge moves through the model (Fig. 36).

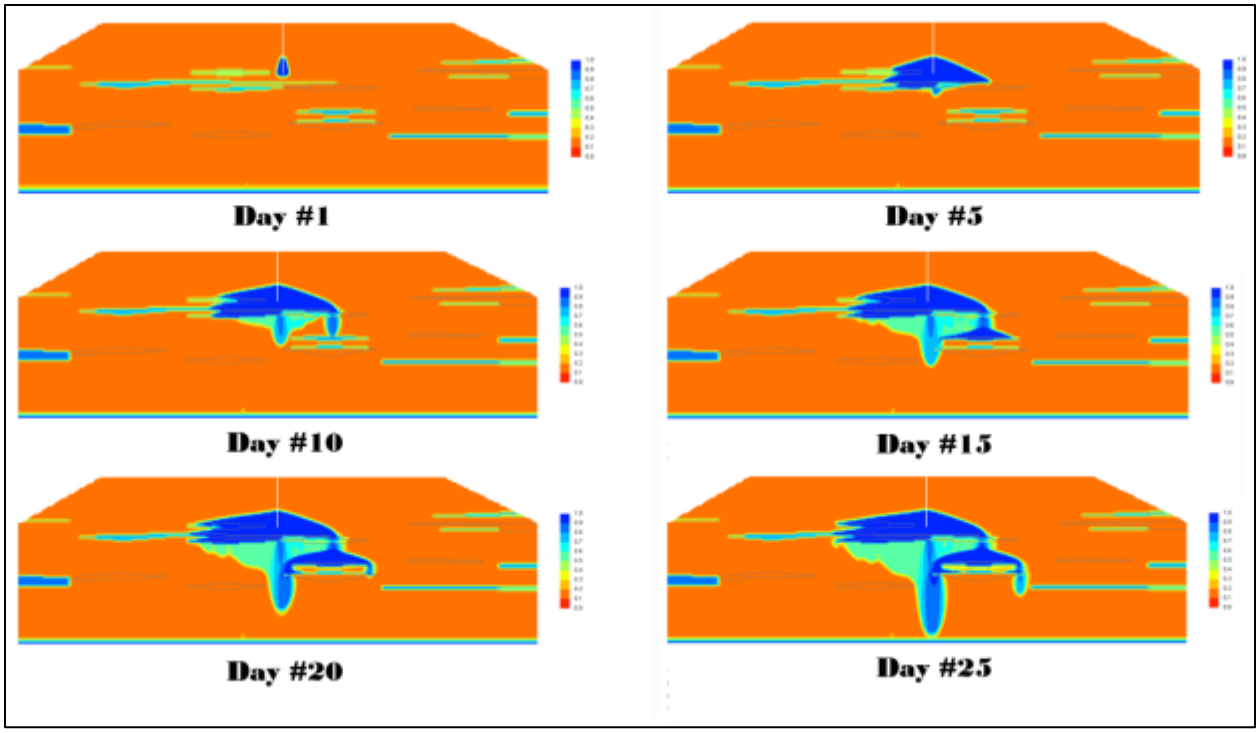

Figure 36: Moisture content at various recharge times, HBA

6.1.1 Unsaturated Zone Results

By comparing vadose zone well recharge rates at different water column heights to the recharge rate of an infiltration basin with a ponded depth of 1m, it was possible to determine how the well performed in relation to the infiltration basin. The 33m deep vadose well infiltration rate correlates positively with increasing water column height; a linear regression of the data yields the equation $y = 8.5221x$, where y is the infiltration rate in m^3/d and x is the height of the water column in meters inside the 33m deep well. Extrapolating from this equation allows a determination of the increase (or decrease) in infiltration rate as the water level in the well is raised or lowered—each meter of water column height added (subtracted) provides an increase (decrease) of just over 8.5 m^3 per day per unit width.

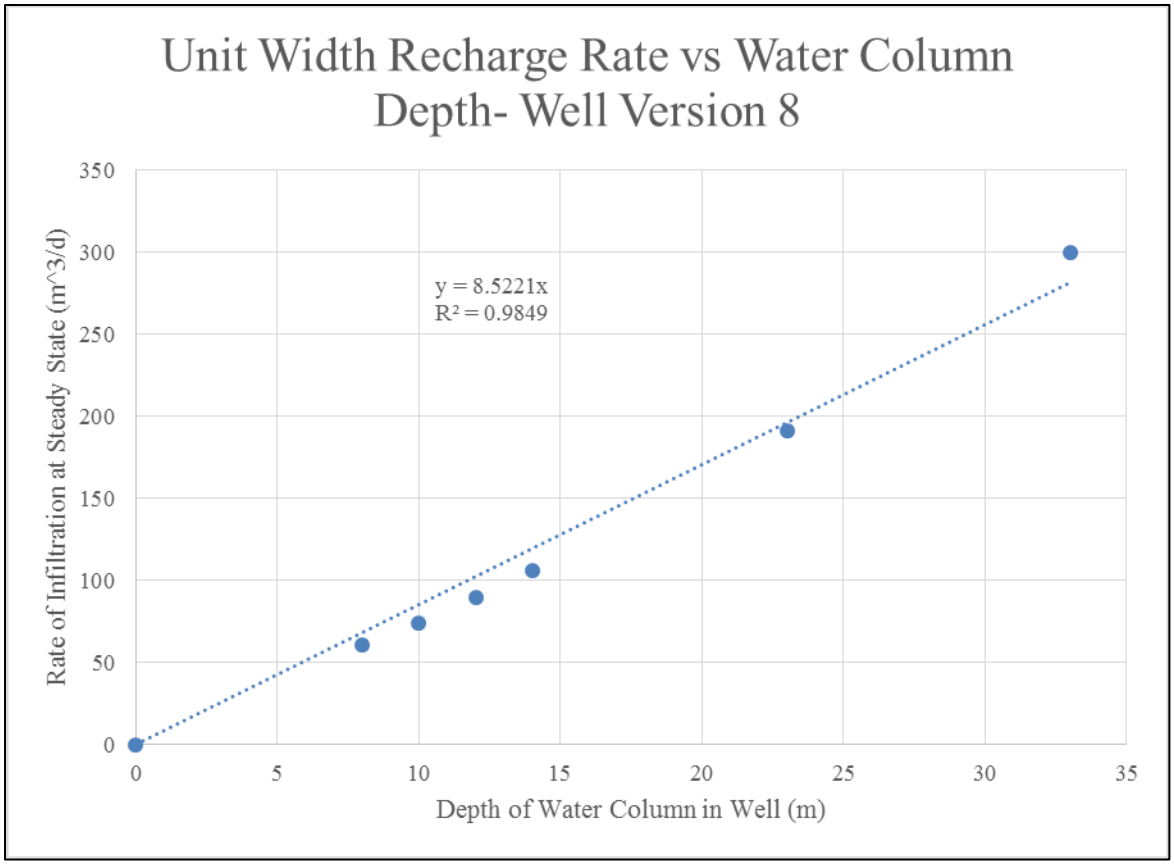

Figure 37: Vadose well infiltration rate vs water column depth, HBA

Scaling from two dimensional recharge rate (8.5221m^3/d per meter of screen length) to estimate total volume in three dimensions requires using the circumference of the well screen and the length of the well screen as outlined in Chapter 5 (Equation 13). A new recharge rate vs water column graph can then be produced (Fig. 38). Linear regression of these data yields the equation $y = 13.38x$, where y is the infiltration rate in m^3/d and x is the height of the water column in meters inside the 33m deep well.

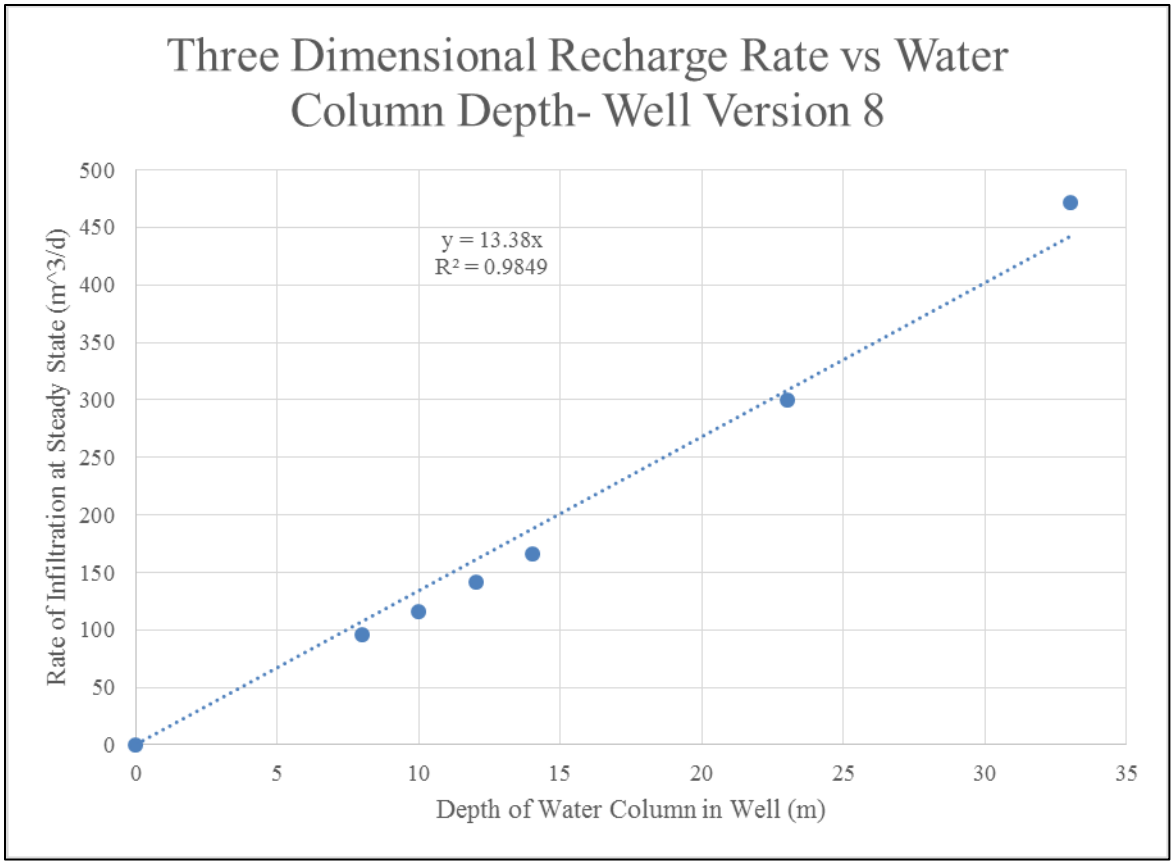

Figure 38: Total flow volume from vadose well vs water column depth, HBA

VS2DTI output for the infiltration basin, modeled at 1m, infiltrated water at a rate of 143 m^3/d per unit width (table 17). Since a half acre basin is essentially a 45 x 45m square, the total volume that could be infiltrated is:

$$\frac{143\ \mathrm{m3/d}}{m} \times 45\ \mathrm{m} = 6{,}435\ \mathrm{m3/d}.$$

To match this in the modeled vadose well the recharge rate equation for the well is set to the recharge rate of the infiltration basin:

$$6{,}435\frac{m^3}{d} = 13.38\frac{m^3}{d}\ x$$

where *x* is the water column height in the well. Solving the equation provides a value of *x*=480.94 meters. Clearly, even a totally "full" well with a water column 33m high is not sufficient to recharging the same total volume as a ½ acre infiltration basin. Using our slope

equation from Fig. 38 the highest recharge rate possible in the modeled vadose zone well is 13.38 m^2/d x 33m, or 441.54 m^3/d.

Knowing the maximum possible recharge of the vadose well and the recharge from the basin allows calculation of the number of vadose zone wells required to match the basin's recharge rate. **It would take a minimum of fifteen vadose zone wells to achieve the same recharge rate as a half-acre infiltration basin** (6435 m^3/d ÷ 441.54 m^3/d per well).

6.1.2 Validation of Unsaturated Model

Validation of the HBA vadose zone model was done using historical data from the 2003 American Water Works Association Research Foundation (AWWA) report. As detailed in this report, monitoring wells were constructed adjacent to the proof of concept infiltration basin to measure soil moisture content and potential perched layers. The resulting data showed a rise in the water table below the infiltration basin beginning 28 days following startup of the pilot project basin, which translated to an average vertical water velocity of 4.2 m/d (AWWA, 2003) (Fig. 39).

The average saturated seepage velocity for the fine sand matrix used in the model is determined by dividing *vertical conductivity* by *porosity*. Using the vertical conductivity value (chapter 4) and the porosity (33.7%) chosen as model input yields:

$$\frac{2.1 m/d}{0.337}$$

This provides a vertical seepage velocity value of 6.2 m/d. This value is closely aligned with the theoretical matrix-only value of 6 m/d described in the AWWA report (3.3% higher) implying the hydraulic characteristics of the fine sand matrix used in the model are closely aligned with the observed measurements made during the project.

With the inclusion of low-permeability horizons in the model, simulated travel time in the model becomes very close to the observed travel time during the AWWA project. Simulations of the basin with 0.31m and 0.5m of ponded water gave a model output with the wetting front arrival between day 24 and day 28 of the simulation.

This very close alignment between observed and simulated wetting front arrival at the water table implies a valid HBA physical hydrology model. The low permeability layers chosen for the model, which are based on lithology from well logs at depths known to cause perched conditions during the American Water Works Association field test (AWWA, 2003), retard the flow of water long enough to bring the simulated wetting front to the water table at the same time as it was observed to arrive at the AWWA project.

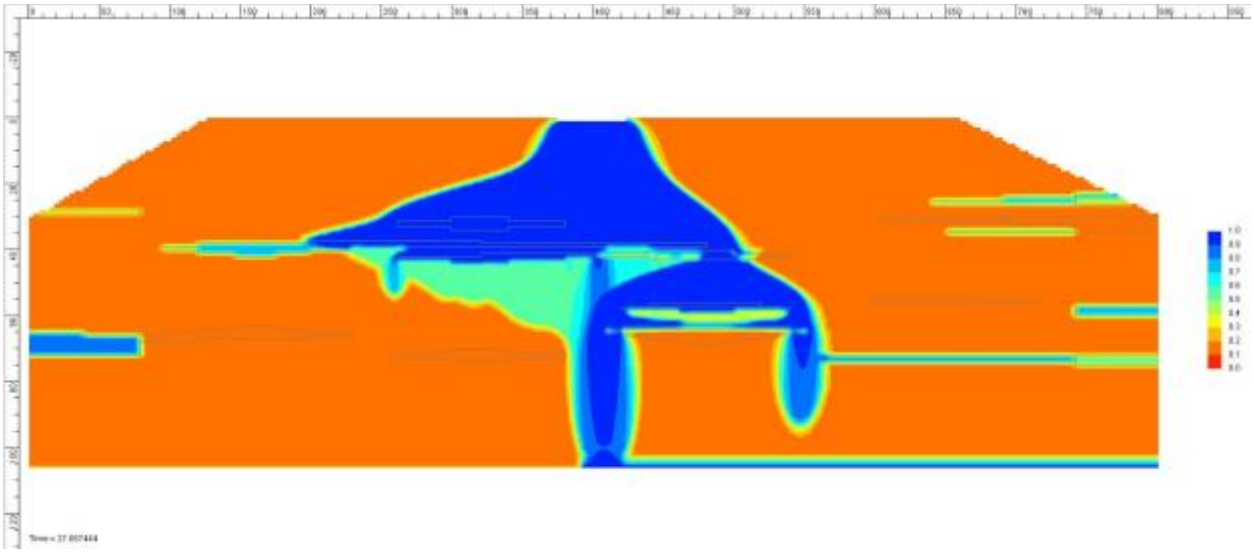

Figure 39: Infiltration basin model at day 27, HBA

Dark blue shows saturated conditions and red shows completely dry conditions with zero moisture content. Residual moisture volumes in pore spaces are shown using a blue to red gradient, and recharge water is seen as the large blue (saturated) section moving from model top to bottom and spreading laterally along low permeability horizons.

Comparing volume of water infiltrated into the subsurface calculated by the model with observed volumes during the pilot program provides another method to test the validity of the model. A perfectly calibrated model would show the same amount of simulated recharge and

observed recharge. Table 17 shows the volume of water infiltrated per day in the three basin models.

Table 17: Simulated and actual recharge rates, HBA

Modeled Basin Depth	Simulated Infiltration Rate (m^3/d)	% Difference from Actual Recharge, 15JAN-03FEB	%Difference from Actual Recharge: 08FEB-20FEB
0.213m	131	27.6%	19.6%
0.5m	138	23.8%	15.3%
1m	143	21.0%	12.3%
*Recharge rate is *per unit width* of 1m. Observed basin stage was less than 0.5m			
Actual average *unit width* infiltration rate (m^3/d) for 15JAN-03FEB 2002*		Actual average *unit width* infiltration rate (m^3/d) for 08FEB-20FEB 2002*	
181		**163**	

The infiltration rates simulated in the model are smaller than the observed infiltration rates and provide less clarity than wetting front travel time for model calibration. Any volume of water moving in three dimensional lateral dispersion during initial wetting at the AWWA project was not captured in VS2DTI even after 2D-to-3D interpretation. This could account for some of the "missing" volume of water from VS2DTI. During the AWWA study infiltration rates during two periods of uninterrupted basin operation averaged 181 m^3/d and 163m^3/d. These values can be thought of as the observed "steady state" for the infiltration basin. The modeled infiltration rate for a basin with 0.213m of ponded water has a 27.6% and 12.3% difference from these two observed rates. The model results using 1m of ponded water, which is higher than observed during most of the AWWA project, has a 21.0% and 13.1% difference from these observed rates.

The absence of evaporation in the model may also contribute to the higher volume of observed recharge compared to modeled recharge. The simulations provide a value only for water crossing the flux boundary and entering the model, whereas the volume rate for the pilot study is the total flow into the infiltration basin required to maintain a constant ponded depth at the surface of approximately 0.3m. Once the water was applied to the infiltration basin, some would evaporate and the rest would infiltrate. This would result in a higher observed volume.

The year-2002 lake surface evaporation rate for the HBA area was 2.65 inches per month in January and 3.31 inches for February (Texas Water Development Board, 2017). Precipitation during the same period was negligible, <1in for either month. Using the evaporation data, a refined difference between actual and simulated infiltration can be obtained, which provides a modest reduction in difference between simulated and actual infiltration (Table 18):

Table 18: Simulated and actual recharge rates with evaporation, HBA

Modeled Basin Depth	Simulated Infiltration Rate (m^3/d)	% Difference from Actual Recharge, 15JAN-03FEB	%Difference from Actual Recharge: 08FEB-20FEB
0.213m	131	26.8%	18.6%
0.5m	138	22.9%	14.3%
1m	143	20.1%	11.2%
*Recharge rate is *per unit width* of 1m. Observed basin stage was less than 0.5m			
Actual average *unit width* infiltration rate (m^3/d) for		Actual average *unit width* infiltration rate (m^3/d) for	
179		**161**	

Another consideration that may cause differences in modeled and observed recharge is the model's two dimensional volume of water output being converted to three dimensions. A direct comparison from 2D to 3D is difficult to make because water in a 2D simulation spreads down in the *z* direction and laterally in the *x* direction, whereas in the real-world 3D application water can also spread laterally in the *y* direction. The observed volume of water infiltrated during the AWWA project may include a fraction that spread in the *y* direction which was not modeled in VS2DTI. Water flowing laterally like this does not contribute to a change in wetting front arrival time at the water table, even though it is a greater volume infiltrated per unit width of the basin than was modeled. The 2D-to-3D conversion of model results does not consider any water that may flow in the *y* direction.

6.1.3 Additional Unsaturated Simulations

Four different depths of vadose zone wells were modeled. The primary well depth considered was 33m BGL, or 1/3 of the distance to the water table, as defined in the hypothesis.

This 33m depth was referred to as "Well Model #8" (WM8), since it was the eighth version of the model that provided the best fit to observed data. The three other well depths modeled were at 20m BGL (WM9), 50m BGL (WM10), and 45m BGL (WM11). Well model #9 was the shallower well and well models #10 and #11 were chosen to simulate a vadose well screened below and partially below the first perching layer.

In addition to simulating several well depths, the height of the water column in the wells was varied to observe the effects on vadose recharge. The model assumed that water would quickly fill the well to the modeled water column height and recharge rate could be adjusted to maintain this height. This assumption was also made by Handel (et al. (2014) and is analogous to what was done during the AWWA recharge study where water column height was maintained between two predetermined elevations (AWWA, 2003). During the AWWA project three combinations of water column heights were attempted until ultimately flow was adjusted to maintain a constant water column height within the well. The various well models and a description of their differences appears in Table 19.

Table 19: Wells simulated, HBA

Well Name	Depth of Well (m BGL)	Height of Water Column in Well (m)	Notes
W8.1	33m	8	Well Model #8 screened entirely above perching layers
W8.2	33m	10	
W8.3	33m	12	
W8.4	33m	14	
W8.5	33m	33	"Full" well
W9.1	20m	10	Shallow Well
W10.1	50m	10	Screened below first perching layer
W10.2	50m	15	Screened mostly below first perching layer
W11.1	45m	10	Screen centered on first perching layer
Awwa RF Well	49-28m	21.5-15	Water column height was adjusted three times to within the three ranges annotated. After the third adjustment, flow rate was reduced to maintain a steady water height.

This table is a summary of the different well parameters simulated in the HBA unsaturated zone models.

6.2 Saturated Zone Modeling

6.2.1 Saturated Zone Results

(a) Iteration #1

An infiltration rate of 441.54 m^3/d was used for both the infiltration basin and vadose zone well. This number was chosen by interpreting two dimensional results of VS2DTI modeling for a "full" vadose zone well (WM8.5, Table 19) and then scaling up to three dimensions.

Results show almost no difference in water table elevations between the two models, except for the area adjacent to the well. Figure 40 shows water table contours created by subtracting the difference between water table heights in the vadose zone well model from the water table from the infiltration basin model. In the immediate vicinity of the well (center of

image) there is a maximum rise of 2.7cm and a progressive decrease in water table height difference as difference increases radially from the well. Stated simply, if recharge rates for the two structures are the same in both models, the vadose zone well creates a water mound only 2.7cm higher than that created by recharge from the infiltration basin.

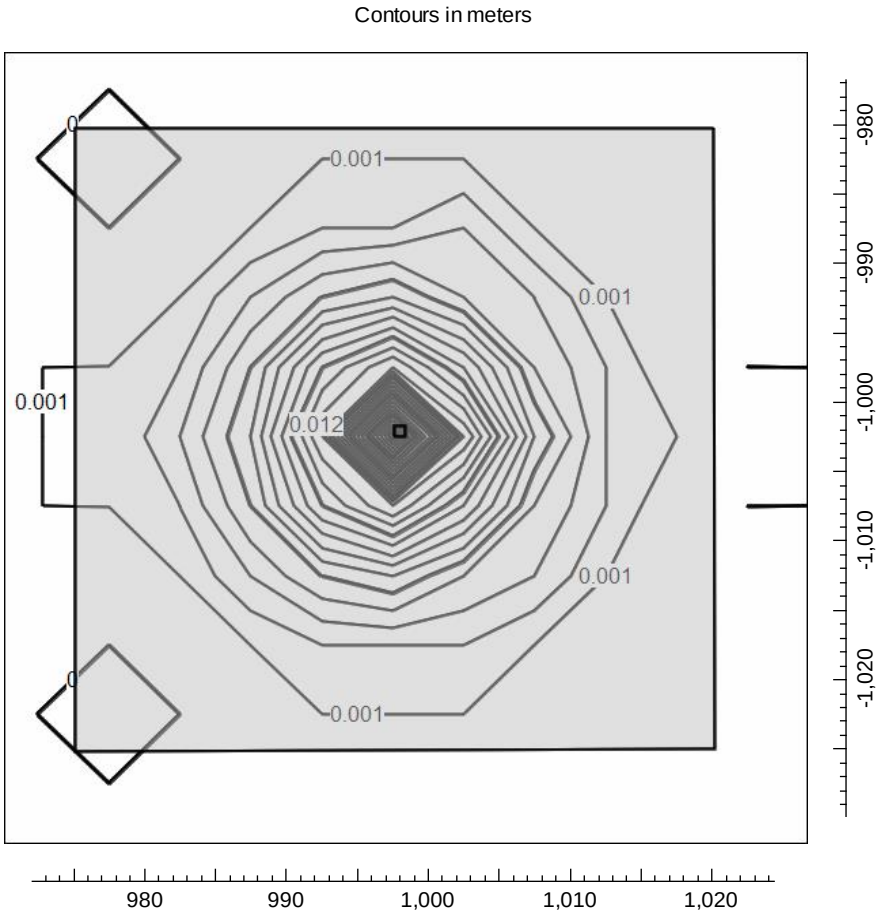

Figure 40: Water table height difference @ Day 90, 0.1mm contours, iteration #1, HBA
Shaded area is the infiltration basin. Vadose zone well is in the very center of the image. Contour intervals are 0.1mm.

The small difference between infiltration basin and vadose zone models is expected when recharge rate is equal for both setups. The high permeability of the HBA aquifer allows for rapid movement of water laterally away from the recharge source, creating a very flat water table mound even directly beneath the recharge structures.

Given the scale of the model ($4km^2$) compared to the scale of the recharge basin ($0.002km^2$) and the input parameter placing recharge immediately at the water table below each recharge structure, the infiltration basin almost appears as "point source" of recharge in the saturated zone simulation (the vadose well, of course, IS modeled as a point source of recharge). Beyond proving a slightly different water mound shape produced from the two recharge structures, iteration #1 does little to answer the research hypothesis.

(b) Iteration #2

Iteration #2 used the VS2DTI calculated infiltration values as the recharge input for the saturated zone model. The vadose zone well model used the "full" well rate of 441.54 m^3/d for a 33m deep well (WM8.5). The infiltration basin used the rate calculated for 1m deep ponding conditions of 6,435 m^3/d, since this value was closest to the value observed at the AWWA project.

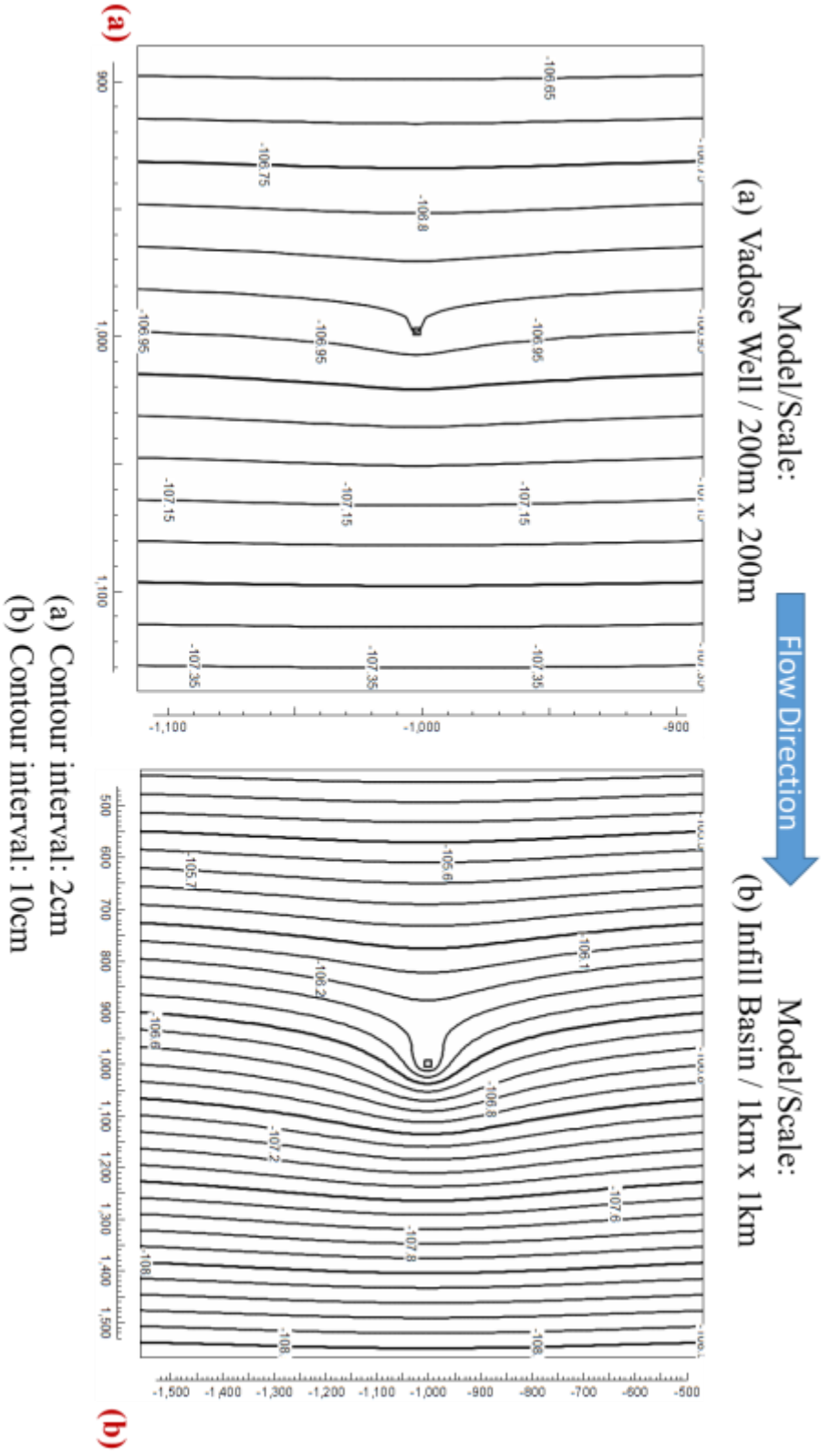

Figure 41: Water table rise @ day 90, iteration #2, HBA.

Results (Fig 41) show a larger increase in water table elevation in the infiltration basin model. This is not surprising given the much greater infiltration rate used in the basin model. Even though it is clear more water infiltrates in the basin model, storage values must be considered for a complete understanding, just as they were for the SLA model. Recall that in these unconfined models, change in head is synonymous with water table change. Storage values are then the volume of water retained in the cells as the water table rises due to recharge in the HBA model. There is a natural groundwater flow gradient created by establishing fixed head values along the east and west boundaries of the model. Although the effect of this gradient is too small to be easily detected on contours of water table height, it nonetheless exists. Some of the recharged volume flows across these boundaries and "disappears" from the model. Water that does not cross the boundaries but is retained in the model area contributes to an increase in storage. Storage values are the "actual" volumes of recharge within the model boundaries. Table 20 provides values for cumulative recharge and storage for iteration #2.

Results from iteration #2 provide clear evidence in support of the hypothesis that a vadose zone well will recharge a greater volume of water to a well 402m away**. Instead, an infiltration basin is capable of a much greater volume of recharge over a given period of time, and this greater recharge through the vadose zone ultimately creates a higher water table 402m away from the recharge structure** (Fig. 41).

Table 20: Saturated zone model outputs, iteration #2, HBA

	Day 30- Infiltration Basin	Day 30- Vadose Well	Day 30 Difference	Day 90- Infiltration Basin	Day 90- Vadose Well	Day 90 Difference
Cumulative Recharge (m^3)	192,238.14	13,246.20	178,991.94	576,714.44	39,738.60	536,975.84
Water in Storage (m^3)	117,375.30	8,090.02	109,285.28	153,698.34	10,595.00	143,103.34
Rate of Storage Influx (m^3/d)	2,000.32	137.90		173.51	11.97	

After vadose and saturated zone modeling was complete a final check on recharge volume accuracy was done by converting the modeled recharge volumes to acre-feet and comparing it with values from historical data published by EPWU. After thirty days of infiltration through a modeled basin the total volume recharged was 155.85 AF (192,238.14 m^3). Historic data from 2014 indicate the recharge through infiltration basins varied from a high of 340.65 AF in January to a low of 42.96 AF in June. The average infiltration for 2014 was 199.48 AF/month. During the first few months of 2017, infiltrated volume at the cluster of four southern basins that ran for a continuous month averaged 78.78 AF/month per basin. During this time three of the four basin were typically running and each basin is slightly smaller than 0.5 acres. Monthly totals through May are given in Table 21. EPWU does rotate through several infiltration basins instead of using just one, so the recharge values are not perfectly comparable, but the comparison indicates that 155.85 AF of recharge in the saturated zone model is a reasonable quantity of recharge. The author has observed basins 9E, 9W, and 8N receiving inflows of approximately 600 GPM (2.65 AF/D, 82.15 AF/M) which sank into the soil without ponding. EPWU historical data for 2014 is available in Appendix L.

Table 21: EPWU recharge volumes, Year 2017

	Volumes (AF)			
Month	**Basin 8N**	**Basin 8S**	**Basin 9W**	**Basin 9E**
Jan	50.025	27.396	82.188	82.188
Feb	0.000	74.234	74.234	74.234
Mar	0.000	82.188	70.285	82.188
Apr	3.369	48.606	64.955	58.106
May	65.176	0.000	56.688	56.688

6.3 Microgravity Survey Results

6.3.1 Initial Results

Microgravity readings must undergo several layers of corrections before accuracy is assured. At the most fundamental level, a microgravity reading is supplied as a *counter reading* that is converted to milligals using an interval factor unique to each instrument. Even these values are not a direct measure of gravity in a narrow sense, since the instrument is designed to measure relative gravity. To determine the absolute gravity at a site, the milligal value obtained from the counter reading must be calibrated at two calibration stations. Corrections for this project were applied using instrument-specific values in the formula:

$$dg_{corrected} = dg * 41.43866 + 43.246$$

Equation 13: Microgravity correction factor

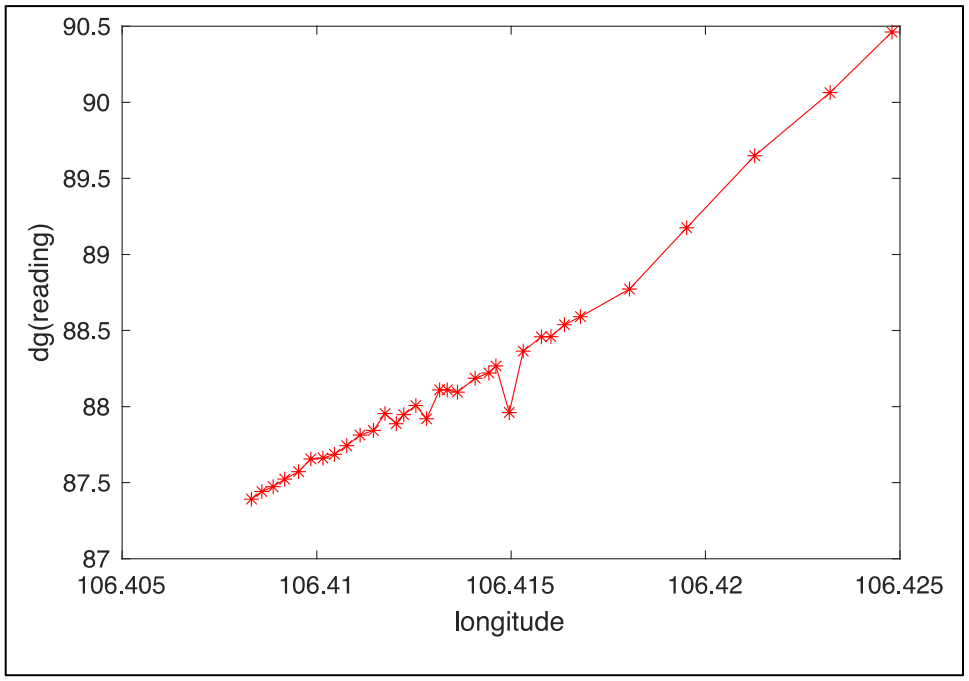

Figure 42: Uncorrected microgravity readings, East-West transect

Corrections must then be applied to account for topography. To correct for topography we apply the Bouguer correction. The correction was made to account for the Franklin Mountains, located west of the study area and believed to cause the large regional gravity trend observed in the data (Fig. 42). This was accomplished by removing the five outlying points,

which represented measurements made closest to the mountains and furthest from the infiltration basins, and fitting a straight line, shown in blue, to these points (Fig. 43a). Corrections were made by fitting the blue line in MATLAB and removing the slope. Relative gravity change along this transect was then plotted (Fig. 43b).

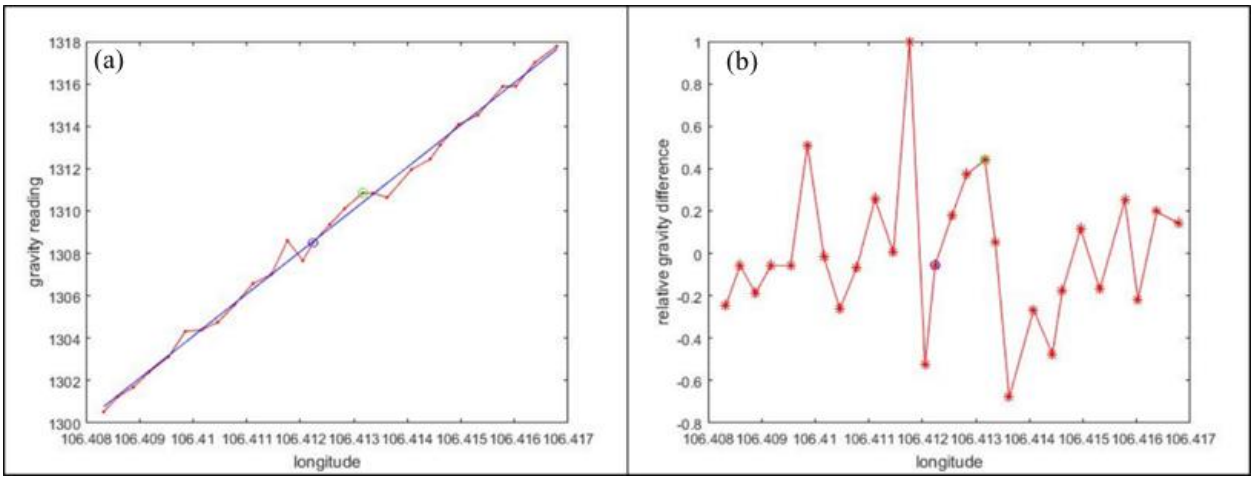

Figure 43: Gravity readings plotted against longitude

The north-south transect was also corrected to account for drift but the Bouguer correction was not applied because this profile ran parallel to the Franklin Mountains (the expected density anomaly). The corrected results are shown in Fig. 45.

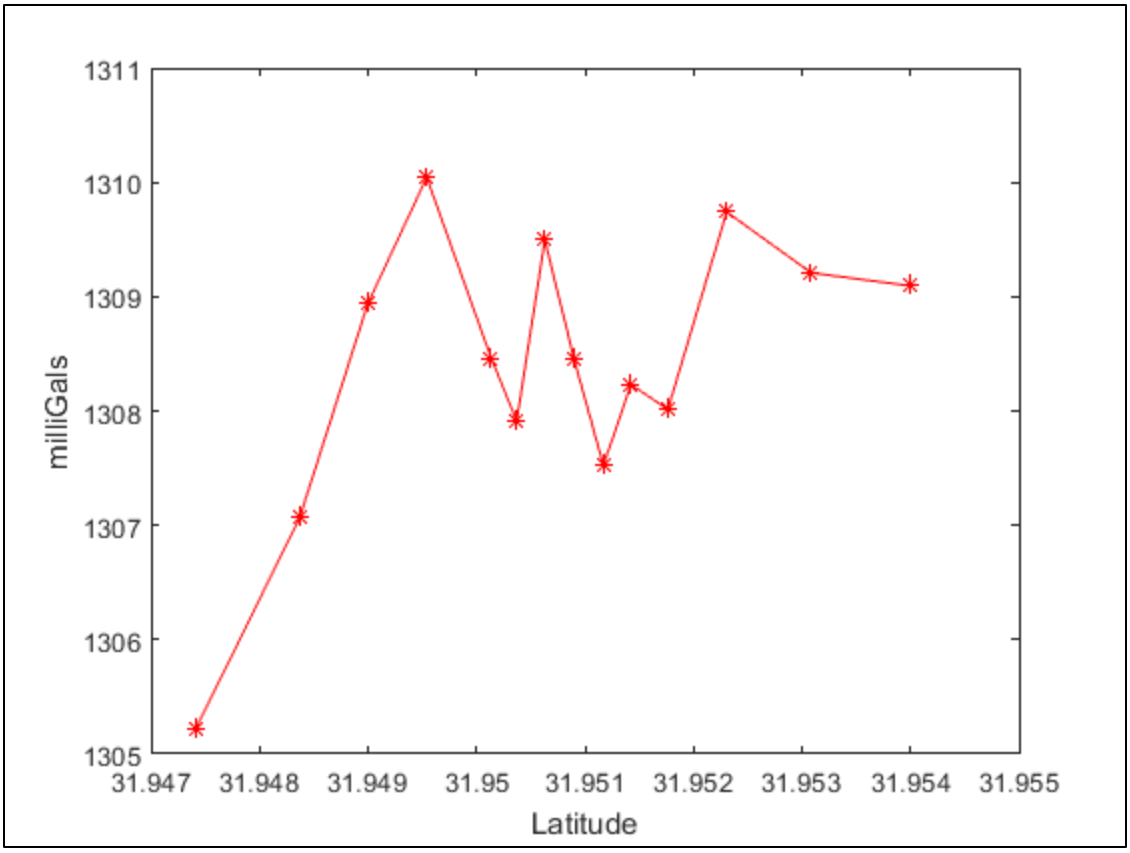

Figure 44: Gravity readings N-S transect plotted against latitude

Final analysis of gravity data will be made following the second survey to provide contrast between the low infiltration summer month and high infiltration fall month, but initial results show areas that appear to have some volume of infiltrated water affecting the gravity values. These are shown in Fig. 45.

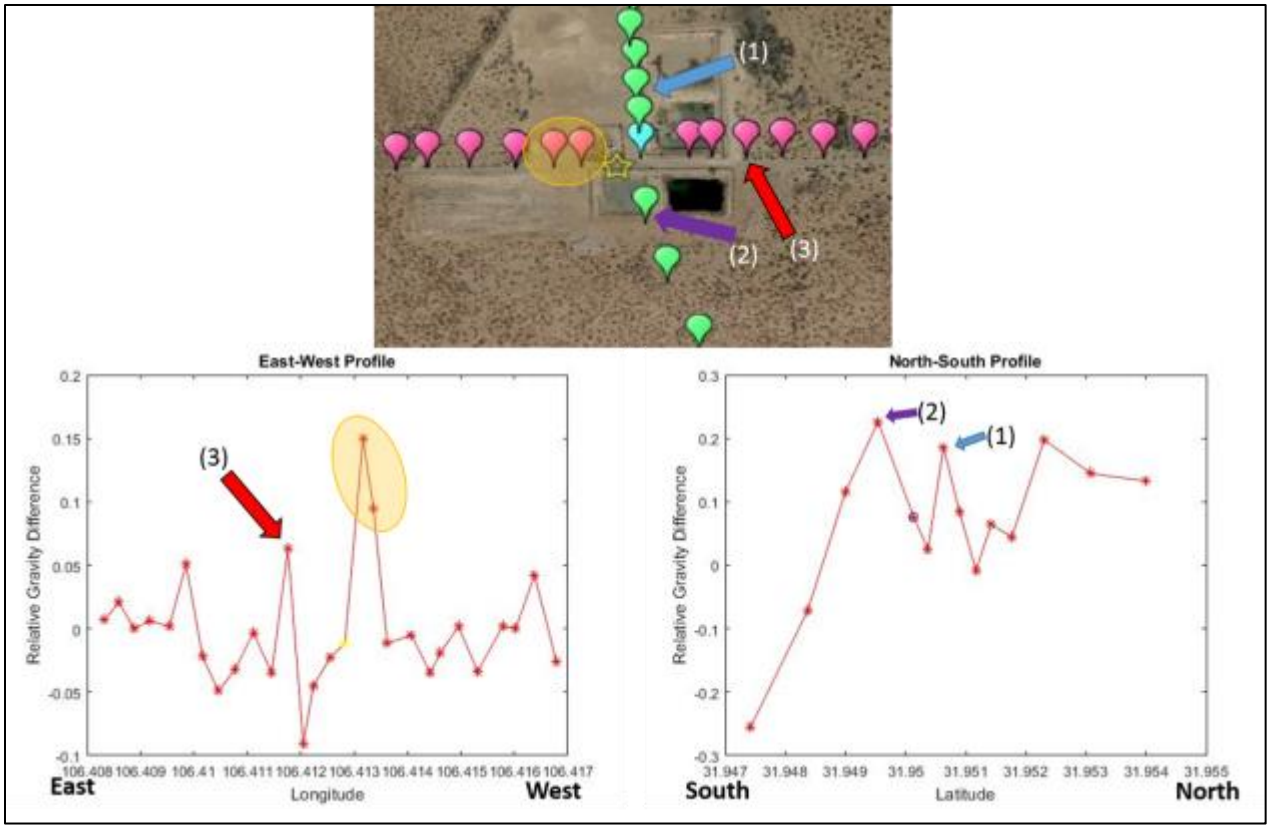

Figure 45: Areas of initial interest, HBA

(1), (2), and (3) represent relative gravitational highs adjacent to basins which were actively receiving water during the microgravity survey. The tan shaded area represents the location of a proposed preferential flow path to the northwest.

Locations (1) and (2) on the N-S transect (Fig. 45b) are gravity anomaly highs adjacent to infiltration basins which were actively receiving water during the survey. The high measurements are reassuring, because the influx of water should result in higher gravity readings. Location (3) on the E-W transect (Fig. 45a) is also located next to an active infiltration basin. Lithologic variation could also produce high readings but on such a small spatial resolution, reading changes from lithology could be expected to be seen across multiple adjacent points. To confirm this, the subsequent survey will have even finer spatial resolution between points near the basins.

Location (4) (left side, Fig. 45) is a little more enigmatic. This location may represent a local perched layer. Follow on field work should assist in resolving these gravitational readings. If this does represent a local perched layer, gravity readings taken during a second survey in the fall should measure even higher to account for the additional water recharged by EPWU during the "wet" fall month. If the gravitational reading trend is not caused by a perched layer, the same readings can be expected.

6.4 Soil Grain Size and Permeability Analysis Results

6.4.1 Grain Size

Under the Unified Soil Classification (USC) System, 95.99% of the sample consists of sand-sized particles. The remaining 3.99% are "fines" and 0.02% of the sample volume was not recorded during the sand procedure analysis.

The sample was very well sorted with a single bell-shaped curve (Fig. 46). Peak particle size occurs between 0.586mm and 0.666mm diameter, making the USC designation for the sample *SP* for sand, poorly graded. "Graded" refers to the mix of particle sizes. Samples with a single dominant size are said to be poorly graded or well sorted—the terms "graded" and "sorted" having an inverse connotation. -Gravel-size particles weren't sufficiently abundant to give the sample a "gravelly sand" designation.

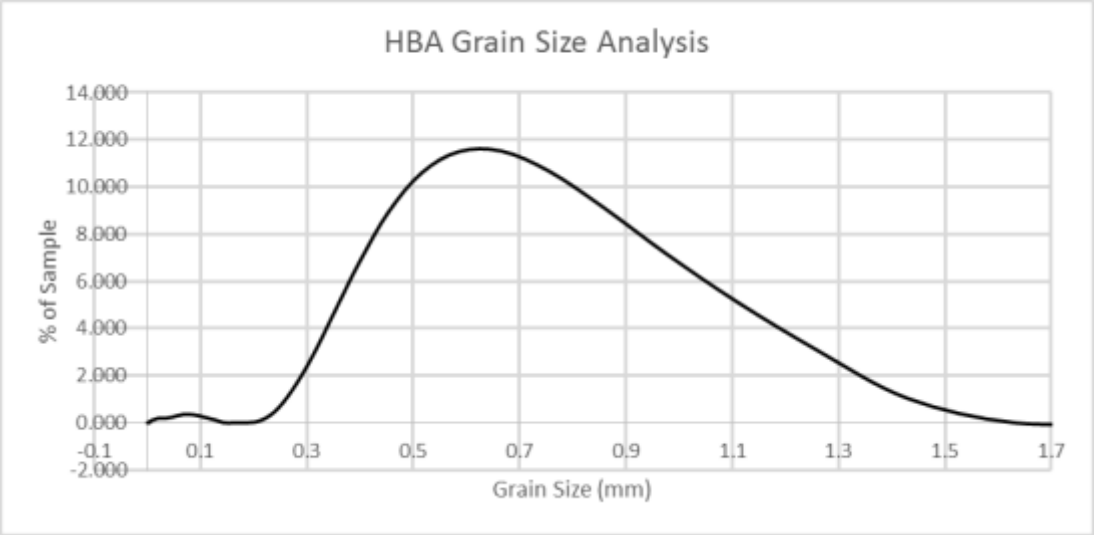

Figure 46: HBA grain size analysis

Laboratory analysis using the Mastersizer 3000.

The Wentworth scale may be used to further refine the range of sand sizes (Table 22).

Table 22: Wentworth Scale, sand fraction of HBA soil sample

	Very Fine Sand	Fine Sand	Medium Sand	Coarse Sand	Very Coarse Sand
%Volume of Sample	1.67	0.56	35.31	49.95	9.21

The sand fraction of the sample was 96.7% of the sample according to the Wentworth scale.

The author would like to speculate that the silt-size fraction of the sample, although small (<4% total), may have an effect on basin infiltration rates. Furthermore, the curve of grain size shows a small secondary peak centered on the silt-sand diameter boundary. Since the sample was taken from near surface, the author proposes that particles around these sizes are aeolian transports into the infiltration basin, not sediments deposited by the ancestral Rio Grande River. Further research may be considered to determine whether these silt-size grains are, in fact, aeolian and, if so, the rate / timing of their deposition in the basin as well as the effect they may have on basin infiltration rates.

6.4.2 Permeability

Results from the permeability analysis returned hydraulic conductivity values higher than anticipated for the HBA. The average *K* value from all four tests is 0.0533 cm/s, or 46.05 m/d. This value is within the range expected for coarse sands (Fetter, 2005, Bell, 2006; Gangopadhyay, 2013) and, therefore, in agreement with the grain size analysis reported above. The most likely explanation for the higher-than-anticipated *K* values is the lack of soil compaction during permeability testing. Soil was sampled only from the surface of the infiltration basins in El Paso. These basins are subject to frequent reworking by earthmoving equipment to prevent clogging and encourage high infiltration rates. The sampled basin appeared to have been recently reworked due to the complete lack of vegetation growing in the basin area. Procuring the sample produced a disturbed sample that was less dense than *in situ* soil.

Further research should be conducted to validate the hydraulic conductivity of the soil horizon at the bottom of infiltration basins. The author proposes that a high *K* value approaching 46.05 m/d is correct for soil at the surface in the infiltration basins, but is not representative of the overall aquifer matrix, which has a lower hydraulic conductivity more similar to the 21 m/d value chosen in the model.

Testing of *in situ* density at the basin could be translated to degree of compaction. Samples being prepared for laboratory permeability analysis could be tested first for density to see whether they are similar to *in situ* density results. Alternatively, undisturbed samples could be taken from the infiltration basins and tested. Using a technique like a split spoon sampler or thin wall tube would produce a mostly undisturbed soil sample and provide a deeper sample than the shovel technique used in this research.

Chapter 7 - Discussion

"Groundwater has become an interdisciplinary subject. Professionally, it is no longer the almost exclusive domain of hydrogeologists and engineers; it is also receiving a good deal of attention from economists, sociologists, ecologists, climatologists, lawyers, institutional experts, communication specialists and other. Analysis groundwater from these different perspectives puts it in a wider context, resulting in changing views on this natural resource." –Jac van der Gun, United Nations World Water Assessment Programme

7.1 Overview of the Discussion Section

Making models of two dissimilar sites, as was done for this thesis, provides detailed insight into *how* water moves through those exact location, including volumes infiltrated from the two different recharge methods. Understanding *why* water moves the way it does requires some additional interpretation. In SLA models it was clear that boundary conditions and depth to water table influences the shape of water mounds in homogenous aquifers. From the shape of these water mounds and the infiltration rates it became apparent that infiltration rate is negatively correlated with shallowly sloping water mounds. In HBA models it was clear that heterogeneous lithology can create perched layers leading to vadose zone water mounds. These water mounds also reduced infiltration rates.

This discussion section extends that results from HBA and SLA models in an attempt to draw some general conclusions about water mounding from vadose well recharge. Specific results as outlined in the two chapters above will be referenced, but this section will also introduce additional, simplified models. Section 7.2 of this discussion will be based on the SLA model and define how water mounds affect infiltration rates from basins. Subsequent sections explore how water mounds affect infiltration from vadose wells, especially when these mounds

are created by perched conditions in heterogeneous vadose zones. Finally, section 7.5 lessons learned from extending SLA and HBA results is used to demonstrate how perched conditions could affect the design of vadose wellfields in a "real world" application.

Results from Chapters 5 and 6 shows quantitatively that a single vadose well cannot achieve recharge rates comparable to an infiltration basin when the vadose well is screened above perching layers. This is true at both locations, including the SLA location when using revised boundary conditions (discussed below). Also quantitatively proven by this research is that a vadose zone screened above perching layers will create a water table mound similar but not identical to the mound caused by an infiltration basin. Since the vadose well is above the perching layers, water from the well mounds above and must still travel horizontally along perching layers just like water recharged from the infiltration basin. The small "head start" the water receives by being recharged some depth below the surface does not make much difference if low permeability layers are deeper than the start depth.

7.2 Boundary Conditions, Infiltration Rates, and Darcy's Flow

7.2.1 Boundary Conditions

Chosen boundary conditions used to constrain the vertical left and right limits of SLA models had a significant influence on recharge rates. By considering only a 600m cross section of aquifer, the shape of the water mound from infiltration basin or vadose well was artificially constrained. To determine the actual shape of water mounding from these recharge methods, additional unsaturated zone models were run with cross sections ranging from 800m to 2,500m. At a width of about 1,500m, the recharge rate at ten days stabilized and no change to water mound shape occurred in subsequent model runs with greater cross sectional widths (Fig. 47). This implies that the SLA model described in chapter 4 should have used a minimum model

cross section of 1,500m instead of 600m and demonstrates how important correctly sizing boundary conditions can be in a model. Expanding the expected infiltration volumes to three dimensions also gives a reduced total infiltration rate-approximately half the rate given in chapter 5 (Table 23).

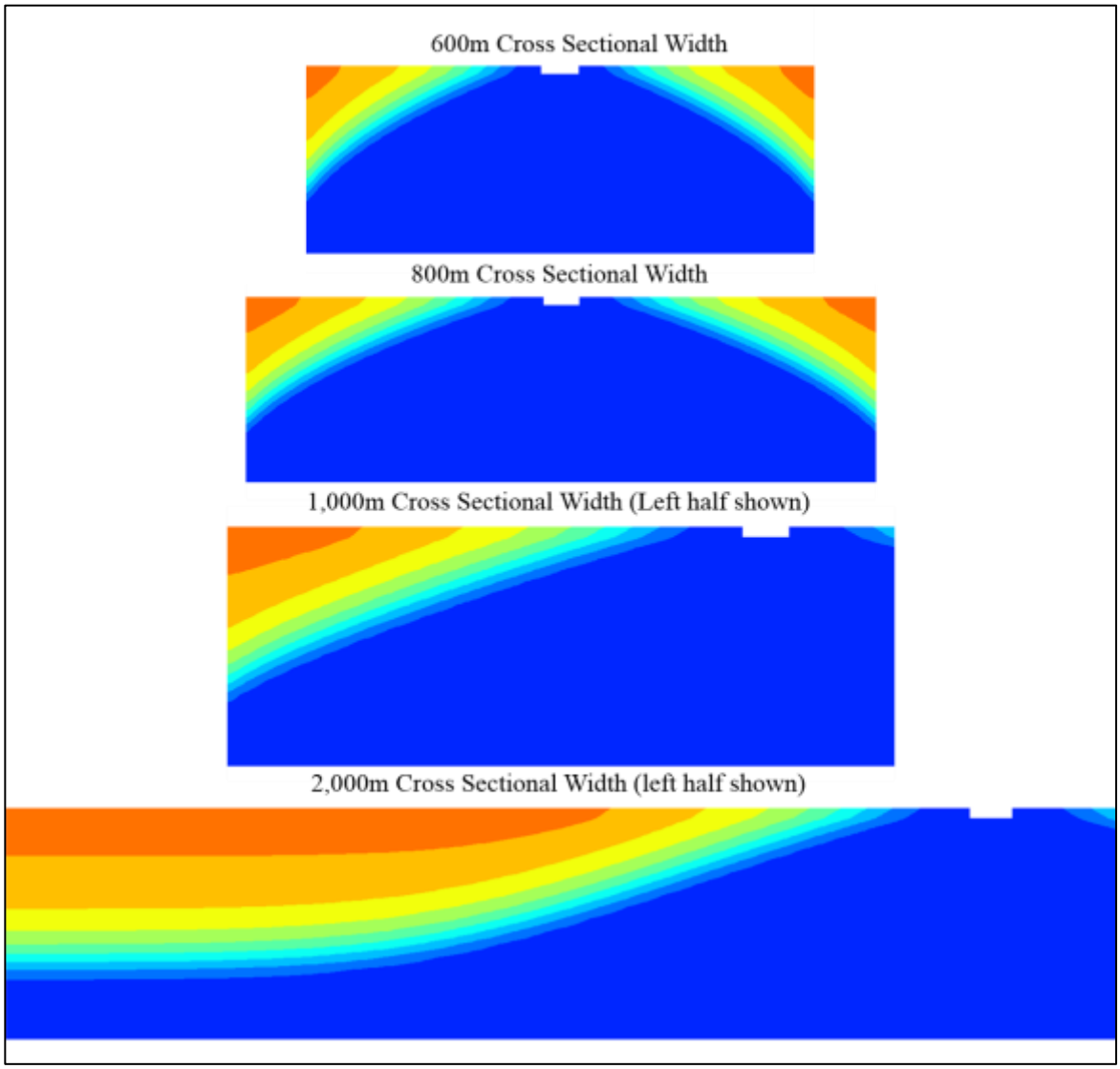

Figure 47: Water mound shapes at various cross sectional lengths

Dark blue represents saturated conditions. Water mounding shape is influenced by vertical boundary conditions unless these boundary conditions are sufficiently distant from the recharge location.

Table 23: Revised infiltration volumes, SLA model

Cross Sectional Width of Model (m)	2d Infill Rate (m^3/d)	3D Infill Rate (m^3/d)
600	284.88	12819.6
800	160.8	7236
1000	142.56	6415.2
1500	138.72	6242.4
2000	138.72	6242.4
2500	138.72	6242.4

With the reduced infiltration rate observed when using the modified boundary conditions (6,242.4 m^3/d instead of 12,819.6 m^3/d), the total standing water column that would pass through the basin floor in each twenty-four hour period is just over 3m. This is a large amount of water and would necessitate rapid subsurface flow but falls in the range of observed volumes infiltrated through basins of similar size. An example of such large flow volumes into a similar sized infiltration basin occurred at El Paso during the 2002 American Water Works Association aquifer recharge feasibility study. Maximum flows into a 0.4 acre basin were recorded as high as 1,500 GPM, or 8,176 m^3/d (AWWA, 2003). This corresponds to a water column 5.05m tall infiltrating in a 24-hour period, greater than the modeled 3.07m tall water column in SLA simulations done with revised boundary conditions. The overall lesson from is that boundary conditions strongly affect model performance and ensuring correct boundary conditions can ensure a model provides realistic, real world results.

The reduced infiltration rates do not change the major findings of this thesis- the chosen vadose wells still do not infiltrate water at rates similar to infiltration basin. Revisiting the SLA model results with the new value of flow from an infiltration basin (6,242.4 m^3/d) shows that 15 vadose wells would be required to achieve that same infiltration rates. While this number is certainly smaller than the 30 wells required when using 600m cross section boundary conditions

as stated in chapter 5 *results* it is still not close to approaching equivalency between the vadose well and infiltration basin recharge rates. Further complicating recharge comparison is the effect of low permeability layers, discussed in section 7.3 and 7.4.

7.2.2 Darcy Flow and the Reynolds Number

Both modeling programs used in this research are based on variants of Darcy's law and understanding limitations to Darcy's law is important to understanding how model flows affect results. Darcy's law is valid when groundwater flow in laminar, which experimentation has shown to occur when the flow's Reynolds number is less than 1-10 (Fetter, 2001, Hornberger et al., 1998). The Reynolds number equation is:

$$R = \frac{\rho q D_{10}}{\mu}$$

Equation 14: Reynolds number equation

where ρ is the density of the flowing water, q is the discharge velocity of the water, D_{10} is the effective grain size, used as a proxy for the diameter of passageways through which fluid can move, and μ is the viscosity of the flowing water.

While it is sufficient to assume most natural groundwater flow is laminar, occurring at Reynolds numbers less than 1, areas of steep hydraulic gradient, such as occurs in the vicinity of a well or the interface between recharged water and the water table, can result in much higher Reynolds numbers (Fetter, 2001). It is possible to determine the maximum q value which satisfies laminar flow. Using the revised value for infiltration basin flow given in section 7.2.1 (3.07 m/d), R is found by the following equation:

$$R = \frac{(1000\frac{kg}{m^3}\left(\frac{3.55 * 10^{-5}\frac{m}{s}}{0.3}\right)0.001m}{0.00114\ \frac{kg}{s * m}}$$

where all values are directly substituted for variables in *equation 14* except for *q*, which is determined as the infiltrated water column (in seconds, not days) divided by porosity to give velocity. The Reynolds number *R* calculated above is 0.1, which satisfied Darcy's law and by extension the governing equations used in the model.

7.3 Low Permeability Horizons and Infiltration Rates

7.3.1 Effect of Perched Layer on Vadose Well Recharge Rate

Most surprising was the discovery of the negative effects to recharge that are created by a poorly placed vadose well. This concept is explored further in this chapter, but by choosing to place the vadose zone well at 33m depth with a 10m high water column, conditions were created to drastically reduce recharge rates from their maximum potential. At 33m depth in the HBA there is one perching layer 5m below the well and another layer directly adjacent to the well at 32m depth (Fig. 48). Almost immediately after recharge began perched conditions formed on these layers. Perched water on the layer below the well created a water mound adjacent to well screen, decreasing hydraulic gradient between the well screen and the aquifer matrix.

Here the math on how this reduces water flow. Darcy's law (equation 6, chapter 4) states that flow volume (*Q*) is proportional to hydraulic gradient (*i*). When no water is mounded adjacent to the well screen the only pressure is atmospheric in the aquifer matrix but the hydraulic head inside the well is the entire water column (plus atmospheric pressure) so hydraulic gradient (*i*) approaches its maximum possible value because $i=\frac{\Delta h}{\Delta d}$ (change in head between well and aquifer matrix divided by change in distance across the screen). However, when different hydraulic heads exists at two distances, such as the hydraulic head from the well and the hydraulic head from the perched water mound, *i* can become small. The higher the perched water mounds along the well screen the greater the hydraulic head "pushing back against" water flow from the well.

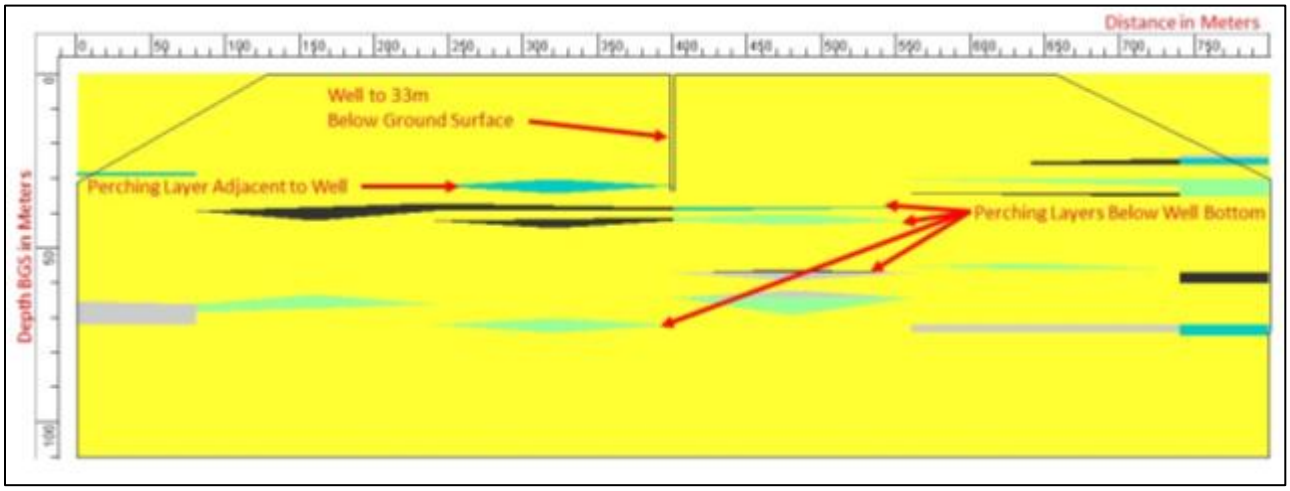

Figure 48: Pre-recharge conditions for HBA well model #8.3

Lithologic horizons that created perched conditions. Yellow indicates the area is aquifer matrix.

7.3.2 Effect of Perched Layers on Basin Recharge Rate

Perched layers can affect infiltration from basins. If the depth to water table below an infiltration basin is small, flow from the basin will be mostly lateral and controlled by the slope of the water mound (Fig. 49a) (Bouwer, 2002). This is also true if the water table in question is formed by a perched aquifer provided the perching layer has sufficient lateral extent. At locations with deeper water tables flow is controlled by gravity with flow occurring mostly in the vertical direction (Fig. 49b). Bouwer (2002) states that for basins which run for long periods of time without clogging, such as are observed in the HBA and modeled during this research, infiltration rates are affected by the depth to water table below the surface of the basin only if this depth is less than twice the basin width or diameter ($2W < Dw$, where W is basin width and Dw is depth to water). If the depth to water table is less than twice the width of the infiltration basin, infiltration flow is lateral along the slope of the water table instead of being mostly controlled by gravity in the vertical direction (Fig. 49(a)) (Bouwer, 2002). Infiltration rates decrease almost linearly with decreasing depth to the saturated zone (Fig. 49 (c), when x axis <

2). If the depth to water table (or perched layer) is greater than twice the width of the basin, infiltration rates are not affected by depth to groundwater.

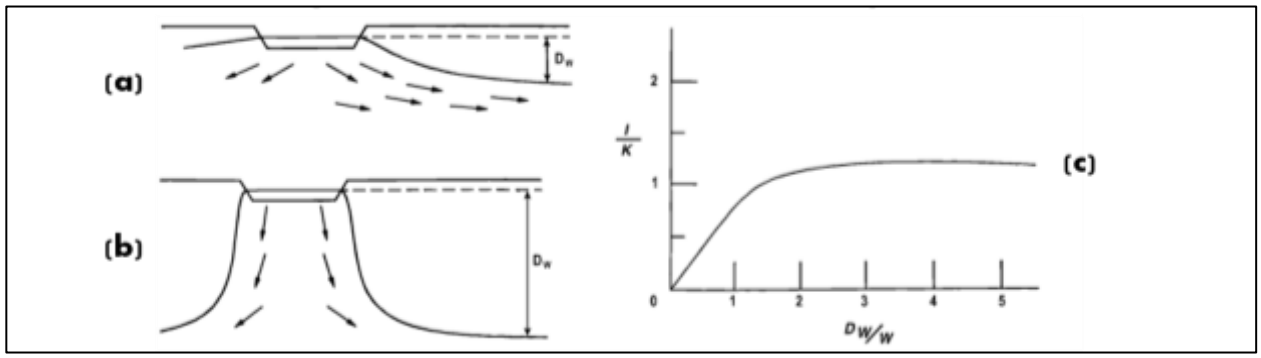

Figure 49: Effect of water table depth on basin infiltration rates, no clogging (Bouwer, 2002)

(a) basin and shallow water table. Infiltration is controlled by the slope of the water mound because the distance from basin to water table is less than twice the width of the basin. (b) basin and deep water table. Infiltration is controlled by gravity, not water mound slope, resulting in greater infiltration rates than in (a). The left image (c) shows a plot of infiltration rate on the y-axis versus the ratio of water table depth to basin width on the x-axis. Beyond a ratio of 2, depth to water table ceases to have an effect on infiltration rate.

While the phenomena has been researched extensively for surface infiltration (Hantush, 1967; Bouwer, 1969; Marino, 1975), the infiltration effect on vadose wells has not been studied so extensively. Depth to water table or a perching layer effects infiltration from vadose zone wells at even greater depths than it does for infiltration basins. Modeled infiltration from a 10m high water column in a 1m diameter vadose well is still measurably affected by a perched layer over 40m below the base of the well.

The linear-type decrease in infiltration rate observed for basins with $2W < Dw$ also appears to occur as the bottom of a vadose well approaches water table or perched layer. These concepts are explored further in the next part of this chapter.

7.4 Isolating the Effect of Perched Layers on Vadose Wells

7.4.1 Vadose Zone Wells Modeled

While attempting to answer this research's hypothesis, the HBA vadose well models provided some surprising data. When water column height was kept equal across all HBA models, the vadose well at 33m BGS recharged less total water than wells screened deeper (45m, 50m BGS) and less than the well screened shallower (20m BGS). It seems to make intuitive sense that a deeper well will recharge more water- after all they're closer to the water table and more likely to be screened below perching layers- but why then did a shallower well (20m) outperform the deeper (33m) one? After reviewing the model results it became apparent that the location of perching layers relative to the well bottom has a significant influence on recharge rates. By happenstance, this research's hypothesis about a 33m deep well in the HBA model placed that well in about the worst possible location to maximize recharge rate. The rate of recharge volume per meter of screen length in well model #8.3 (WM8.3) at a water column height of 10 meters was just over 8.5 m^3/d (Fig. 36, chapter 5).

7.4.1.A Perched Layers below the Vadose Well

Perhaps the most original research in this numerical modeling study was the effect that perching layer have on vadose well recharge rates, and perhaps the best modeled location to see this is 5m below the bottom of WM8.3 (Fig. 47, previous section). This layer began 38 m below ground level and simulates the effect of the first perching layer encountered during the American Water Works Association Research Foundation (AWWA) project.

The modeled infiltration rate from WM8.3 was 85.5 m^3/d and can be contrasted with the rate from a similar model having the same well but no adjacent or underlying perched layers (Fig. 50). This "matrix only" model has an infiltration rate of 200.6 m^3/d. This rate can be

thought of as the maximum possible recharge potential of the aquifer for this well since the perched layers that constrained downward water movement were removed.

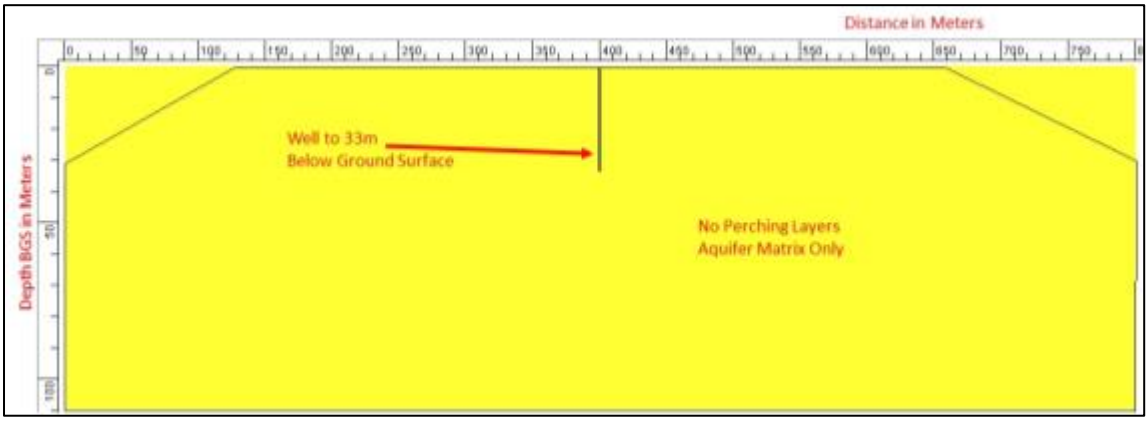

Figure 50: Theoretical maximum recharge potential, HBA well model #88

This study shows the value of 200.6 m^3/d obtained by using the Richard's equation based numerical model is not in agreement with the value expected from Bouwer's equation for flow from a vadose well even after accounting for the additional volume expected if the two dimensional model is expanded to three dimensional flow. The model described in section 7.4.1.A returns 200.6 m^3/d in the model can be expected to produce ~314.94 m^3/d in three dimensions by using a scaling factor of 1.57.

Bouwer's equation is (Bouwer, 2002):

$$Q = \frac{2\pi K {L_w}^2}{\ln\left(\frac{2L_w}{r_w}\right) - 1}$$

Equation 15: Bouwer's Equation for Flow From a Vadose Well. Bouwer, 2002

Where Q is the flow rate, K is the hydraulic conductivity of the soil, L_w is the height of water column in the vadose well, and r_w is the radius of the well. For inputs used in the model, this equation provides a value of 490.46 m^3/d. The author interprets the difference in values to the difficulty in determining an accurate *K* to use in Bouwer's equation and possibly the effects of discretization on apparent well radius in the model. Bouwer stated that, "The proper value for *K* is difficult to assess because the wetted zone is not always saturated and the streamlines have horizontal and vertical components, which complicates matters for anisotropic soils." A *K* value of 1.348 m/d will make Bouwer's equation result in 314.94 m^3/d; on the scale of *K* values for sand this is not a very large difference from the 2.1 m/d used as K_v in the model and is within the range of expected values for sand (Fetter, 2002).

To determine the effects of a perched layer 5m below a well, a series of simplified models were conducted based on the HBA well #8 (WM8.3). These models stripped out all except a single perching layer so the effects of that single layer could be analyzed (Fig. 51). All boundary conditions and recharge parameters were left unchanged from those used in the original HBA WM8.3 simulation. These wells were recorded as "well #88" (WM88) to denote that they were based on the original HBA model. A similar set of models, denoted as well #99 (WM99), also be discussed. These models differ from WM88 in that the perched layer is laterally continuous across the model.

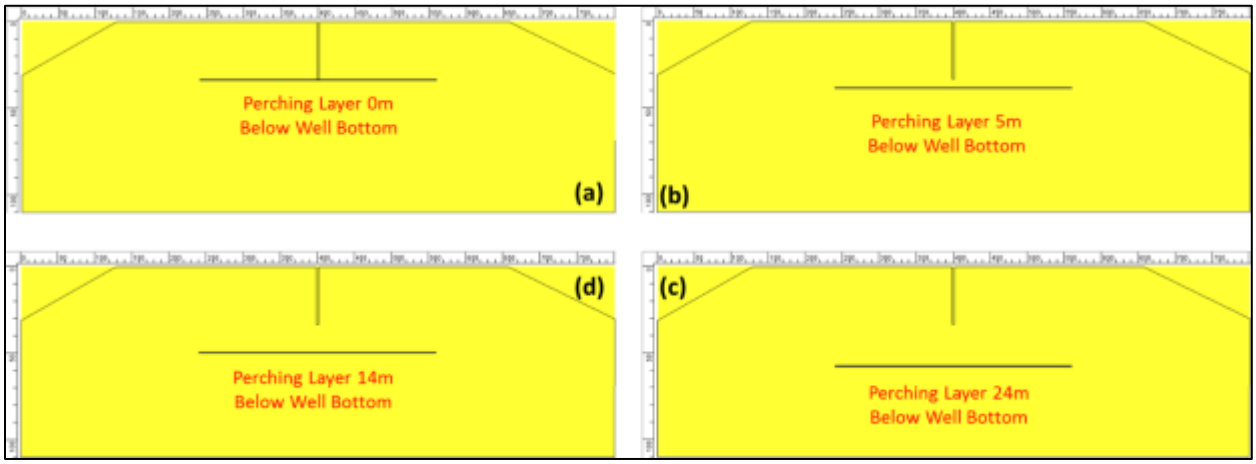

Figure 51: Four examples of HBA well model #88

Table 24: Recharge Rates Associated with Fig. 52

Depth to Perched Layer	Unit Width Recharge Rate (m^3/d)
0	54.5
5	85.5
14	128.5
24	161.7
Theoretical Maximum Recharge	
N/A	200.6

With a perched layer 5m below the bottom of a well, performance is only 48% of its theoretical maximum ($85.5 m^3/d$ compared to $200.6 m^3/d$) . This finding is similar to the concept of decreasing recharge per unit screen length published in Handel et al (2014), however, that research included a low-*k* layer adjacent to the well screen to simulate clogging. The paper attributed changes in recharge rate to variations in horizontal conductivity caused by this low-*k* layer and in the aquifer matrix, not vertical conductivity ("much stronger dependency on the horizontal component of hydraulic conductivity than on the vertical component," Handel et al., 2014). This research indicates that vertical conductivity, especially the presence of perched layers with conductivity values orders of magnitude lower than the aquifer matrix, also strongly affects recharge rates.

The tests were rerun with the perching layer extending completely across the model domain to determine if lateral extent of the layer had an effect on infiltration rates from the well. Left and right vertical boundary conditions remained "possible seepage face" to simulate aquifer continuation (but not perching layer continuation) by allowing water to exit the model, creating the effect of an end to the perching layer 400m away from the well in either direction. Surprisingly, there was no significant change in recharge rate. Models run for 50 days, at which point the infiltration rate was assumed to have reached steady state, show the same recharge rate for W88 models with a non-continuous perched layer and the W99 models with a continuous perched layer (Fig. 52). Horizontal conductivity was sufficient to allow water movement away from the well before water mounding on the additional perching layer length could interfere with recharge rate. It is possible that additional study on models with much long run times, different boundary conditions, and models with varying horizontal to vertical conductivity may eventually determine a condition where a laterally continuous perching layer affects recharge rate, but for

conditions modeled the slope of the water mound was the same between W88 and W99 models. There is probably a minimum lateral extent that a perching layer must have to create the water mound slope that minimizes recharge, after which the lateral extent ceases to affect recharge rate. No attempt was made in this research to find this "minimal extent".

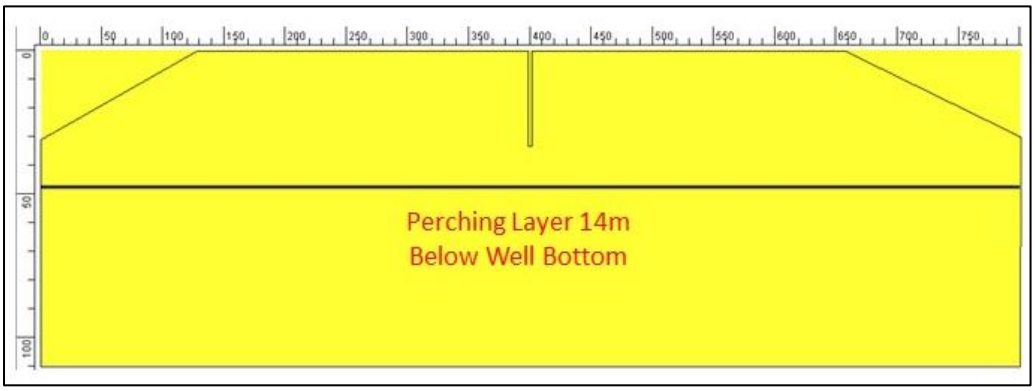

Figure 52: Example of well model #99 with laterally continuous perching layer

There are implications to this finding. Since a perched layer's lateral extent does not noticeably affect infiltration rates, vadose wells may be successfully employed in locations with extensive perching layers. In such areas water may have to travel significant lateral distances before ultimately reaching the end of the perching layer and continuing downward to recharge the aquifer. Provided eventual recharge is the only goal (as opposed to recharge at a specific location) and residence time is not a concern, this means vadose zone wells could be employed without loss of efficiency even in locations with extensive perched layers.

Results from twelve WM88 models simulating perched layers below a vadose well are shown in Fig. 53. Recharge rate increases from a minimum when a perching layer is immediately below the well to around 80% of the theoretical maximum efficiency when the perching layer is 24 meters below the bottom of the well. Plotted as an independent point on this graph (red square) is WM8.3- the 33m deep, 10m of water column well in the original model that was shown in Fig. 48. If the perched layer 5m below Well #8 is assumed to be the only factor

influencing that well's recharge rate then the red square datum point should fall along the blue "recharge rate" curve. Instead the datum point plots below the recharge curve, suggesting there is an additional factor decreasing WM8.3 recharge rate.

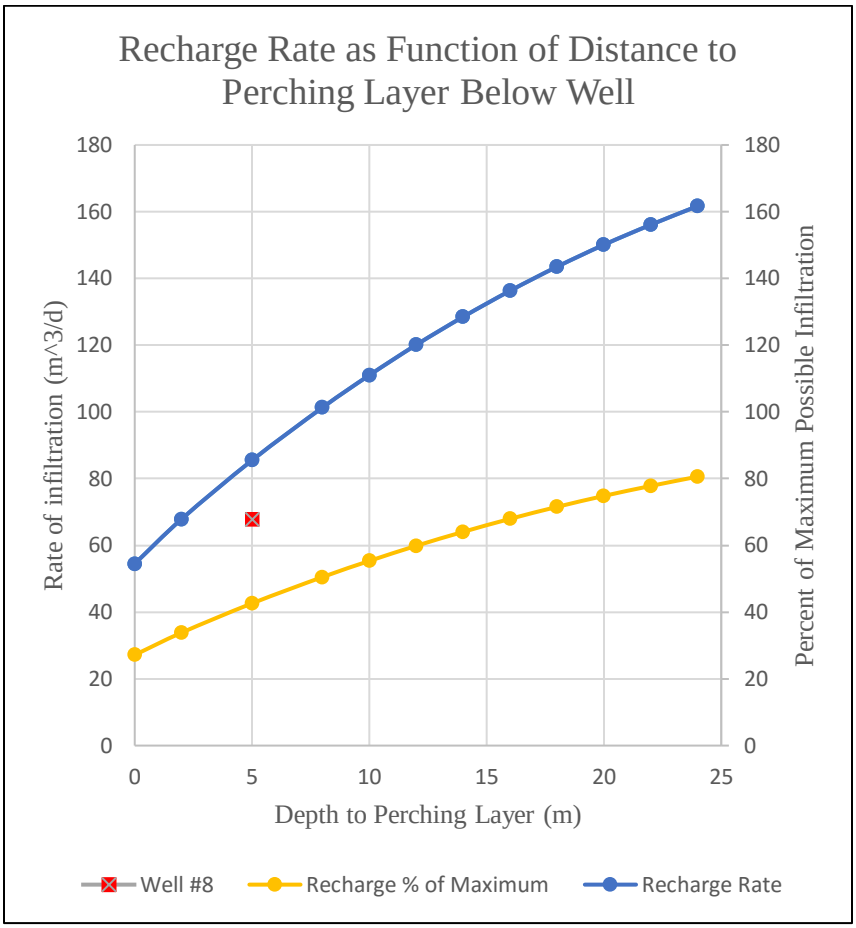

Figure 53: Recharge rates vs distance to perched layer

7.4.1.B Perched Layers Adjacent to the Vadose Well

While the depth to perched layer below the well screen had a clear influence on the recharge rate, the simulated recharge for WM8.3 was only 67m^3/d, lower than the rate of 85.5m^3/d that would be expected if the lower perching layer was the only influence on recharge (Fig. 53, red square is below the blue recharge rate curve). This discrepancy of 18.5 m^3/d can be explained by the presence of an additional low-permeability layer adjacent to the well screen at approximately 31m depth (Fig. 48, previous section).

To test the influence of the perched layer adjacent to the vadose zone well in WM8.3, models were set up with a single perching layer adjacent to the well screen. This single perching layer was tested on only one side of the well (referred to as "Well #77" (WM77) models) and as a continuous layer adjacent to both sides of the well screen ("Well #66" (WM66) models). The perching layer thickness was set at 2m and the depth of the perching layer was varied from the top of the well screen to its base.

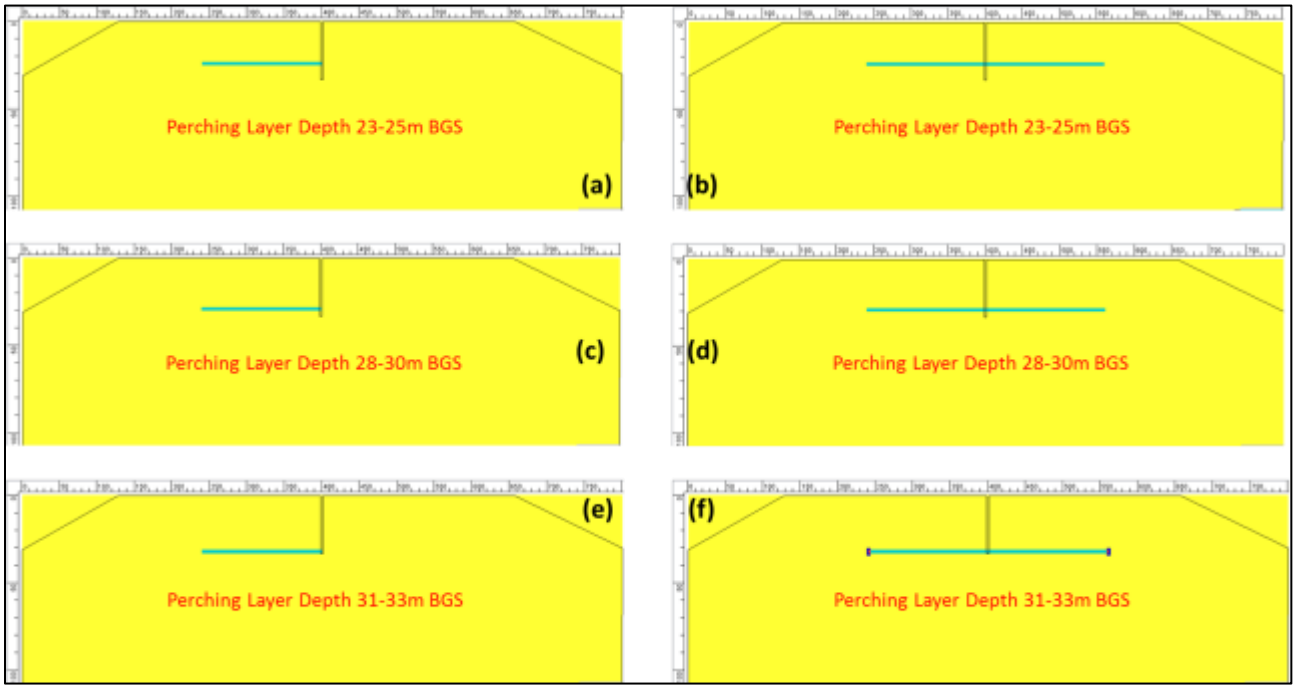

Figure 54: Three examples of well #77 (left) and well #66 (right)

(a) and (b) WM77 and WM66 perching layer between 23-25m; (c) and (d) WM77 and WM66 perching layer between 28-30m; (e) and (f) WM77 and WM66 perching layer between 31-33m

Fig. 55 shows the recharge rate curve for a vadose well with a 2m thick perching layer modeled on a single side of the well screen. If the perched layer is at the very bottom of the well screen, such as is the case for well at the bottom left of Fig. 54, the expected result is a decrease in infiltration rate of ~33%. Starting with theoretical maximum recharge of 200.6 m^3/d obtained

from our "matrix only" model, this would result in a recharge rate decrease of 66.2 m^3/d for a total recharge value of 134.4 m^3/d.

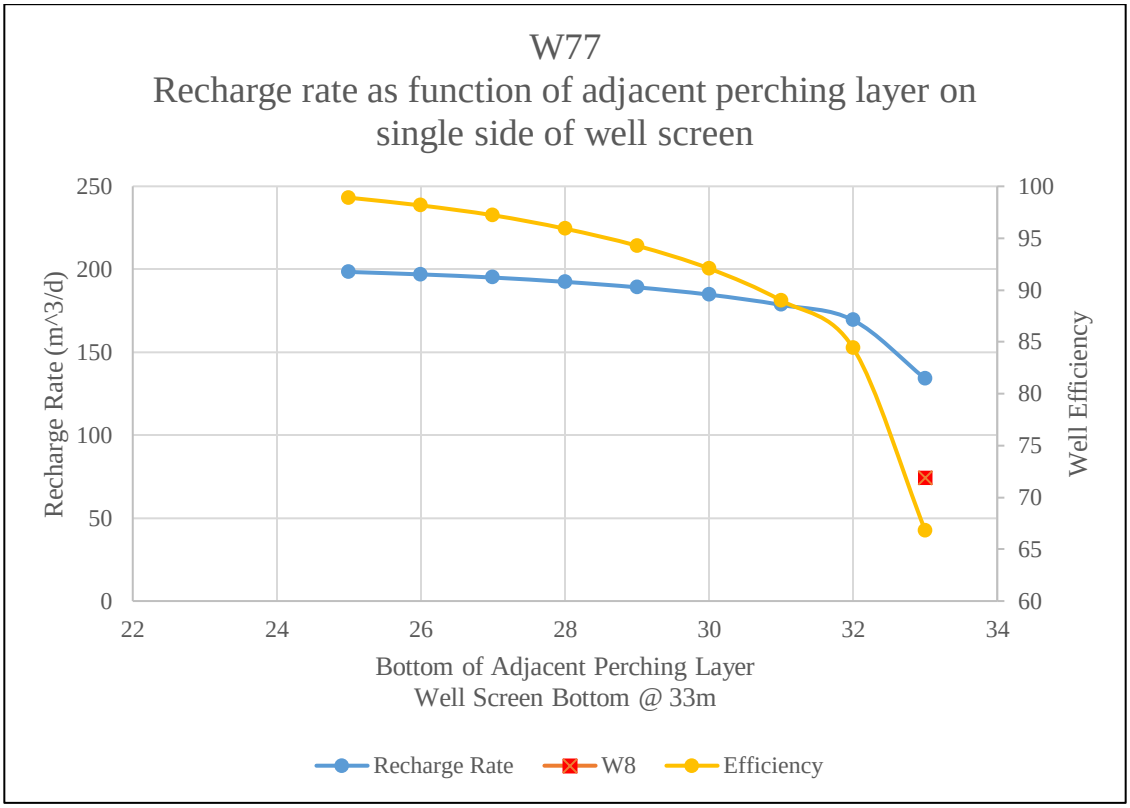

Figure 55: Effects of perched layer adjacent to one side of well

If the expected recharge rate decreases from both a perched layer 5m below and a perched layer adjacent to WM8.3 are combined, the total recharge should be found by the equation:

Maximum recharge possible – Decrease from adjacent perching layer – Decrease from perching layer below = Recharge value expected

Or

200.6 m^3/d – (.33*200.6 m^3/d) = 134.40 m^3/d [recharge adjusted for adjacent perching layer]
134.40 m^3/d – (.52*134.40 m^3/d)=64.51 m^3/d [recharge adjusted again for lower perching layer]

This value 64.51 m^3/d is lower than but close to the observed modeled recharge rate of 67 m^3/d suggesting that most of the reduction from maximum possible recharge is attributed to these

two layers. The higher value of 67 m^3/d may be a product of model discretization because the adjacent perching layer in WM8.3 appears as if it is several meters away from the well screen after the model is discretized.

Overall, these simulations suggest that screening a well at 1/3 the distance to the water table (33m) is a very poorly selected depth in this part of the HBA.

During real-world construction of a vadose zone well it is unlikely that there would be a low permeability layer on only one side of the well screen. It is probable that the perching layer would fall adjacent to all sides of the well screen at some depth as the well screen passed through the layer. This possibility was considered by creating "Well #66" (WM66) models that extended the adjacent perching layer to both sides of the well screen (Fig. 54, right side images).

It becomes clear that a perched layer adjacent to the well screen has a large effect of recharge rate when adjacent to the bottom half of the well screen. Fig. 56 shows how the efficiency curve of a vadose zone recharge well remains at or above ~90% provided that the perching layer is adjacent to the upper half of the screen. In Fig. 56, this top half corresponds to a depth of 27.5m. Above this point there is sufficient screen length below the perched layer to allow recharge in the section of screen with higher pressure head. If the perched layer is adjacent to the well in the lower half of the screen length the well efficiency begins to suffer. This becomes especially pronounced if the perched layer is both adjacent to the bottom section of screen and below it. Such a condition would occur if the bottom of a vadose well was installed in the perching layer (Fig. 54, bottom right image). Recharge rates associated with this condition occurs at 33m in Fig. 56. Water mounds on the perching layer and decreases the pressure difference that drives water from the well into the surrounding aquifer matrix.

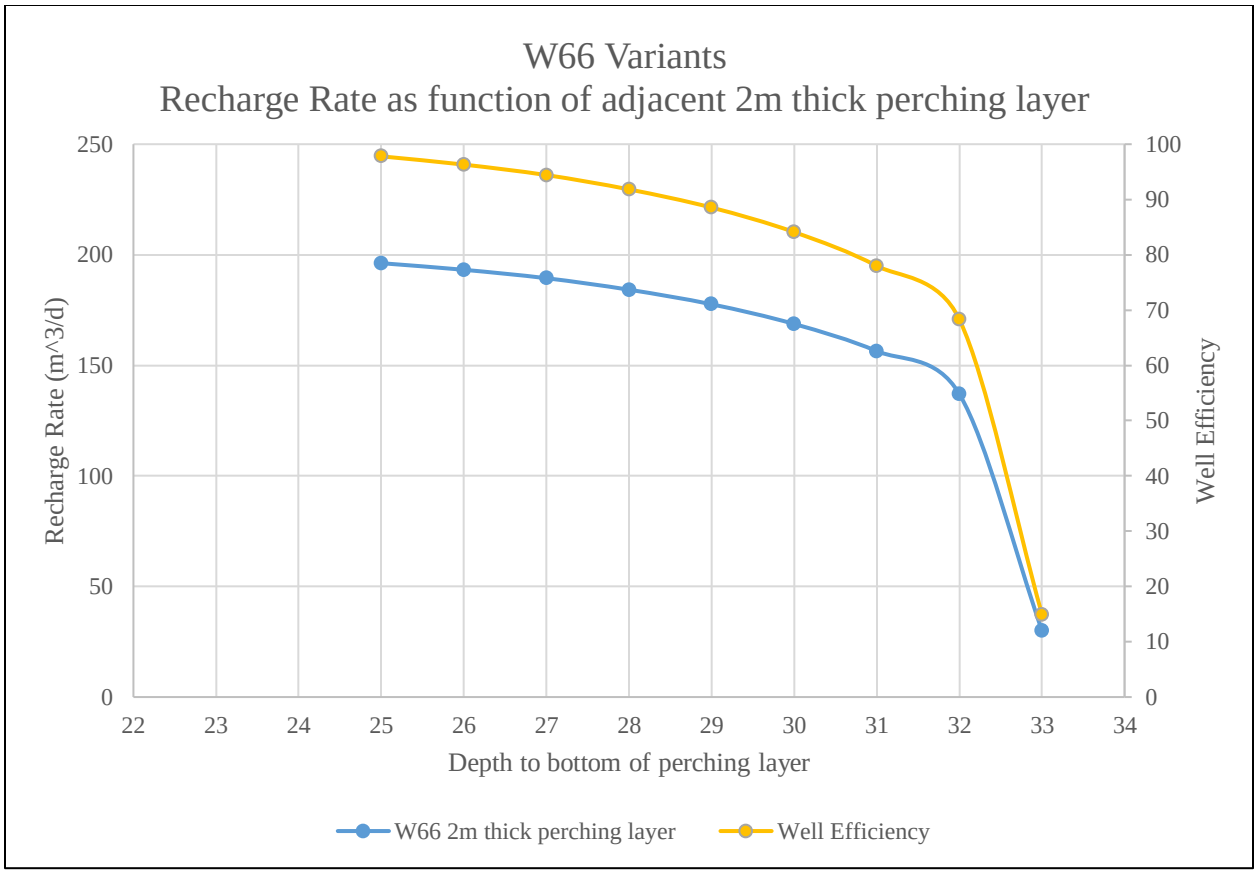

Figure 56: Effects of adjacent perched layer, well model #66

7.4.1.C Consequences of Perched Layer Depth Relative to Vadose Well

Results from simulating perching layers adjacent to and below a well screen can be combined to provide an estimate of infiltration efficiency as a function of relative perched layer location. Fig. 57 demonstrates the effect on recharge for a perched layer relative to the bottom of the well screen. In Fig. 57 the vadose well is fixed at 33m BGS with a screened area between 23-33m BGS. The y-axis shows the location of the perching layer depth. Moving top to bottom on the y axis is progressively deeper below ground.

There is a brief but rapid decrease in recharge rate as the perching layer approached the bottom of the well then a long and steady recovery in recharge rate as the perching layer moves further from the well bottom (Fig. 57).

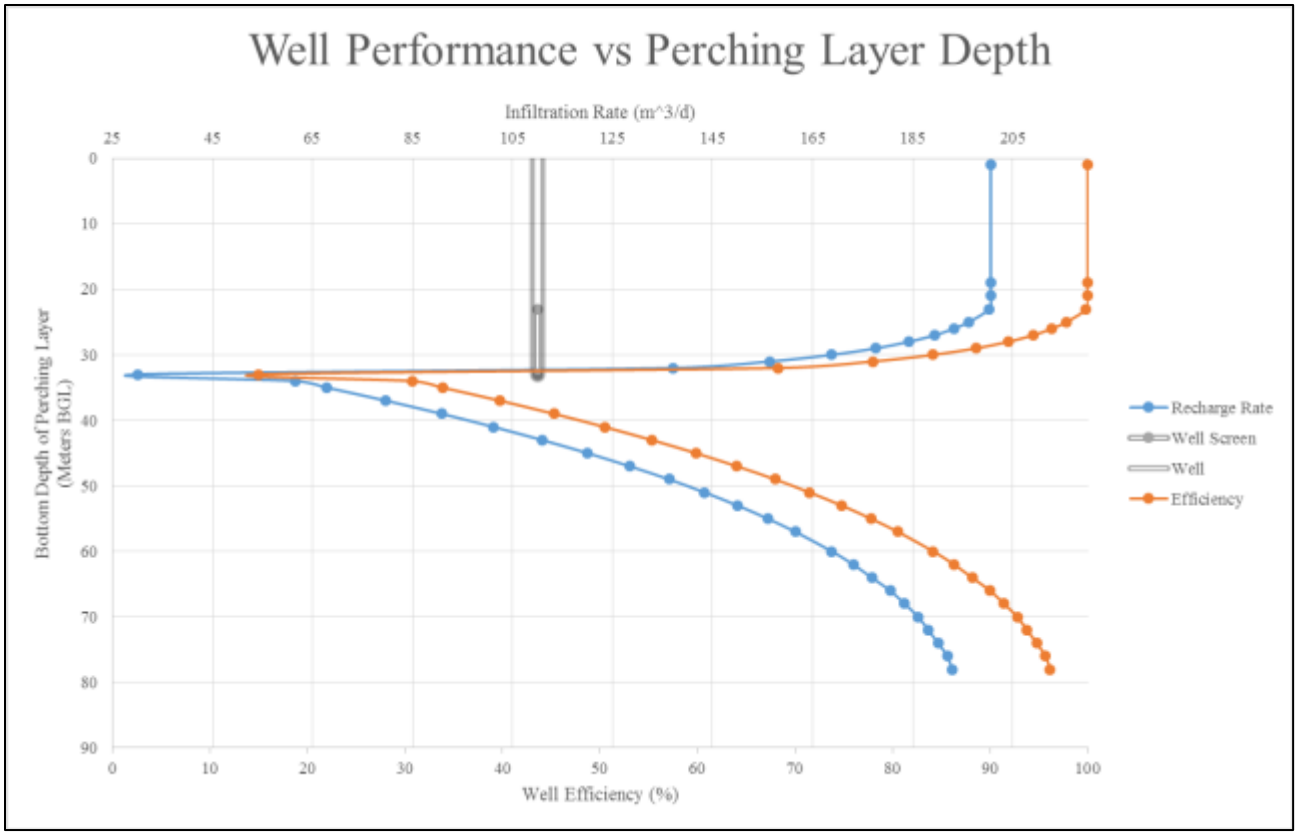

Figure 57: Effects of perched layer on vadose well recharge

There is one important assumption to this chart- the water column in the well and the well depth are constant while the perching layer is moved. In reality perching layers are fixed in the subsurface but the bottom of the well and well screen length are varied depending on emplacement depth. Examples in the next section consider the additional screen area and pressure head associated with drilling a deeper well relative to a fixed perched layer depth.

Even with this caveat the chart can have significant implications for the design of vadose wells in unconfined, heterogonous vadose zones. The efficiency of recharge per unit length of screen decreases as the well screen approaches the perched layer, reaches a minimum value when the well bottom is inside the perched layer, and increases as the well screen extends below the perched layer. Using the knowledge of relative efficiencies, a geotechnical firm could design

the most efficient well field obtaining a desired infiltration quantity within budgetary and land availability constraints.

7.5 Accounting for Greater Well Screen Area in Deeper Vadose Wells

As a vadose well is drilled deeper there is additional length available for the well screen. All lithologic considerations equal this creates a condition where a deeper well will have more screen length and more water column height, resulting in greater recharge rate. For example, consider two wells of 1m diameter placed side by side in the same aquifer. Both wells are screened beginning 5m BGS. The first well has a bottom depth of 15m BGS while the second well have a bottom depth of 25m. The first well will have a possible recharge area of $31.4m^2$ (circumference of a 1m diameter circle times the height of the screen) but the second well will have a total recharge area of $62.83m^2$. Assuming the well is filled to the ground level the maximum possible water column, also known as pressure head, in the first well is 15m. The maximum possible pressure head in the second well is 25m. As the area adjacent to the well screen is saturated, Darcian flow occurs, and the greater pressure head and larger screened area in the 25m deep well will allow more water to flow into the aquifer matrix.

This concept can be visualized using Figs. 58 and 59. The vadose well at the far right in Fig. 58 is deepest and so has a greater recharge rate than the wells on the left. If there were no perched layers, recharge rate increases according to a linear function. Since there are perched layers, recharge rates will still increase as wells progress deeper, but the recharge rate increase is no longer a steady linear function.

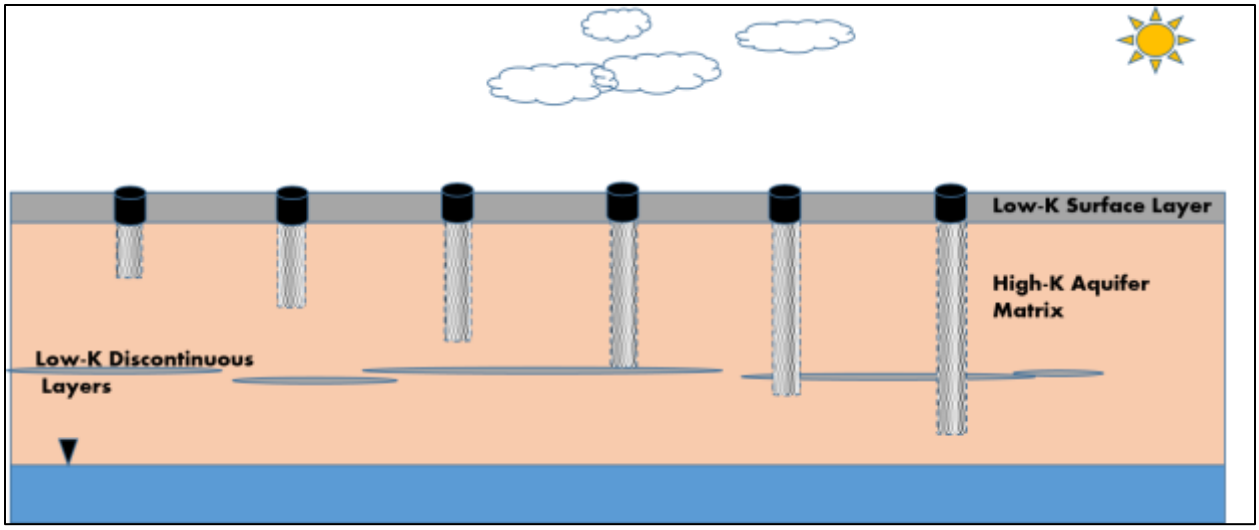

Figure 58: Example of six vadose wells

Well depths vary, with the last two wells penetrating past the deep, discontinuous low permeability layer.

The following example serves to demonstrate a situation where the effects of perching layers on recharge rates may influence the calculations on how deep and how many vadose wells to emplace in heterogeneous lithology.

7.5.1 Example of Perched Layer Effect on Recharge Project Design and Vadose Well Sizing

Suppose a small city plans to implement a recharge program targeting an alluvial aquifer with a water table one hundred meters BGS. Thick clay layers in the uppermost 5-20m of the aquifer preclude basin infiltration as an option. Non-laterally extensive, thin clay layers also exist, especially at seventy five meters BGS.

A maximum design recharge rate of 10 AF/D is desired (12,350 m^3/d) in order to allow the city to maximize seasonal winter rain recharge.

The aquifer matrix is characterized as fine sand with some localized horizons grading to coarse sand and gravels. The clay layer at 75m depth causes perched conditions while other clay

lenses have sufficient secondary porosity to not noticeably slow infiltration through the vadose zone. A cross section of this aquifer with three potential wells (option #1, #2, and #3 from left to right) is shown in Fig. 59.

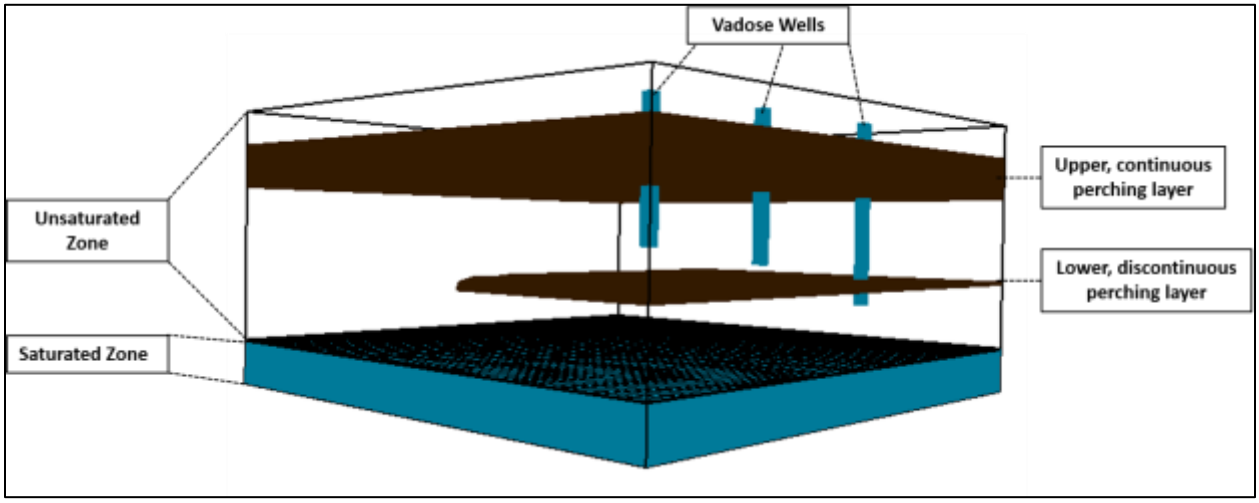

Figure 59: Example aquifer section and vadose wells used to demonstrate section 7.5.1

The effects of perching layers on recharge rate are seen in Fig. 60. There is an overall increase in recharge rate as the well extends deeper into the subsurface. Initially this increase is subdued by the effects of the perching layer until the well passes below it.

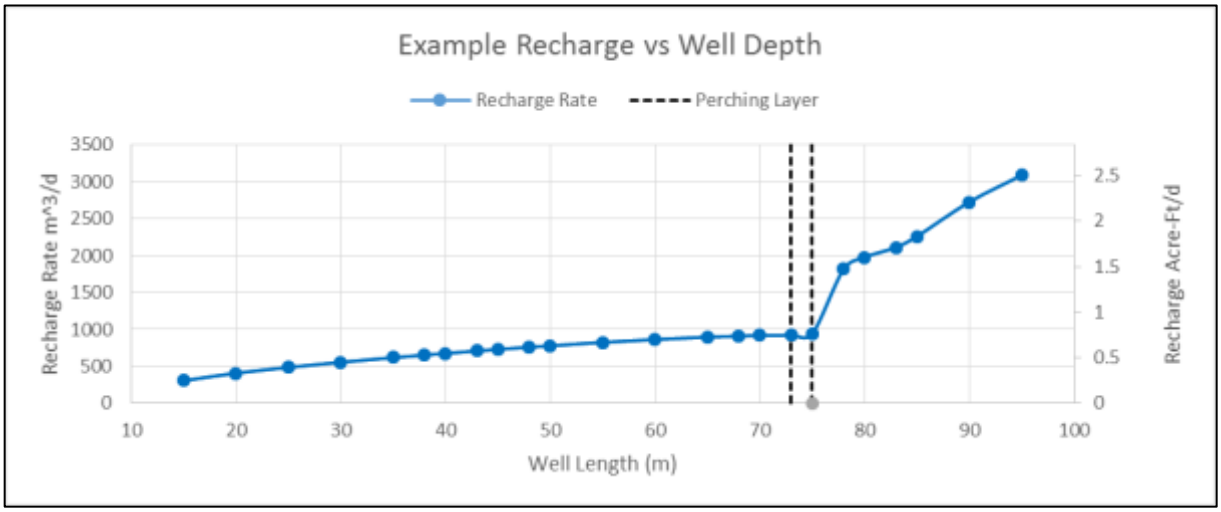

Figure 60: Example recharge rate vs well depth.

Recharge rates are scaled to 3D volumes by the same procedure as described in previous chapters.

Effects from the perching layer at 73-75m BGL are most clearly seen by showing the recharge rate per unit area. This is the total recharge rate divided by the well's screened length. Fig. 61 shows how the average recharge rate decreases as the well bottom approaches the perching layer- each additional meter drilled provides decreasing gains.

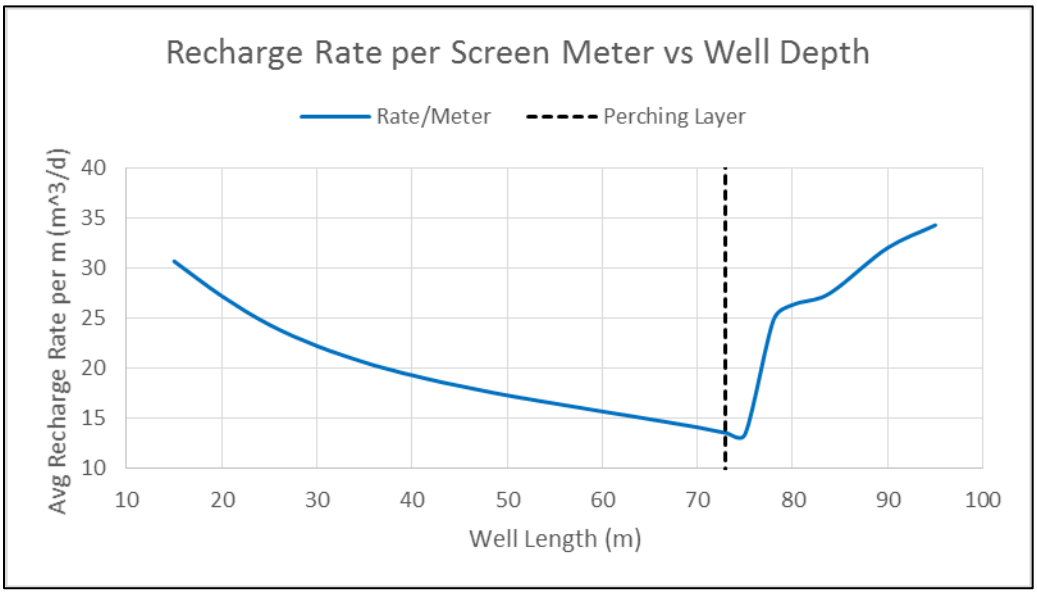

Figure 61: Example average recharge rate per meter vs well depth

The cost for each m^3 of recharge capacity can now be considered. For shallower wells, direct push technology is being considered as a very low cost method for emplacing small vadose zone wells (Handel et al., 2014). Most large diameter vadose wells are emplaced by auger type rigs. For this example the cost of drilling a meter of well is arbitrarily set to $100 (costs associated with installation of pumps, well housing, supporting infrastructure, water, etc. can be ignored because those costs will be applied regardless of well depth). The recharge rate per meter for each well depth is then divided by the cost to drill to that depth. The result is the cost per cubic meter recharge capacity for a well at each depth. As Fig. 62 shows, the cost per cubic meter of recharge rate actually goes up for a well drilled between 50m to 75m BGL.

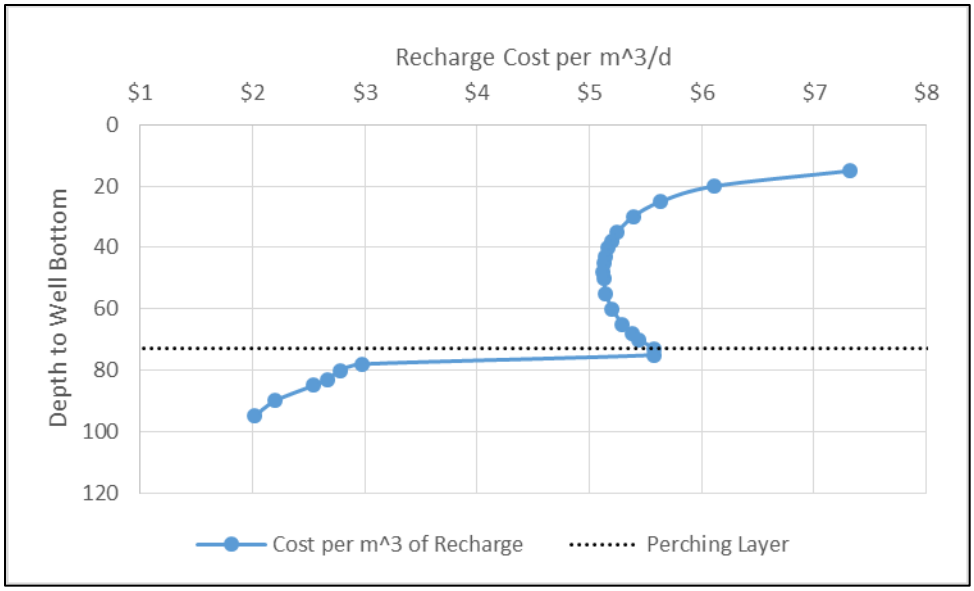

Figure 62: Price for m^3 of Recharge vs Well Depth @ arbitrary $100 per meter emplacement cost

Blue circles are output values (x-axis) for a model run with vadose well depth given on y-axis

Shallow vadose wells look most attractive when realistic well emplacement costs are considered. Literature review shows the cost for direct push well installation is $40/m based on field tests done in Kansas (Liu et al, 2016), while deeper requires the use of bucket auger rig at $300/m. It is notable that other tests of low-cost, shallow recharge wells have quoted costs as low as $14/m such as one experiment done as a well field in Austria (Handel et al, 2016). By contrast, a USDA fact sheet quotes $610/m for large diameter auger drilling, although it also quotes rotary methods at $55/m as an alternative method for well construction. Auger drilling or cable tool drilling is preferred since the minimal amount of drilling fluid is used and local permeability is usually maintained (AWWA 2003).

Personal communications with Mr. Mayer of Torrent Resources indicated that any well shallower than ~27m cost around $90,000 and well costs increase by ~$3,281 per meter ($1,000/ft) from 27m to a depth of around 55m. Past 55m it becomes difficult to use the large diameter bucket augers typically applied to these projects. These costs are higher than the

literature review because more of the well installation is included in this price (as opposed to just drilling the hole).

Fig. 63 provides a cost curve for recharge rate vs well depth using Mr. Mayer's quoted costs. To achieve a desired 10 AF/D of recharge with wells shallower than 55m, 23 wells should be drilled to a depth of 30m. In this scenario each 30m deep well has a 25m screen length and a recharge rate of 556.4 m^3/d (about 0.45 AF/d). The cost per m^3/d of recharge capacity is $176.90 and the overall cost to meet 10 AF/d is $2,263,890.

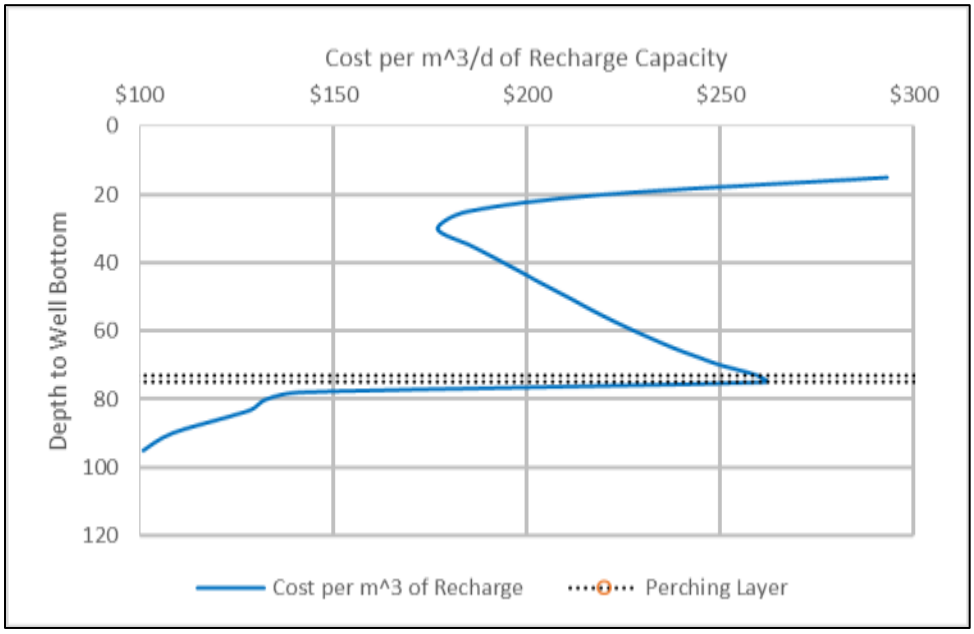

Figure 63: Price of recharge vs depth of well @ ~$3,281 per meter emplacement cost

If drilling can continue below 55m, possibly by some method other than bucket auger, the screen length for the vadose well could be brought lower than the perching layer. Assuming the cost for each additional meter of drill length remain constant and there are no constraints on the depth a vadose well can be emplaced (a poor assumption if switching to a more expensive drilling method, but useful for demonstrative purposes) the cheapest option for a 10 AF/D vadose well field is four wells drilled to 95m.

Factors such as land availability, drilling cost, rig type, and life expectancy/clogging potential will all influence the calculations in the generalized examples above but some important conclusions become clear. Above a perching layer, well recharge per meter of well depth decreases as the perching layer is approached. Once the well screen is extended below the perching layer there is a rapid increase in recharge. The above examples indicate it would usually be most economical to install the wells below the perching layer. More numerous but shallower and less efficient wells should be drilled when the cost of installing wells below a perching layer is high or when the target recharge amount is relatively small.

7.6 Application in Kansas

"In southwest Kansas, hydraulic connection between the Arkansas River alluvial aquifer and the underlying High Plains aquifer is poor because low permeability clay layers inhibit the downward flow of groundwater (Fig 64). Thus, the upper Arkansas River alluvial aquifer is a perched aquifer. However, the Cimarron River alluvial aquifer is well-connected to the underlying High Plains aquifer because there are no clay layers immediately beneath the alluvium to inhibit the flow of groundwater between the aquifers." (Macfarlane et al, 2000).

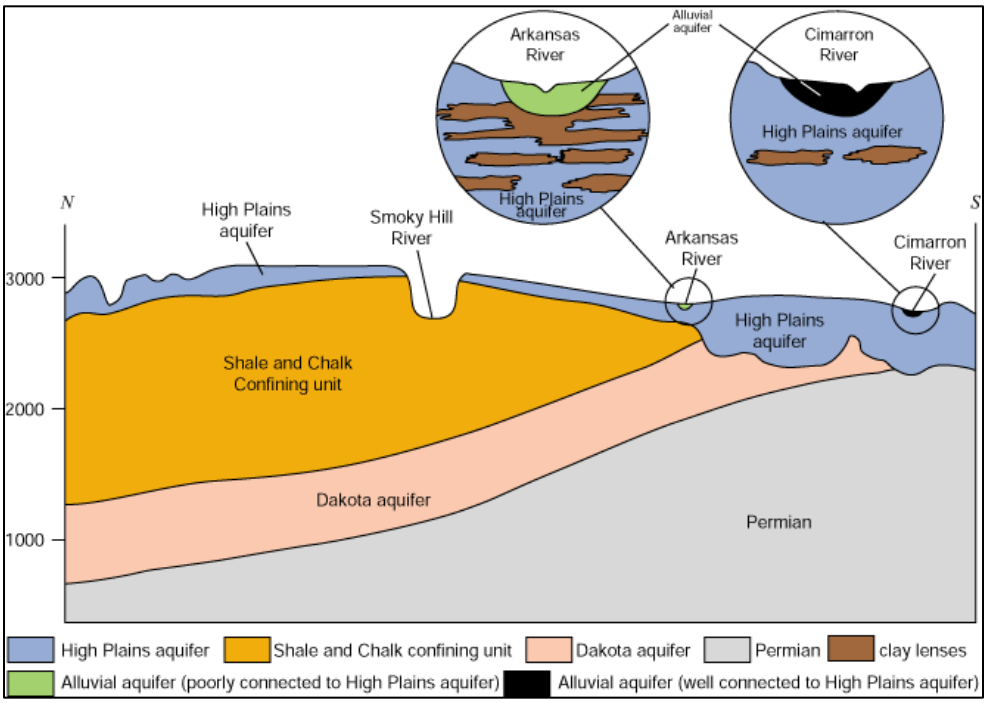

Figure 64: Connection between surface and High Plains aquifer in southwestern Kansas (Macfarlane et al, 2000)

The goal of recharging the High Plains aquifer may be achieved using different methods depending on where recharge is implemented. If artificial recharge occurred in the Cimarron River alluvial aquifer, an infiltration basin could take advantage of the high conductivity between surface and High Plains aquifer water table, whereas if the recharge was to occur in the Arkansas River alluvium, recharge may require vadose or direct injection wells. The results of this research could be applied to understanding the feasibility of aquifer recharge at either site.

7.7 Clogging

All of the recharge methods in this research made several key assumptions to allow direct comparison. The first and potentially most influential assumption made was to ignore the effects of sedimentation and biofouling. Some degree of clogging during aquifer recharge is generally expected (Bhuiyan, 2015) and most literature on MAR and ASR at least addresses the issue.

Three distinct forms of clogging occur in MAR and ASR projects: particulate clogging from suspended solids, chemical clogging from geochemical reactions between infiltrated water and native groundwater, and biological clogging. The amount of Total Suspended Solids (TSS) are the most influential factor in well clogging (Bloestscher et al, 2014) and can be mitigated by settlement or pretreatment of water. Chemical clogging susceptibility can be identified by high Total Dissolved Solids (TDS) which usually indicates the presence of chlorides and dissolved metals. Infiltrated water with high cation concentrations causes the geochemical equilibrium to become unbalanced and undergo chemical reactions leading to release of metals (possibly rendering the water unusable) or precipitate out minerals (clogging pore spaces). Prevention of chemical clogging is done first by selecting recharge sites with groundwater chemistry compatible with the infiltrated water, then by treating the infiltrated water using techniques like acidization treatments as needed (Bloestscher et al, 2014). Biological clogging occurs when microorganisms encrust or corrode well screens and, in the case of infiltration basins, may form algae mats that cover the bottom of the basin. Plants such as grasses may also grow on the floor of infiltration basins, reducing infiltration and causing transpiration losses. Treatment for biological clogging is different for vadose wells and infiltration basins (Bloetscher et al, 2015).

No matter what infiltration method, the best defense against all clogging is use of high quality, treated water. When lower quality water such as storm water runoff is used, settlement prior to infiltration is a key step to maximizing a vadose well or infiltration basin's lifespan.

Since clogging occurs near the initial source of infiltration, basins can be easily and cheaply redeveloped by removal and/or reworking of the upper sediments using bulldozers, scrapers or graders. EPWU does this any time the water level in a basin begins to pond above several feet (Eric Bangs, Personal Communications, 2017). Multiple basins can also be rotated

to allow cyclical drying and wetting periods which discourages the growth of biologicals and desiccates the upper soil, encouraging cracks.

Vadose zone wells are more difficult to remediate after clogging. Because they are not screened within the saturated zone they cannot be redeveloped. Chemicals may be periodically added to discourage microbiological fouling. Vadose well designs may include chemical feed and recirculation tubes to help flush vadose wells and maintain a working lifespan. Fig. 65 shows a vadose well design from a project in Goodyear, Arizona, that includes two such tubes alongside the main well screen.

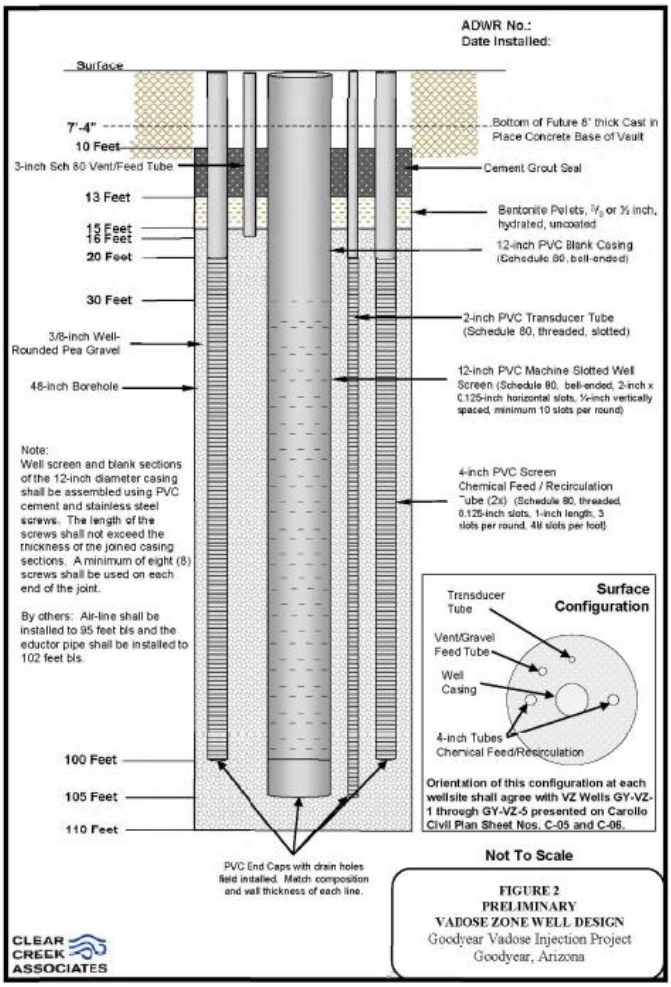

Figure 65: Vadose well design

Showing 4-inch Recirculation Tubes Adjacent to Main Well Screen. Courtesy of Torrent Resources.

Chapter 8 - Conclusion

"Thanks to the centrifugal pump, places like Nebraska, Kansas, Oklahoma, and Texas had thrown on the garments of fertility for a century, pretending to greenery and growth as they mined glacial water from ten-thousand-year-old aquifers. They'd played dress-up-in-green and pretended it could last forever." – Pablo Bacigalupi, "The Water Knife"

8.1 Closing Summary

When choosing infiltration methods for Managed Aquifer Recharge in unconfined aquifers, site lithology seems to control the most effective method for aquifer recharge. All considerations equal, infiltration basins are usually the best choice. Due to their large surface area, infiltration basins allow large volumes of water to naturally infiltrate into the vadose zone and ultimately reach the water table. At both sites modeled, an infiltration basin far outperforms a vadose zone well. Steady state rates infiltrating from basins was 6,243m^3/d and 6,435m^3/d at the Sagamore Lens Aquifer (SLA) and Hueco Bolson Aquifer (HBA) locations, respectively, and total steady state rates infiltrated from vadose wells using well depths proposed in the hypothesis were 429.2m^3/d and 133.8m^3/d at the SLA and HBA locations. To compare the vadose well with the infiltration basin at the HBA location, a full vadose well with a 33m water column, provided a recharge rate of 441.5m^3/d. This leads to the conclusion that in the HBA model it requires fifteen 33m deep vadose zone wells to obtain the same infiltration rate as a single half-acre infiltration basin. For the more homogenous SLA model, thirty 10m deep vadose wells would be required to obtain the same infiltration rate as a single half-acre infiltration basin using the original boundary conditions, and fifteen 10m deep vadose wells would be required using revised boundary conditions.

Complex lithology influences recharge rates, and additional models were run to isolate the effect of perched layers on recharge rates from vadose wells. A vadose well screened above a perched layer will be influenced by the water mounds that builds on the perched layer with the result being a reduced infiltration rate. As the bottom of the well approaches the top of the perching layer, this infiltration rate is reduced to less than 20% of the value expected for that same well in the absence of perched layers. In modeling based on HBA location hydrogeological conditions, recharge from a 33m deep vadose well with a 10m water column was 200.6m^3/d. This rate decreased to 85.5m^3/d when a low permeability layer was installed 5m below the bottom of the vadose well. This rate decreased to a minimum of 54.5m^3/d when that same low permeability layer was placed directly below the well screen. In both these scenarios the decrease in infiltration rate was due to the formation of perched conditions. Perching layers also decrease recharge rate if a well is screened through the layer and below it, although this effect is small when the perching layer is adjacent to the upper half of the well screen. Using the same 33m deep vadose well with a 10m screened interval but including a 2m thick low permeability layer halfway down the well screen returned an infiltration rate of 184.2m^3/d.

To constrain the model and validate model input parameters, soils analysis and a microgravity survey were conducted at El Paso Water Utility's (EPWU) managed aquifer recharge basins, the location that HBA models were based on. Grain size distribution analyzed by a Mastersizer 3000 showed a well medium to fine sand composition. This information was validated by permeability testing which returned a value of 0.054cm/s hydraulic conductivity, within the range expected from well sorted sands. The microgravity survey is an ongoing effort, but preliminary results indicate a possible preferential flow path and perched conditions to the northwest of one of EPWU's recharge basins.

In the HBA model all perching layers were non-continuous and below 33m. This negated the greatest advantage of vadose wells- that is, recharge can begin below perching layers if the vadose well is emplaced sufficiently deep. The vadose well depths chosen for this research did not penetrate the unsaturated zone sufficiently far to allow this. A location with similarly complex lithology but perching layers closer to the surface would allow vadose wells to be screened below the perching layers. This may result in situations where a single vadose well outperforms an infiltration basin.

8.2 Further Research

Lithology at both Cape Cod and El Paso allows easy surface infiltration and favors a basin approach to Managed Aquifer Recharge. Many locations, including some in western Kansas, have near surface lithology which does not permit basin style recharge. The understanding and management of groundwater in western Kansas is critical to maintaining the area's economy. This study further indicates that this research could be applied in conjunction with storm water runoff capture and changes in wastewater discharge to help western Kansan cities and towns ensure sufficient water table elevations in municipal wellfields. A partnership between KGS, KDHE, local government, and Kansas State University could prove beneficial to all in executing this.

While this research would assist with the selection of MAR method based on site specific lithology, additional research into clogging, geochemistry and water quality changes due to MAR must be addressed. While there is a wealth of literature on aquifer water quality effects of MAR-induced recharge, results are influenced by specific local conditions. If reclaimed wastewater is to be widely used in western Kansas- as it already is in much of the American Southwest- the water quality effects must be evaluated for western Kansas locations.

Finally, this study also points towards the need to understand how virus and pathogens respond during vadose recharge. While soil aquifer treatment (SAT) is generally acknowledged to be "good" for water quality, a quantitative assessment of SAT benefits could go a long way in guiding regulatory requirements for MAR implementation. With the NBAF facility opening in the near future, studies in waterborne pathogen response and lifecycle during recharge could inform requirements for minimum water residence times in the vadose zone prior to aquifer recharge or the maximum contaminant level of certain pathogens in effluent or storm water used as a source for aquifer recharge.

References

Abeyta, C., and Frenzel, P., 1999. Geohydrology of the Unsaturated Zone and Simulated Time of Arrival of Landfill Leachate at the Water table, Municipal Solid Waste Landfill Facility, U.S. Army Air Defense Artillery Center and Fort Bliss, El Paso County, Texas. USGS Water-Resources Investigations Report 97-4036.

Abeyta, C., Frenzel, P., 1999. Geologic and Hydrologic Data for the Municipal Solid Waste Landfill Facility, U.S. Army Air Defense Artillery Center and Fort Bliss, El Paso County, Texas. USGS Open File Report 99-271.

Adam, C., 2017. Personal Communications, Kansas State University, Kansas. From January 2017 to October 2017.

AMEC Foster Wheeler, 2003. Log of Borehole MS-255. Recovered from USACE NAE District Document Repository. Accessed 04 November 2016.

Anderholm, S., and Heywood, C., 2003. Chemistry and Age of Ground Water in the Southwestern Hueco Bolson, New Mexico and Texas. USGS Water-Resources Investigations Report 02-4237.

AWWA Research Foundation, 2003. Comparison of Alternative Methods for Recharge of a Deep Aquifer.

AWWA Research Foundation, 2008. Design, Operation, and Maintenance for Sustainable Underground Storage Facilities.

Barbaro, J., Masterson, J., LeBlanc, D., 2014. Science for the Stewardship of the Groundwater Resources of Cape Cod, Massachusetts. USGS Fact Sheet 2014-3067.

Bekele, E., Toze, S., Patterson, B., Fegg, W., Shackleton, M., Higginson, S., 2013. Evaluating Two Infiltration Gallery Designs for Managed Aquifer Recharge Using Secondary Treated Wastewater. Journal of Environmental Management, Vol 117, pp 115-120.

Bell, F., 2006. Engineering Geology. Elsevier Science, available from ProQuest Ebook Central, http://ebookcentral.proquest.com/lib/ksu/detail.action?docID=285826.

Bloetscher, F., Sham, C., Danko III, J., Ratick, S., 2014. Lessons Learned from Aquifer Storage and Recovery (ASR) Systems in the United States. Journal of Water Resource and Protection, 2014, Vol 6, pp 1603-1629.

Botros, F., Onsoy, Y., Ginn, T., Harter, T., 2011. Richards Equation-Based Modeling to Estimate Flow and Nitrate Transport in a Deep Alluvial Vadose Zone. Vadose Zone Journal, 2011.

Bouwer, H., 1969. Theory of Seepage from Open Channels. Advances in Hydroscience, Academic Press, New York, pp 121-170.

Bouwer, H., 2002. Artificial Recharge of Groundwater: Hydrogeology and Engineering. Hydrogeology Journal, Vol 10, pp 121-142.

Bouwer, H., Pyne, R., Brown, J., St Germain, D., Morris, T., Brown, C., Dillon, P., Rycus, M., 2008. Design, Operation, and Maintenance for Sustainable Underground Storage Facilities. AWWA Research Foundation, Denver, Colorado.

Bredehoeft, J., Ford, J., Harden, B., Mace, R., Rumbaugh, J., 2004. Review and Interpretation of the Hueco Bolson Groundwater Model. Prepared for El Paso Water Utilities. Available from www.epwu.org/water/hueco_bolson/ReviewTeamReport/pdf.

Brown, C., 2006. Lessons Learned From a Review of 50 ASR Projects from the United States, England, Australia, India, and Africa. Session 12 of the UCOWR Conference, Paper 68.

Brown, G., 2002. Henry Darcy and the Making of a Law. Water Resources Research, Vol 38, No 7.

Buszka, P., Brock, R., Hooper, R., 1994. Hydrogeology and Selected Water-Quality Aspects of the Hueco Bolson Aquifer at the Hueco Bolson recharge Project Area, El Paso, Texas. USGS Water-Resources Investigations Report 94-4092.

California Department of Water Resources, 2017. California Groundwater website, www.water.ca.gov/cagroundwater. Accessed 08 March 2017.

Carlson, C., Walter D., Barbarao, J., 2015. Simulated Responses of Streams and Ponds to Groundwater Withdrawalals and Wastewater Return Flows in Southeastern Massachusetts, Scientific Investigations Report 2015-5168.

City of Tucson, 2017. Central Avra Valley Storage and Recovery Project. Available from www.tucsonaz.gov/water/cavsarp. Accessed 09 March 2017.

City of Wichita, 2017. Wichita Area Future Water Supply: A Model Program for Other Municipalities. Available from www.wichita.gov. Accessed 09 March 2017.

Darcy, H., 1856. Les Fontaines Publiques de la Ville de Dijon. Victor Dalmont, Paris.

Das, B., 2010. Principles of Geotechnical Engineering, 7th Edition. Cengage Learning, Stamford, CT, USA.

Department of the Interior Press Release, 2017. Secretary Zinke Announces $23.6 Million for Water Reclamation and Reuse Projects and Studies. 12 May 2017. Available from www.doi.gov/pressreleases.

Denver Water, 2017. Construction Projects, Aquifer Storage and Recovery Study. Available at www.denverwater.org/ConstructionProjects/ConstructionWorkAffectingCustomers/ASR/. Accessed 09 March 2017.

Dillon, P., Pavelic, P., Toze, S., Rinck-Pfieffer, S., Martin, R., Knapton, A., Pidsley, D., 2006. Role of Aquifer Storage in Water Reuse. Desalination Vol 188 pp 123-134.

El Paso Water Utilities, 2016. Water Resources. Available from www.epwu.org/water/water_resources/html. Accessed 17 August 2016.

Elhadj, E., 2004. Camels Don't Fly, Deserts Don't Bloom: an Assessment of Saudi Arabia's Experiment in Desert Agriculture, Occasion Paper No 48, School of Oriental and African Studies, King's College London, University of London, United Kingdom.

El-Kadi, A., 2005. Validity of the Generalized Richards Equation for the Analysis of Pumping Test Data for a Coarse-Material Aquifer. Vadose Zone Journal 4 pp 196-205.

Fairchild, G., Lane, J., Voytek, E., LeBlanc, D., 2013. Bedrock Topography of Western Cape Cod, Massachusetts, Based on Bedrock Altitudes from Geologic Borings and Analysis of Ambient Seismic Noise by the Horizontal-to-Vertical Spectral-Ratio Method. USGS Scientific Investigations Map 3233.

Fetter, C., 2000. Applied Hydrogeology, 4th Edition. Pearson Education Limited, Harlow, Essex, England.

Freeze, R., 1994. Henry Darcy and the Fountains of Dijon. Ground Water, v32, pp 23-30.

Frenzel, P., and Abeyta, C., 1999. Leachate at the Water table, Municipal Solid Waste Landfill Facility, U.S. Army Air Defense Artillery Center and Fort Bliss, El Paso County, Texas. USGS Water-Resources Investigations Report 97-4036.

Gaisheng, L., Knobbe, S., Reboulet, E., Whittemore, D., Handel, F., Butler, J., 2016. Field Investigation of a New Recharge Approach for ASR Projects in Near-Surface Aquifers. Groundwater, Vol 54, No 3, pp 425-433.

Gangopadhyay, S., 2013. Engineering Geology. Oxford University Press, New Delhi, India.

Ghanbarian-Alavijeh, B., Liaghat, A., Huang, G., van Genuchten, M., 2010. Estimation of the va Genuchten Soul Water Retention Properties from Soul Textural Data. Pedosphere, 2010, pp 456-465.

Green, W., Ampt, G., 1911. Studies of Soil Physics, Part I- The Flow of Air and Water Through Soils. J. Agr. Sci., Vol 4, pp 1-24.

Grimestad, G., 2002. A Reassessment of Ground Water Flow Conditions and Specific Yields at Bordon and Cope Cod. Ground Water, Vol 40, No 1, pp 14-24.

Hallett, B., Poppe, L., Brand, S., 2004. Petrography and Character of the Bedrock Subsurface Beneath Western Cape Cod, Massachusetts. Northeastern Geology & Environmental Sciences, v. 26, pp 230-241.

Handel F, Liu G., Dietrich P., Liedl R., Butler J. J., 2014. Numerical assessment of ASR recharge using small-diameter wells and surface basins, Journal of Hydrology 517, pp 54-63.

Handel F, Liu G., Fank J., Friedl F., Liedl R., Dietrich P., 2016. Assessment of Small-Diameter Shallow Wells for Managed Aquifer Recharge at a Site in Southern Styria, Austria, Journal of Hydrogeology 24, pp 2079-2091.

Hantush, M., 1967. Growth and Decay of Ground Water Mounds in Response to Uniform Percolation. Water Resources Research, Vol 3, No 1, pp 227-234.

Haywood, C., and Yager, R., 2003. Simulated Ground-Water Flow in the Hueco Bolson, and Alluvial-Basin Aquifer System near El Paso, Texas. USGS Water-Resources Investigations Report 02-4108.

Harbaugh, A., 2005. MODFLOW-2005, The US Geological Survey Modular Ground-Water Model—the Ground-Water Flow Process. Chapter 16, Book 6, Modeling Techniques, Section A. Ground Water.

Healy, R., and Essaid, H., 2012. VS2DI: Model Use, Calibration, and Validation. American Society of Agricultural and Biological Engineers, Vol. 55(4), pp 1249-1260.

Hess, K., Wolf, S., Celia, M., 1992. Large Scale Natural Gradient Tracer Test in Sand and Gravel, Cape Cod, Massachusetts. Chapter 3: Hydraulic Conductivity Variablility and Calculated Macrodispersivities. Water Resources Research, Sol 28, No 8, pp 2011-2027.

Hornberger, G., Raffensperger, J., Wiberg, P., Eshleman, K., 1998. Elements of Physical Hydrology. John Hopkins University Press, Baltimore, Maryland.

Hsieh, P., Wingle, W., Healy, R., 2000. VS2DI-A Graphical Softward Package for Simulating Fluid Flow and Solute or Energy Transport in Variably Saturated Porous Media. USGS Water-Resources Investigations Report 9-4130.

Huff, G., 2005. Simulation of Ground-Water Flow in the Basin-Fill Aquifer of the Tularosa Basin, South-Central New Mexico, Predevelopment through 2040. USGS Scientific Investigations Report 2004-5197.

Hutchison, W., 2004. Hueco Bolson Groundwater Conditions and Management in the El Paso Area. EPWU Hydrogeology Report 04-01.

Izbicki, J., Flint, A., Stamos, C., 2008. Artifical Recharge through a Thick, Heterogeneous Unsaturated Zone. Groundwater, Vol 46, Issue 3, pp 475-488.

Joint Base Cape Cod Impact Area Groundwater Study Program Database. Accessed between September 2016 and October 2017. Not publically available.

Koth, K., Long, A., 2012. Microgravity Methods for Characterization of Groundwater-Storage Changes and Aquifer Properties in the Karstic Madison Aquifer in the Black Hills of

South Dakota, 2009-12. US Geological Survey Scientific Investigations Report 2012-5158.

Koponen, A., Mataja, M., Timonen, J., 1997. Permeability and Effective Porosity of Porous Media. Physical Review E, Vol 56, Number 3, pp 3319-3325.

LaCoste & Romberg, 2004. Instruction Manual Model G and D Gravity Meters. Available from www.LaCosteRomberg.com.

Leiji, F., van Genuchten, M., Yates, S., Russell, W., 1989. RETC: A Computer Program for Analyzing Soil Water Retention and Hydraulic Conductivity Data. US Salinity Laboratory, USDA-ARS, Riverside, CA.

Mace, A., Rudolph, D., Kachanoski, G., 1998. Suitability of Parametric Models to Describe the Hydraulic Properties of an Unsaturated Coarse Sand and Gravel. Ground Water, Vol 36, No 3.

Macfarlane, P., Misgna, G., Buddemeier, R., 2000. Aquifers of the High Plains Region. Kansas Geological Survey. Available from www.kgs.ku.edu/HighPlains/atlas/ataqhr.htm.

Miocool Inc, 2016. Map Plus (GIS Editor + Offline Map + GPS Recorder) version 2.6.7. Available from iTunes App Store.

MathWorks, 2016. MATLAB and Statistics Toolbox Release 2016b, The MathWorks, Inc., Natick, Massachusetts, United States.

Marino, M., 1975. Artificial Ground Water Recharge, I Circular Recharging Areas. Journal of Hydrogeology, Vol 25, pp 201-208.

Marino, M., 1975. Artificial Ground Water Recharge, II Rectangular Recharging Areas. Journal of Hydrogeology, Vol 26, pp 29-37.

Masterson, J., and Walter, D., 2009. Hydrogeology and Groundwater Resources of the Coastal Aquifers of Southeastern Massachusetts. USGS Circular 1338.

Mawer, C., Parsekian, A., Pidlisecky, A., Knight, R., 2016. Characterizing Heterogeneity in Infiltration Rates During Managed Aquifer Recharge. GroundwaterVol 54, Issue 6, pp 818-829.

McCulloch, P., 2011. How to Conduct a Fire Hydrant Flow Test. Plumbing Systems & Design, December-2011, pp 10-12. Available from www.PSDMAGAZINE.org.

Moench, A., 2004. Importance of the Vadose Zone in Analyses of Unconfined Aquifer Tests. Ground Water, Vol 42, No 2, pp 223-233.

Moore, J., Raynolds, R., Barkmann, P., 2004. Groundwater Mining of Bedrock Aquifers in the Denver Basin- Past, Present and Future. Environmental Geology, December 2004, Volume 47, Issue 1, pp 63-68.

Musset, A., and Khan, M., 2009. Looking Into the Earth. Cambridge University Press, New York, NY, USA.

National Parks Service, 2017. Physiographic Provinces Interactive Map. Accessed 03 October 2017. Available from https://www.nps.gov/subjects/geology/physiographic-provinces.htm

National Weather Service Forecast Office, El Paso Area. Accessed 07 September 2017. Available from www.weather.gov/climate/local_data.php?wfo=epz

Neto, D., van Lier, Q., van Genuchten, M., Reichardt, K., Metselaar, K., Nielsen, D., 2011. Alternative Analytical Expressions for the General van Genuchten-Mualem and van Genuchten-Burdine Hydraulic Conductivity Models. Vadose Zone Journal, vol. 10, pp 618-623.

Quanrud, D., Hafer, J., Karpiscak, M., Zhang, J., Lansey, K., Arnold, R., 2003. Fate of Organics During Soil-Aquifer Treatment: Sustainability of Removals in the Field. Water Research, no. 37, pp 3401-3411.

Reinert, S., 2016. Aquifer Recharge and Beneficial Reuse. Presented at WESTCAS Annual Coference, Santa Fe, New Mexico.

Salt River Project, 2017. Website available from https://www.srpnet.com/water/waterbanking.aspx; accessed 12 July 2017.

Sheng, Z., Devere, J., 2005. Understanding and Managing the Stressed Mexico-USA Transboundary Hueco Bolson Aquifer in the El Paso del Norte Region as a Complex System. Hydrogeology Journal, 13, pp 813-825.

Simunek, J., Sejna, M., Saito, H., van Genuchten, M., 2009. The HYDRUS-1D Software Package for Simulating the One-Dimensional Movement of Water, Heat, and Multiple Solutes in Variably-Saturated Media. Department of Environmental Sciences, University of California Riverside.

Southern Nevada Water Authority, 2015. Water Resource Plan 2015. First accessed August 2017. Available from wwww.snwa.com/ws/resource_plan.html.

Steward, D., Bruss, P., Yang, X., Staggenborg, S., Welch, S., Apley, M., 2013. Tapping Unsustainable Groundwater Stores for Agricultural Production in the High Plains Aquifer of Kansas, Projectsions to 2110. Proceedings of the National Academy of Sciences of the Unites States of America, vol. 110 no. 37.

Stone, M., Garrett, J., Poulton, B., Ziegler, A., 2016. Effects of Aquifer Storage and Recovery Activities on Water Quality in the Little Arkansas River and Equus Beds Aquifer, South-Central Kansas, 2011-14. US Geological Survey Scientific Investigations Report 2016-5042.

Texas Water Development Board, Water Interactive Data. First accessed September 2016. Available from www.twdb.texas.gov.

Trimble, 2010. Trimble NetR9 GNSS Reference Receiver User Guide. Version 4.15 Revision A. Accessed 05 October 2017. Available from http://trl.trimble.com/docushare /dsweb/Get/Document-495804/NetR9_UserGuide_13506.pdf

U.S. Army Corp of Engineers, New England District, 2013. Demolition Area 1 Environmental and System Performance Monitoring Report Response Action Groundwater Treatment Systems September 2011 to August 2012.

U.S. Army Environmental Command, 2011. Army Environmental Command Impact Area Groundwater Study Program. Groundwater Plume Maps and Information Booklet 2011. Available from https://semspub.epa.gov.

Van der Gun, J., 2012. Groundwater and Global Change: Trends, Opportunities and Challenges. United Nations World Water Assessment Program, UNESCO.

Vandike, James, 2014. Course Material from GEO ENG 331 Subsurface Hydrology. Obtained by the author during classes attended at Missouri Science and Technology.

Van Genuchten, 1980. A Closed-Form Equation for Predicting the Hydraulic Conductivity of Unsaturated Soils. Soil Science Society of America Journal, Issue 44, pp 892-898.

Van Genuchten, M., Leiji, F., Yates, S., 1991. The RETC Code for Quantifying the Hydraulic Functions of Unsaturated Soils. US Department of Agriculture, Riverside, California.

Venkataraman, K., Tummuri, S., Medina, A., Perry, J., 2016. 21st Centruy Drought Outlook for Major Climate Divisions of Texas Based on CMIP5 Multimodel Ensemble: Implications for Water Resource Management. Journal of Hydrology.

Walter, D., and Whealan, A., 2005. Simulated Water Sources and Effects of Pumping on Surface and Ground Water, Sagamore and Monomoy Flow Lenses, Cape Cod, Massachusetts. USGS Scientific Investigations Reports 2004-5181.

White, D., Baker, E., Sperka, R., 1997. Hydrogeology of the Shallow Aquifer and Uppermost Semiconfined Aquifer Near El Paso, Texas. USGS Water-Resources Investigations Report 97-4263.

Wilson, L., Everett, L., Cullen, S., 1995. Handbook of Vadose Zone Characterization & Monitoring. Geraghty & Miller Environmental Science and Engineering Series, CRC Press, Boca Raton, Florida.

Winston, R., 2009. ModelMuse- A Graphical User Interface for MODFLOW-2005 and PHAST: US Geological Survey Techniques and Methods 6-A29.

Appendix A - Cape Cod Cross Section

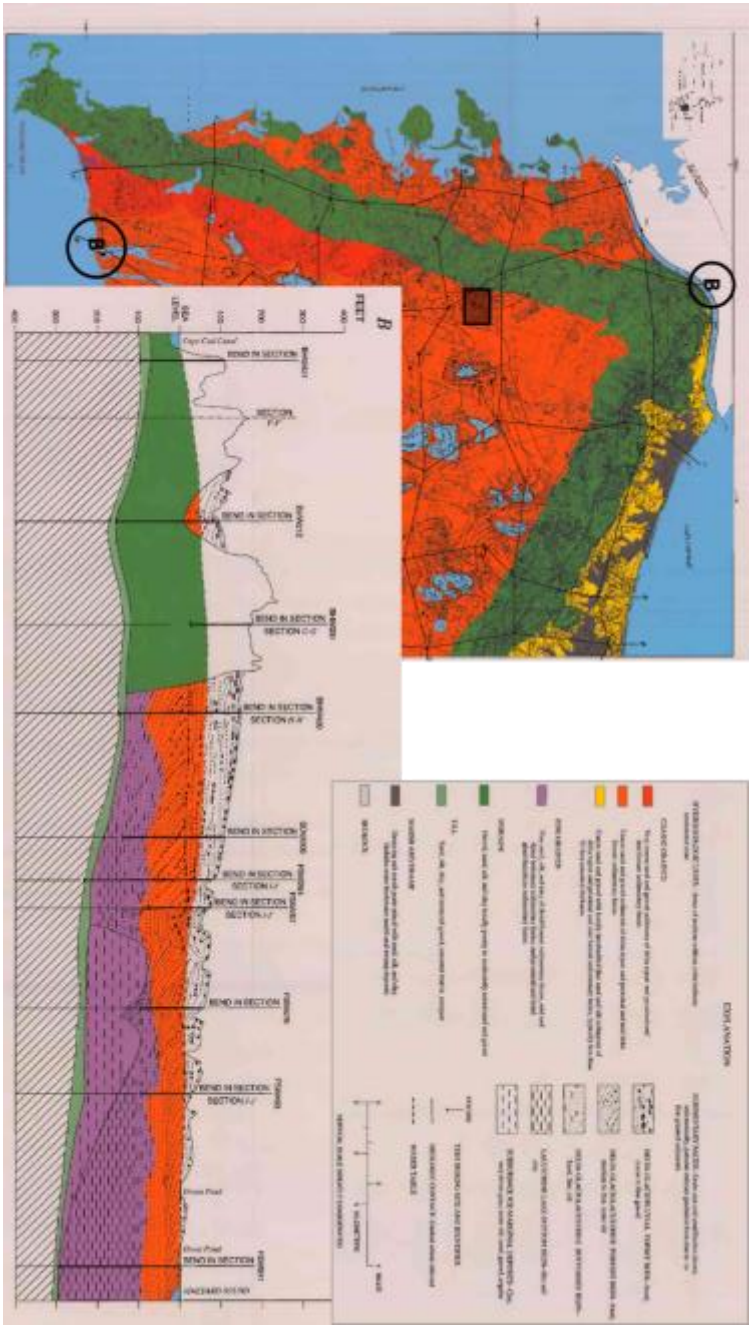

Cross section B-B' shown running north to south across the Sagamore Lens area. Shaded area on the cross section shows the study area.

USGS Groundwater Atlas

Appendix B - Well Logs in the HBA

High, Moderate, and Low Permeability Along Modeled Transect.

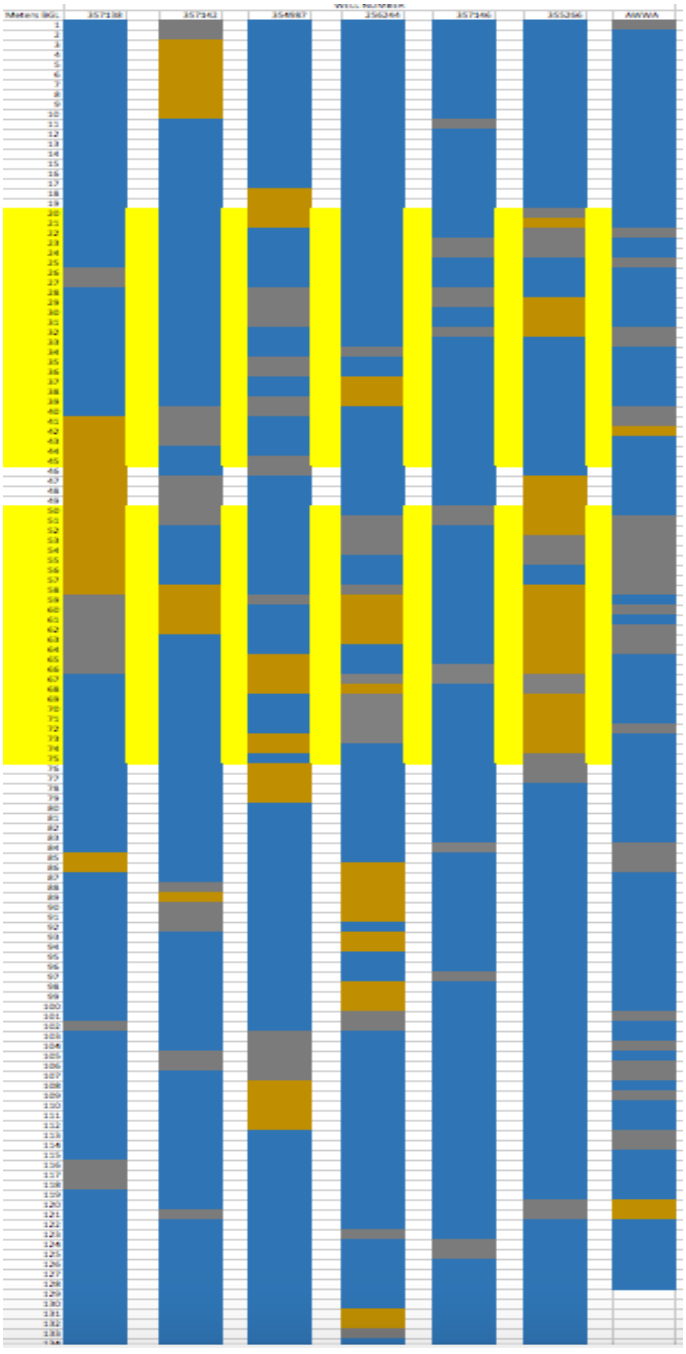

Legend:

Gravel- Sand (high-*K* values)

Silty Sand – Silt (med-*K* values)

Clays (low-*K* values)

Modeled horizons

Layers thinner than 1-meter thick are not shown. Layers shown between the yellow highlights correspond to layers included in the HBA unsaturated zone model.

Appendix C - Lithologic Layering Profile along Modeled Transect, HBA

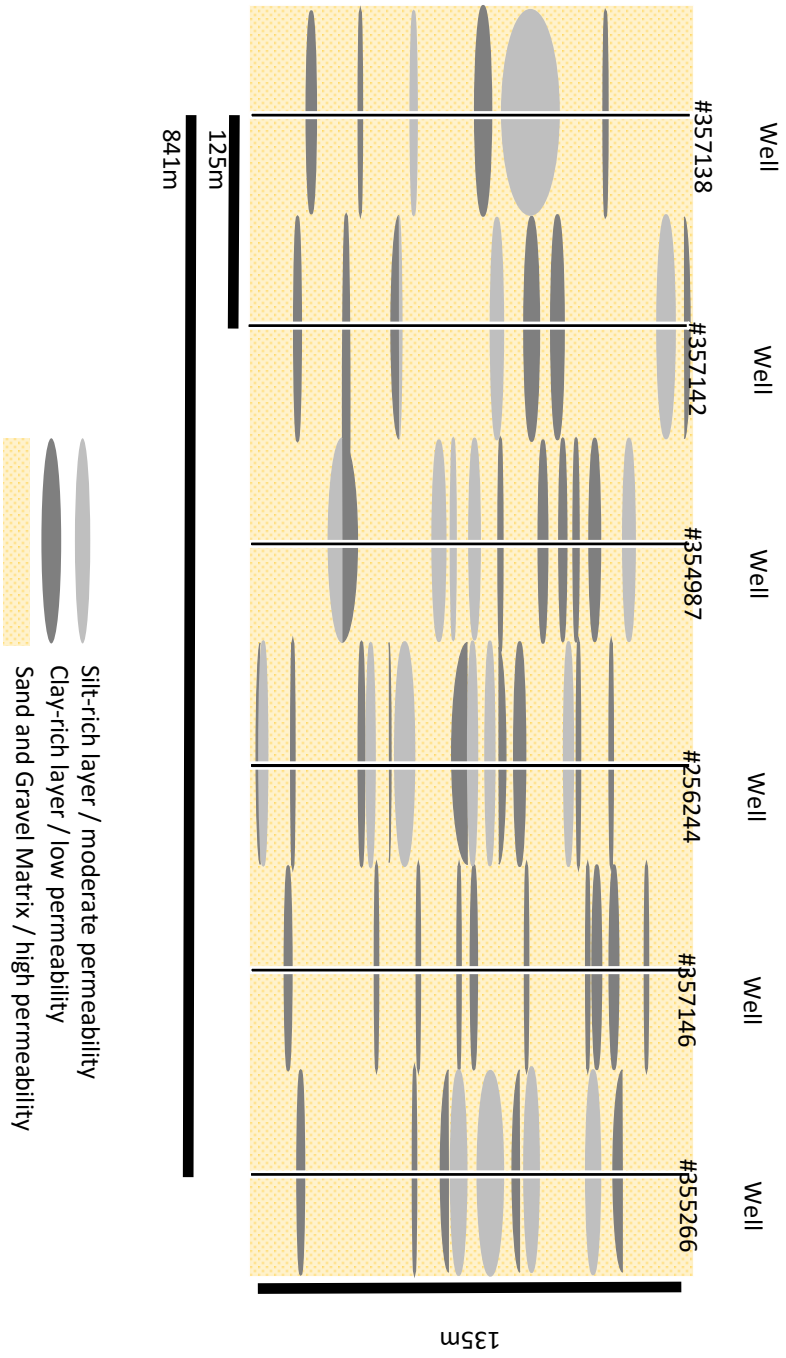

Conceptual model of lithologic complexity in the unsaturated zone, HBA site.

Appendix D - Neutron Log, El Paso (AWWA-RF Study)

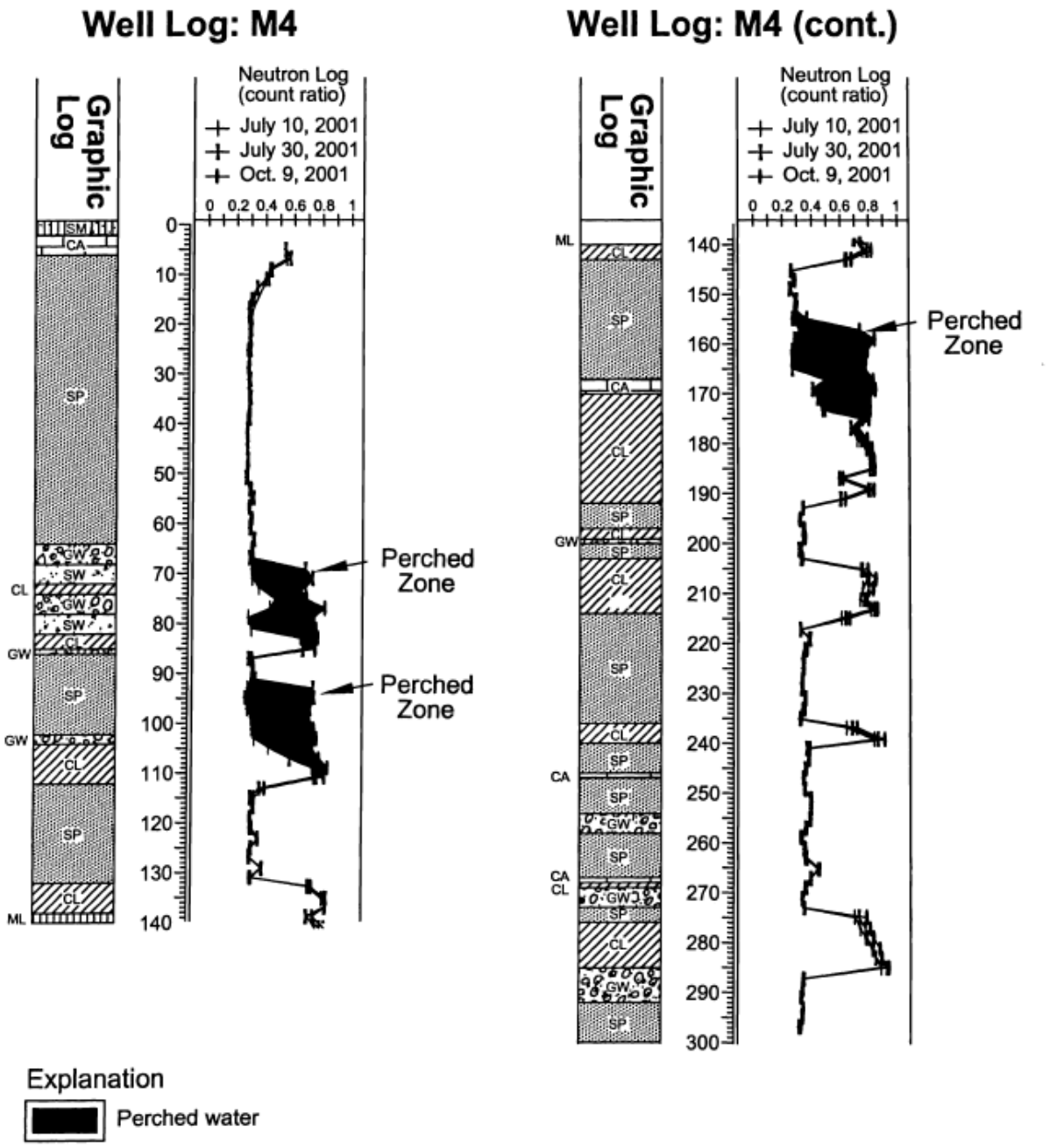

AWWA-RF (2003) modified

Appendix E - Map and Distance from Infiltration Basin to Landfill

Study Site

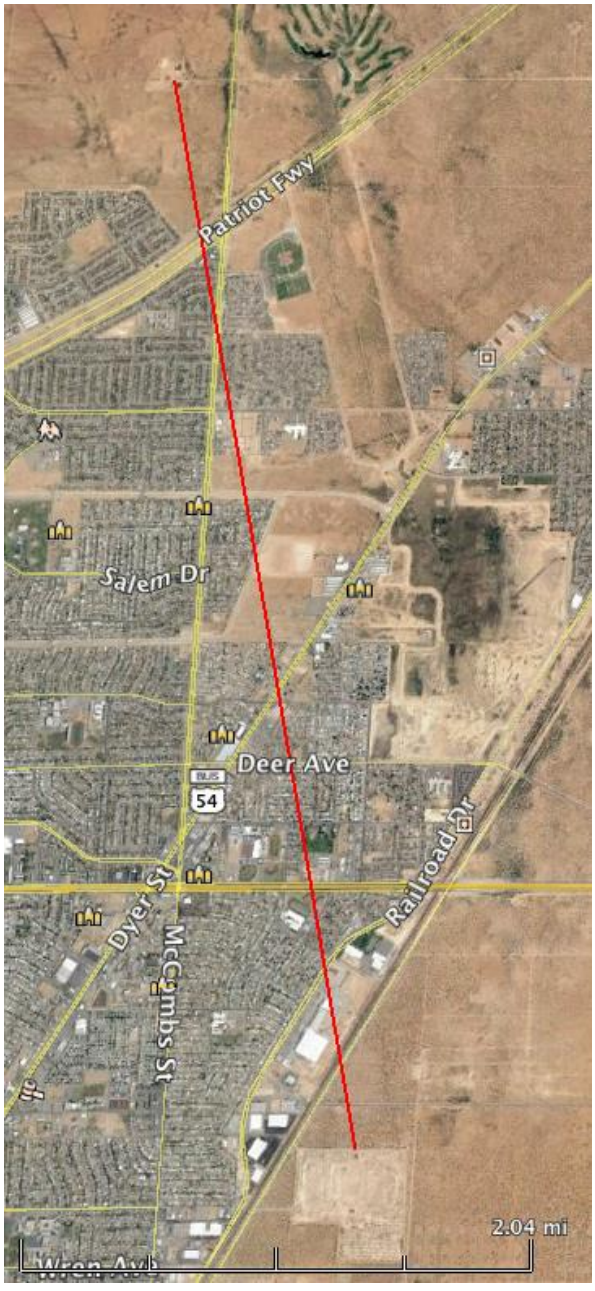

Red line indicates linear distance between two points. This distance is from study site (north point of red line) to the USGS study site (south end of the red line) that was used to provide hydrogeological characteristics of the Hueco Bolson Aquifer. The red line is approximately 2.5 miles in length.

Appendix F - Summary of RETC hydraulic parameters vs USGS published parameters

USGS Report 99-271 Layer# (depth)		Theta R	Theta S	Alpha	n
14ft profile	RETC (calculated)	0.0806	0.4658	0.0064	1.5407
	Given (published)	0.0400	0.4730	0.0081	
29ft profile	RETC:	0.0391	0.3624	0.0343	3.1677
	Given	0.0040	0.3550	0.0348	
45ft profile	RETC	0.0391	0.2611	0.0387	4.9233
	Given	0.0120	0.2600	0.0383	
72ft profile	RETC	0.0914	0.4656	0.0006	1.1546
	Given	0.1310	0.4700	0.0003	
81ft profile	RETC	0.0570	0.3495	0.0021	1.1265
	Given	0.0700	0.3530	0.0076	

92ft profile	RETC	0.1502	0.3956	0.0087	1.7851
	Given	0.0320	0.3940	0.0139	
93ft profile	RETC	0.0807	0.3509	0.0146	1.8296
	Given	0.0210	0.3490	0.0207	
109ft profile	RETC	0.0235	0.3200	0.0147	1.2015
	Given	0.0280	0.3190	0.0094	
140ft profile	RETC	0.1134	0.3170	0.0050	1.4983
	Given	0.0570	0.3190	0.0058	
147ft profile	RETC	0.0709	0.3912	0.0001	1.2969
	Given	0.0980	0.4240	0.0001	
		0.1502	0.3956	0.0087	1.7851
151ft profile	RETC	0.0320	0.3940	0.0139	
	Given				
		0.0807	0.3509	0.0146	1.8296
164ft profile	RETC	0.0210	0.3490	0.0207	
	Given				
		0.0235	0.3200	0.0147	1.2015
180ft profile	RETC	0.0280	0.3190	0.0094	

	Given	0.0810	0.4920	0.0005	
199ft profile	RETC	0.0472	0.3449	0.0252	1.8217
	Given	0.0170	0.3460	0.0257	
220ft profile	RETC	0.1007	0.4805	0.0001	1.3411
	Given	0.1210	0.5060	0.0001	
233ft profile	RETC	0.0328	0.5897	0.0239	1.4602
	Given	0.0260	0.5770	0.0218	
236ft profile	RETC	0.0500	0.3837	0.0076	1.3560
	Given	0.0120	0.3990	0.0109	
245ft profile	RETC	0.0497	0.3338	0.0006	1.2773
	Given	0.0530	0.3490	0.0010	
259ft profile	RETC	0.0680	0.3800	0.0080	1.0900
Caliche layer	Given	N/A	N/A	N/A	N/A
284ft profile	RETC	0.0065	0.3786	0.0588	1.3510
	Given	0.0150	0.3730	0.0521	

289ft profile	RETC	0.0454	0.3673	0.0197	5.4501
	Given	0.0090	0.3730	0.0191	
294ft profile	RETC	0.0908	0.4871	0.0016	1.3962
	Given	0.1210	0.5010	0.0017	
298ft profile	RETC	0.0743	0.3470	0.0187	5.3473
	Given	0.0090	0.3530	0.0217	
318ft profile	RETC	0.0730	0.3896	0.0173	6.0924
	Given	0.0130	0.3970	0.0164	
318.5ft profile	RETC	0.0232	0.3629	0.0280	1.4667
	Given	0.0100	0.3540	0.0263	

"Given" values from Abeyta, 1999

Appendix G- Grid Discretization Example, SLA and HBA Models

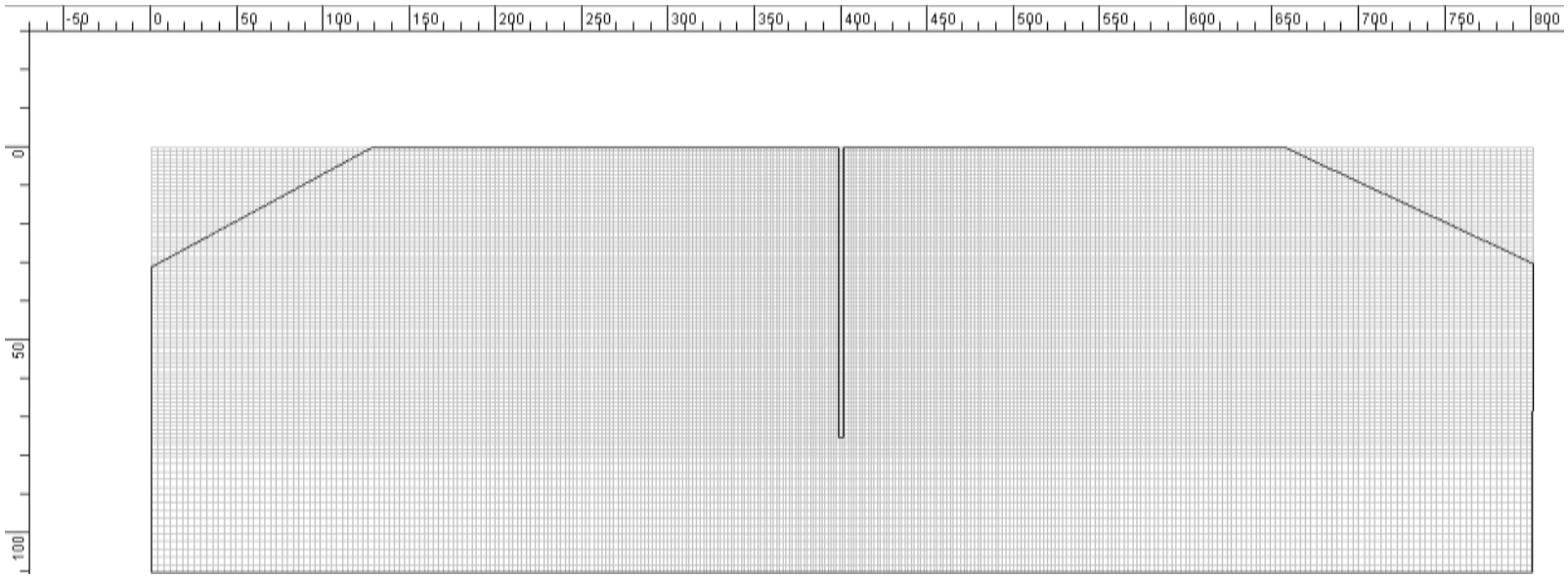

Example shows finer grid discretization in the upper 75m of the model (z-direction) and closer to the well at the horizontal center of the model. A point in the upper half of the model and alongside the well would have a *x* and *z* spacing of no more than 1m between grid lines.

Appendix H - Map and Distance from Infiltration Basin to Monitoring Wells Transect

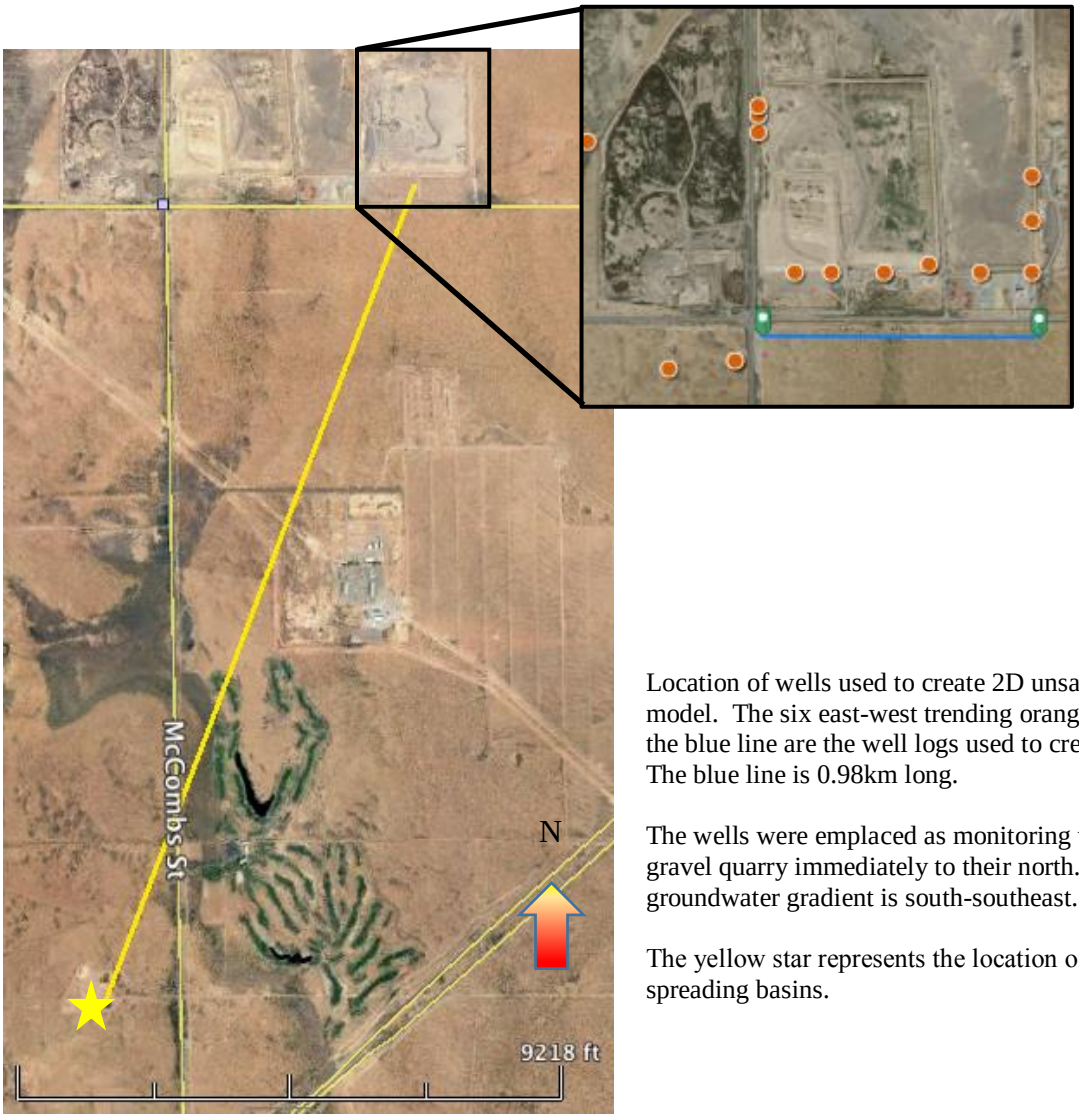

Location of wells used to create 2D unsaturated zone model. The six east-west trending orange circles above the blue line are the well logs used to create the model. The blue line is 0.98km long.

The wells were emplaced as monitoring wells for the gravel quarry immediately to their north. The regional groundwater gradient is south-southeast.

The yellow star represents the location of EPWU's spreading basins.

Appendix I - Historic Recharge Data, EPWU, 2014

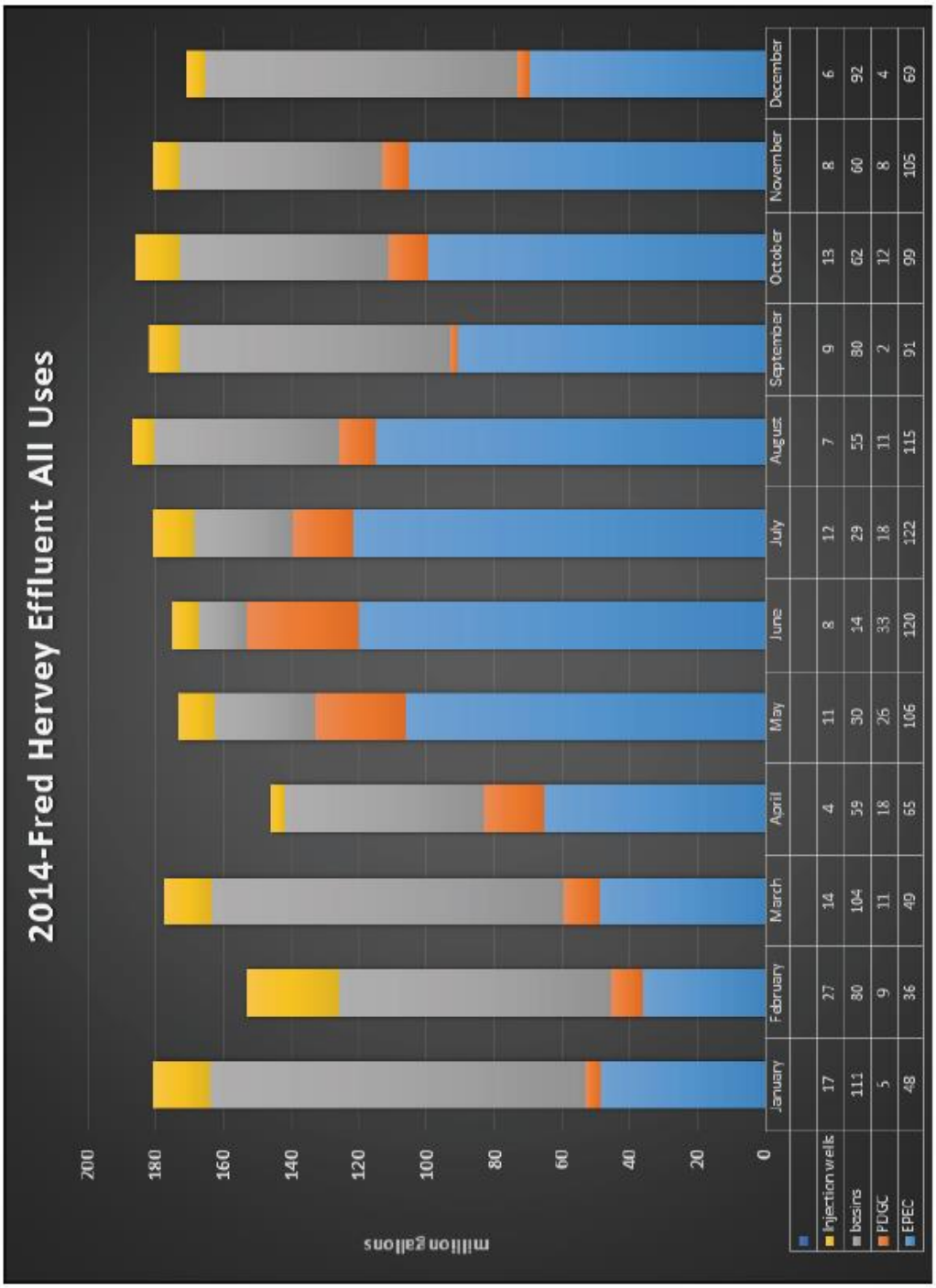

Appendix J - Bedrock Topography of the SLA Area

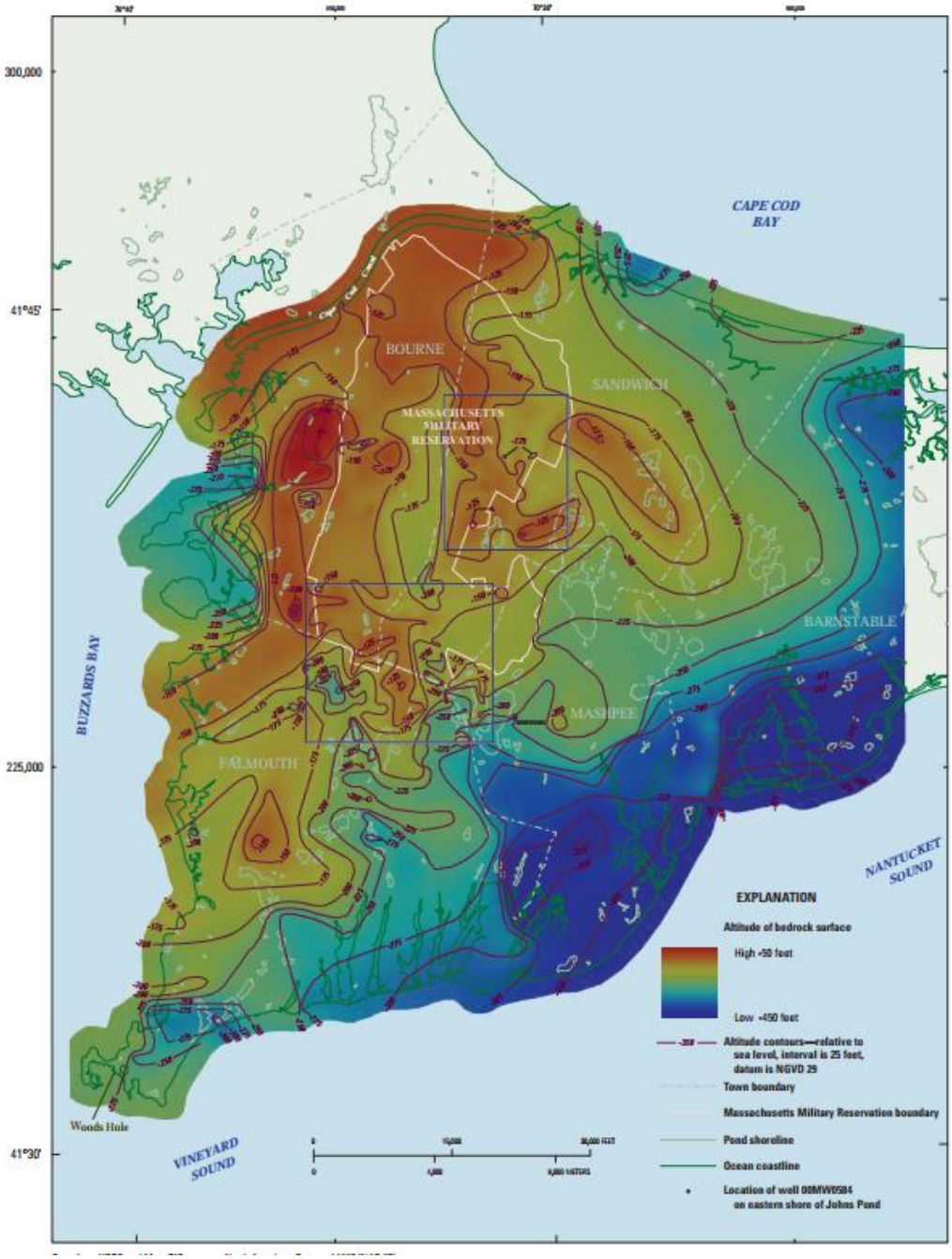

Fairchild et al, 2013

Appendix K - Cape Cod Lithology near MW-255.

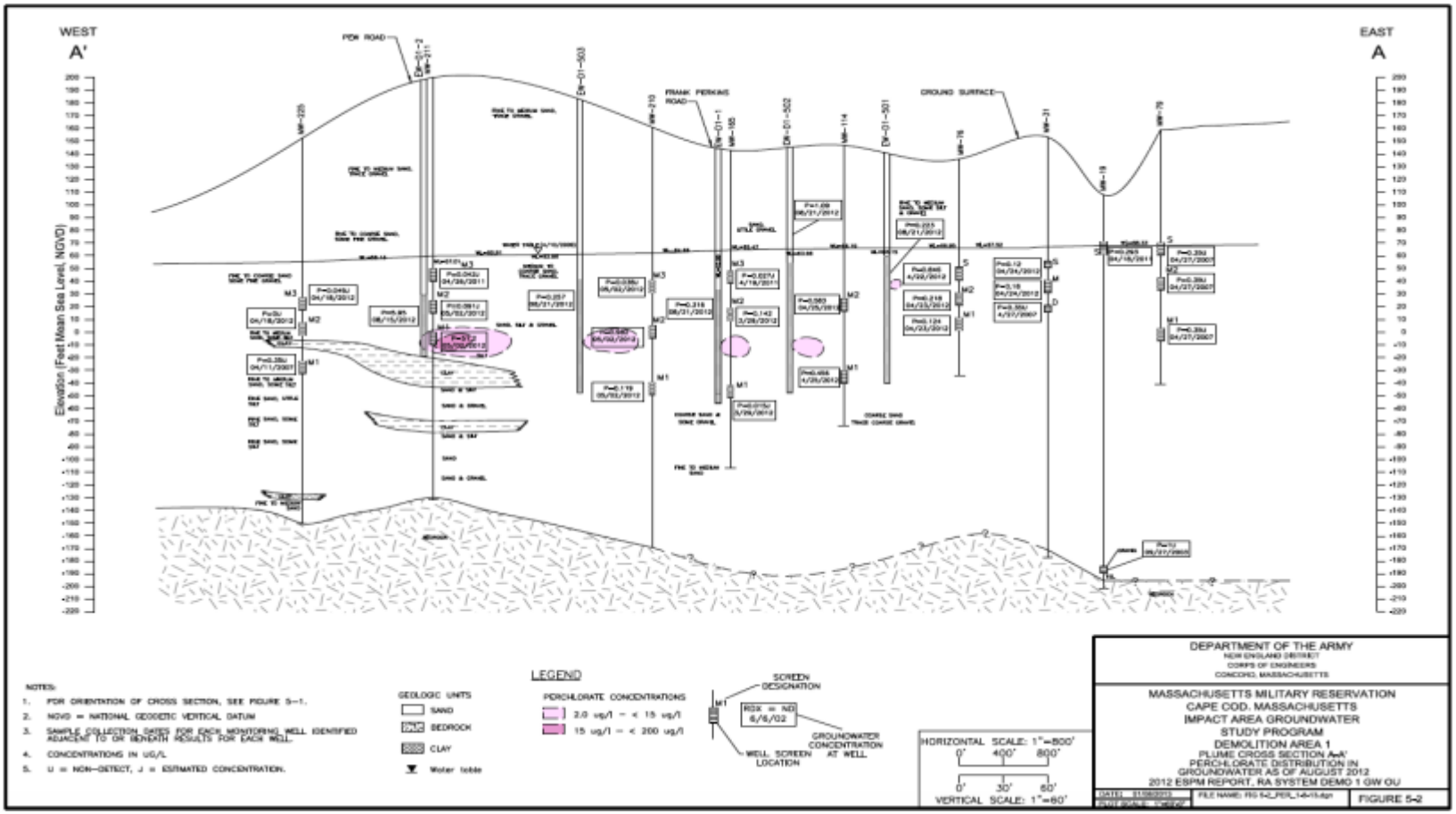

Demolition Area 1 environmental and system performance monitoring report, 2013, U.S. Army Corp of Engineers New England District.

Appendix L - Hydraulic Conductivity and Soil Parameter Values, HBA

Depth BGL	Sand %	Silt %	Clay %		Theta R	Theta S	Alpha
Poorly fitting theta R layers							
86.5m	97	2.8	0.2	Calculated Values	0.00646	0.37864	0.05879
				Published Values	*0.01500*	*0.37300*	*0.05208*
8.8m	97	2.8	0	Calculated Values	0.03908	0.36237	0.03425
				Published Values	*0.00400*	*0.35500*	*0.03480*
28.3m	94	5.8	0.2	Calculated Values	0.08066	0.35091	0.01463
				Published Values	*0.02100*	*0.34900*	*0.02065*
Example welling fitting layers							
24.6m	59	12	29	Calculated Values	0.057	0.34954	0.00207
				Published Values	*0.070*	*0.35300*	*0.00760*
33.2m	91	8.8	0.2	Calculated Values	0.02352	0.32003	0.01471
				Published Values	*0.02800*	*0.31900*	*0.00942*

Hydrogeological parameters used to create HBA model based. Shown in the table are values calculated by author from interpreting moisture retention under suction pressure using the program RETC. Also shown are values published by USGS, derived from the same data set.

"Published Values" from Abeyta, 1999

Appendix M - Vadose Well Schematic

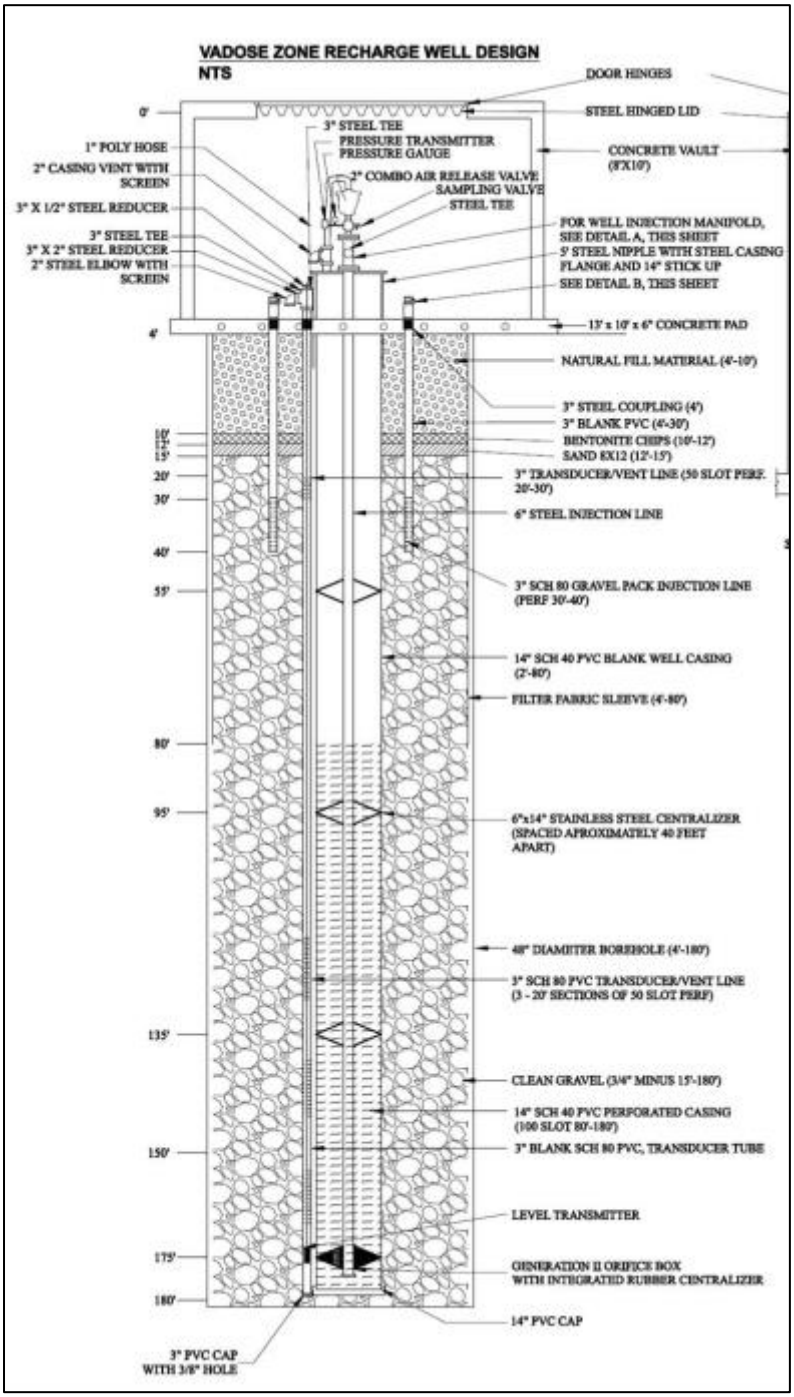

Example of a pre-designed vadose recharge well.

Courtesy of Mr. Meyer, Torrent Resources

Appendix N - Thought Experiment Calculations

Thought Experiment Outputs												
Bottom Depth	Depth to Water Table	Screen Length	Recharge Rate	Scaled Recharge in AF	Scaled Recharge Rate*	Recharge Rate / Screen Length	Wells Needed	ells Needed		Cost per m^3/d of Recharge	Cost Per Well	Total Cost
15	110	10	195.6	0.2490	307.092	30.709	40.164	41		293.07	90000	$ 3,690,000
20	105	15	260.3	0.3313	408.671	27.245	30.181	31		220.23	90000	$ 2,790,000
25	100	20	310.5	0.3952	487.485	24.374	25.301	26		184.62	90000	$ 2,340,000
30	95	25	354.4	0.4511	556.408	22.256	22.167	23		176.90	98430	$ 2,263,890
35	90	30	394.1	0.5016	618.737	20.625	19.934	20		185.60	114835	$ 2,296,700
38	87	33	416.4	0.5300	653.748	19.811	18.867	19		190.71	124678	$ 2,368,882
40	85	35	430.9	0.5485	676.513	19.329	18.232	19		193.99	131240	$ 2,493,560
43	82	38	451.7	0.5749	709.169	18.662	17.392	18		198.94	141083	$ 2,539,494
45	80	40	465.4	0.5924	730.678	18.267	16.880	17		202.07	147645	$ 2,509,965
48	77	43	484.4	0.6166	760.508	17.686	16.218	17		207.08	157488	$ 2,677,296
50	75	45	496.5	0.6320	779.505	17.322	15.823	16		210.45	164050	$ 2,624,800
55	70	50	525.6	0.6690	825.192	16.504	14.947	15		218.68	180455	$ 2,706,825
60	65	55	550.5	0.7007	864.285	15.714	14.271	15		227.77	196860	$ 2,952,900
65	60	60	570.9	0.7267	896.313	14.939	13.761	14		237.94	213265	$ 2,985,710
68	57	63	580	0.7382	910.6	14.454	13.545	14		245.01	223108	$ 3,123,512
70	55	65	585.1	0.7447	918.607	14.132	13.427	14		250.02	229670	$ 3,215,380
73	52	68	588	0.7484	923.16	13.576	13.361	14		259.45	239513	$ 3,353,182
75	50	70	598.9	0.7623	940.273	13.432	13.117	14		261.71	246075	$ 3,445,050
78	47	73	1156.1	1.4715	1815.077	24.864	6.795	7		141.00	255918	$ 1,791,426
80	45	75	1259.3	1.6029	1977.101	26.361	6.238	7		132.76	262480	$ 1,837,360
83	42	78	1350	1.7183	2119.5	27.173	5.819	6		128.48	272323	$ 1,633,938
85	40	80	1445	1.8392	2268.65	28.358	5.437	6		122.93	278885	$ 1,673,310
90	35	85	1736	2.2096	2725.52	32.065	4.525	5		108.34	295290	$ 1,476,450
95	30	90	1967.7	2.5045	3089.289	34.325	3.993	4		100.90	311695	$ 1,246,780
100	25	95		0							400000	
110	15	105		0							440000	

Calculations used to determine cost of a vadose well field in Chapter 7, section 5.

Appendix O - AWWA Report Lithologic Log for El Paso Recharge Program

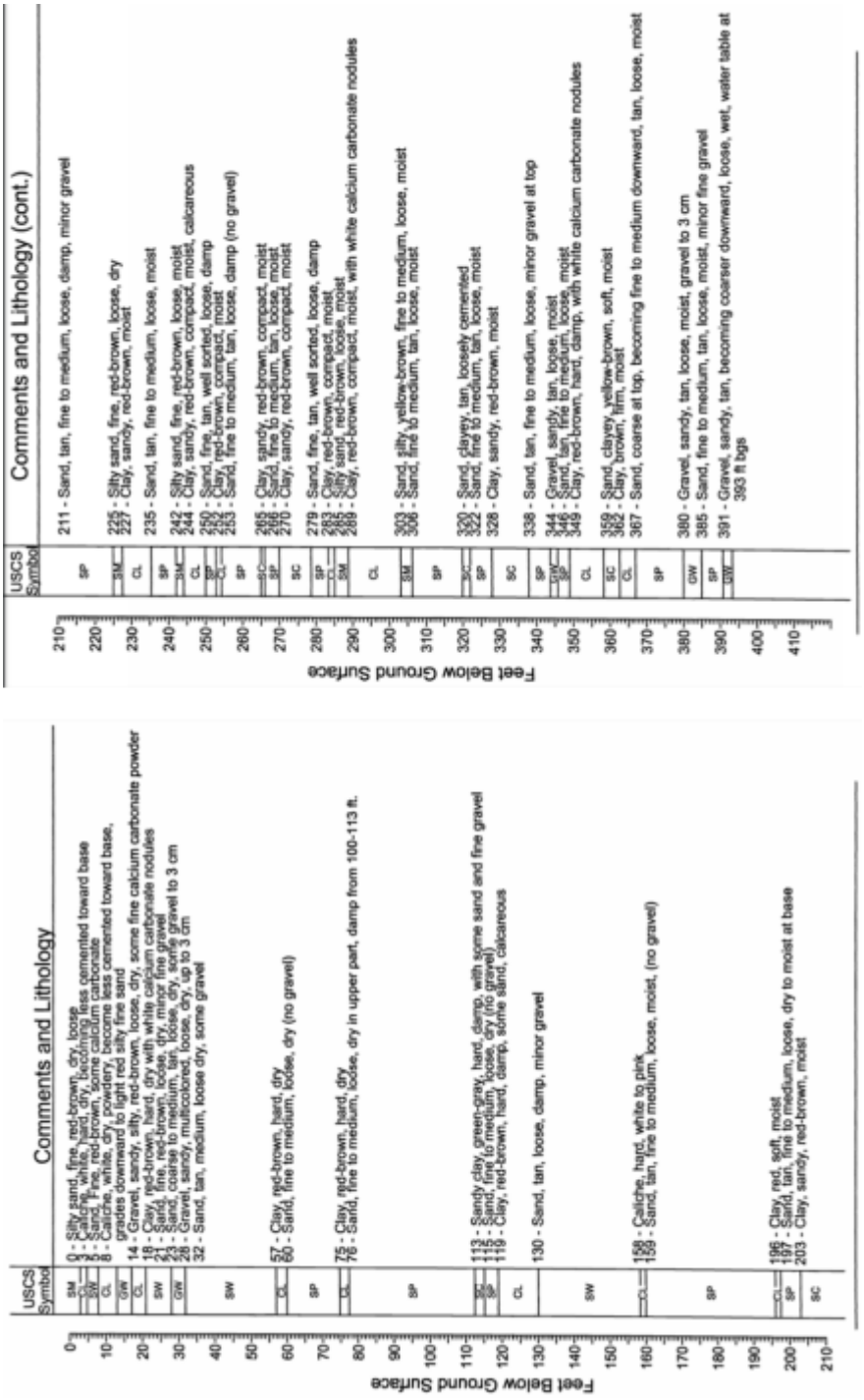

Appendix P - Unit Conversion

Acre-Foot (AF)	Cubic Meters (m^3)	Gallons (Gal)	
1	1,233.48	325,851	
Acre-Feet per Day (AF/D)	**Cubic Meters per Day (m^3/d)**	**Gallons per Day (GPD)**	**Gallons per Minute (GPM)**
1	1,233.48	325,851	226.29
Acre-Feet per Year (AF/Y)	**Cubic Meters per Day (m^3/d)**	**Gallons per Day (GPD)**	**Gallons per Minute (GPM)**
1	3.38	892.15	0.62
Common Conversions from Text:			
GPM to other Rates			
300 GPM =	484.22 AF/Y =	1,635.3 m^3/d	
600 GPM =	968.45 AF/Y =	3,270.6 m^3/d	
Acre-Feet to other Rates			
10 AF/D =	12,334.89 m^3/d =	2,262.87 GPM	
5,000 AF/Y =	16,885.81 m^3/d =	3,097.75 GPM	

Appendix Q - Microgravity Survey Results

East-West Profile				
Latitude	Longitude	Rough Elevation (m)	Time	Counter Reading
31.949956	106.4248	1236		904.62
31.949954	106.423203	1233		900.64
31.950051	106.421261	1228		896.49
31.950059	106.419518	1229		891.76
31.949985	106.418045	1229		887.72
31.950059	106.416787	1227		885.91
31.950055	106.416376	1228		885.38
31.950069	106.416022	1228		884.6
31.950059	106.415779	1230		884.59
31.95007	106.415311	1230		883.65
31.950075	106.414952	1227		883.35
31.9595005	106.414609	1227		882.67
31.950051	106.414426	1225		882.21
31.950056	106.414076	1223		881.87
31.950064	106.413619	1221		880.95
31.950094	106.41336	1223		881.1
31.950098	106.413166	1223		881.1
31.950097	106.412828	1219		879.2
31.95009	106.412553	1225		880.07
31.950147	106.412238	1223		879.47
31.950151	106.412049	1222		878.88
31.950143	106.411761	1220		879.54
31.950152	106.411458	1224		878.43
31.950134	106.411115	1221		878.13
31.950136	106.410772	1218		877.43
31.950146	106.410459	1218		876.86
31.95015	106.410163	1219		876.62
31.950198	106.409854	1219		876.56
31.950206	106.40954	1221		875.73
31.950209	106.409179	1216		875.23
31.950203	106.408884	1221		874.73
31.950203	106.408596	1218		874.42
31.950179	106.408329	1218		873.92